Hydride Generation as a Sample Introduction Technique for Detection of Arsenic by Microplasma

by

Laiba Qadeer

A thesis

presented to the University of Waterloo

in fulfillment of the

thesis requirement for the degree of

Master of Science

in

Chemistry

Waterloo, Ontario, Canada, 2023

Author's Declaration

I hereby declare that I am the sole author of this thesis. This is a true copy of the thesis, including any required final revisions, as accepted by my examiners.

I understand that my thesis may be made electronically available to the public.

Abstract

Microplasma can be used as a portable analytical instrument for elemental analysis of samples due to their small size, low power consumption, low carrier gas consumption, and low cost. This is specifically important for areas where contamination of water by arsenic is prevalent (e.g., because arsenic is indigenous to the soil). Due to the volatility of arsenic and its organic compounds, it is only chemical vapor generation (CVG) that can be used to introduce the sample into the microplasma. In this project, equipment for hydride generation (a type of CVG) was designed and used to test this sample introduction technique for microplasma. It was found that response of microplasma towards water vapors and hydrogen released from the hydride generation reaction was different when it was operated in each of three different carrier gases, namely helium, argon, and mixture of argon with 1000 ppm hydrogen. Similarly, the best observation position for arsenic over the microplasma tube was also different for helium microplasma and argon microplasma (0.84 cm and 1.34 cm away from the front electrode where carrier gas and analyte are introduced, respectively). Arsenic signals were also found to be more intense in helium microplasma, as compared to that in argon microplasma and argon – 1000 ppm hydrogen microplasma. Afterwards, the arsenic peaks at 197.3 nm and 228.8 nm were used to estimate the detection limit for arsenic in helium microplasma and argon microplasma, respectively. The detection limit for arsenic in helium and argon microplasma were estimated to be 31 ppb and 40 ppb, respectively. Although this project proved the feasibility of microplasma for detecting arsenic in liquid samples, it was concluded that more research is needed in this field to improve the reproducibility in the measurement of emission signal and the detection limit for arsenic, by making changes in the equipment and the design of gas-liquid separator.

Acknowledgements

I want to thank Professor Vassili Karanassios for giving me the opportunity to work on this project and for his continued support and guidance throughout my project. He also guided me in setting up several experiments and in trouble-shooting several issues.

I also want to acknowledge the guidance of my committee members, Professor Jean Duhamel and Professor Michael Mayer. Both gave me time for meetings, provided valuable feedback on my project and guided me regarding the content of my thesis.

Lastly, I wish to express my gratitude towards the Associate Chair Graduate Studies and Research Professor Thorsten Diekmann for providing moral support and for guiding me in decision-making regarding my degree. I also want to thank the Administrative Coordinator Catherine Van Esch for her administrative support.

Table of Contents

List of Figures

List of Tables

List of Abbreviations

CVG: Chemical Vapor Generation

DBD: Dielectric Barrier Discharge

GLS: Gas-Liquid Separator

HG: Hydride Generation

ICP: Inductively Coupled Plasma

IT: Integration Time

MS: Mass Spectrometry

NIST: National Institute of Standards and Technology

OES: Optical Emission Spectroscopy

PMT: Photomultiplier tube

PVG: Photochemical Vapor Generation

SNR: Signal-to-Noise Ratio

Chapter 1

Introduction to Microplasma and to Chemical Vapor Generation

1.1 Outline

- Discussion of microplasma as an analytical device and comparison of its function with that of an ICP
- Brief discussion of the issue of arsenic contamination of water
- Description of functionality of microplasma
- Two main sample introduction techniques used for microplasma: electrothermal vapor generation and chemical vapor generation.
- Three types of chemical vapor generation techniques used for sample introduction.
- Summary of the project

1.2 Introduction to Microplasma as an Analytical Instrument

The scientific community has been paying extensive attention to the development of micro-total-analysis or lab-on-a-chip [1]. These analysis systems consist of sensors, microfluidic devices, and microreactors incorporated onto small chips by the help of LSI (large scale integration) microfabrication technologies [1]. Microfabrication consists of design, creation and application of structures, devices, and systems at micrometer range. The properties of materials at this scale vary considerably from those at macroscopic range [2]. Microfabrication techniques are used to make analytical instruments, as decreasing the size of these instruments helps in making them more portable and cost-effective. Furthermore, it also decreases the sample consumption and waste generation of the instrument. This is beneficial as sometimes, the sample to be tested is available

in very small amounts. Microfabrication remains an active area of research due to the benefits of less sample and reagent consumption, and lower waste generation from microfabricated devices.

Microplasmas mimic the functionality of the analytical instrument, inductively coupled plasma (ICP). Microplasmas have the potential to be used as portable analytical instruments because of their small size, low power consumption, low manufacturing cost, and less reagent and sample consumption. Plasma is an ionized gas, consisting of electrons, ions, and neutral atoms/molecules in an excited or fundamental state. A plasma which has one critical dimension in the micrometer range is called a microplasma [3]. Microplasmas can be used for elemental analysis of different samples. Presently, the instrument used for elemental analysis of different samples is Inductively Coupled Plasma (ICP). The detection limits for different elements by ICP can be in the range of parts per million (ppm) to parts per trillion (ppt). This detection limit depends on the element being analyzed and the detector of the ICP, which can be an Optical Emission Spectrometer (OES) or Mass Spectrometer (MS). Mass Spectrometer has a better detection limit [4]. OES allows the quantification of elements by measuring the amount of energy emitted by excited atoms moving to a lower energy state, whereas in mass spectrometry, the elements are quantified by measuring the mass to charge ratio of their ions formed [5]. Inductively coupled plasma is very expensive to operate as it uses 8 – 20 L/min of carrier gas (an inert gas used to carry samples towards plasma) and needs 1 - 2 Kwatt of electric power [6]. This problem of expensive operation is solved by microplasma as it consumes much lower amount of carrier gas, power and sample as compared to ICP. Microplasma can operate at a carrier gas flow rate of 250 mL/minute and a minimum of 5 W power. These microplasma devices use optical emission spectrometers as detectors because of their portability, simple design, and a potential for miniaturization [6]. Thus, microplasmas have

significantly lower operating costs as compared to ICP, making them suitable for their use in a portable analytical instrument. Moreover, development of microplasma as an analytical instrument is an example of micro fabrication technology, and a step towards greening of spectroscopy.

Development of microplasma as a portable analytical instrument will enable low-cost analysis of samples for toxic elements, such as arsenic. Contamination of drinking water by arsenic affects millions of people worldwide. The problem of arsenic contaminated water has been reported in southern and southeast Asian countries, like West Bengal, Vietnam, Bangladesh, Thailand, Nepal, and Taiwan. These places are known to have increased levels of As in ground water [7,8]. Similarly, arsenic contamination of water has also been reported in Canada [9]. In Canada, arsenic is released into the environment by natural weathering and erosion of arsenic bearing rock and soils, and by anthropogenic activities such as gold and base-metal processing, thermal and coal fired power generation, use of arsenal pesticides, etc. [9]. Acute arsenic poisoning usually results in gastroenteritis (inflammation of gastrointestinal lining), followed by hypotension (low blood pressure) [10]. Whereas chronic exposure to arsenic can harm skin, lungs, gastrointestinal tract, kidneys, and liver [10,11]. Even irrigation of crops by water contaminated by arsenic can lead to arsenic contamination of agricultural products [7], allowing arsenic to enter the food chain. Therefore, it is important to analyze water samples for the presence of arsenic before its consumption. In fact, providing safe drinking water and non-contaminated nutritious food to people everywhere is one of the 17 sustainable goals set by the UN. The 17 sustainable goals constitute the 2030 Agenda for Sustainable Development which is an urgent call for action by all countries in a global partnership. It provides the layout for peace and prosperity of people and the

planet [12]. Inexpensive and easy-to-operate analytical instruments are required for analysis of water samples, and microplasma is a candidate for such analysis.

Just like ICP, optical emission spectroscopy is also used for detection of elements in microplasma devices. Optical emission spectroscopy measures the energy lost by an atom when it falls from an excited state to a lower energy state in the form of light, as described in Figure 1.1. The intensity of light depends on the number of emitting atoms in the sample [13]. In the plasma, the excited states are created through collisions between plasma species and electrons, for example through electron impact excitation or dissociation reactions. Radiating atomic, ionic or molecular species can reveal information about the species present in the plasma. Hence, an emission line can act as an identification for the excited species present in the plasma. However, absence of an emission line does not always indicate absence of a particular species in the plasma. Sometimes, no emission line would be seen for a species if the plasma is unable to excite it [14].

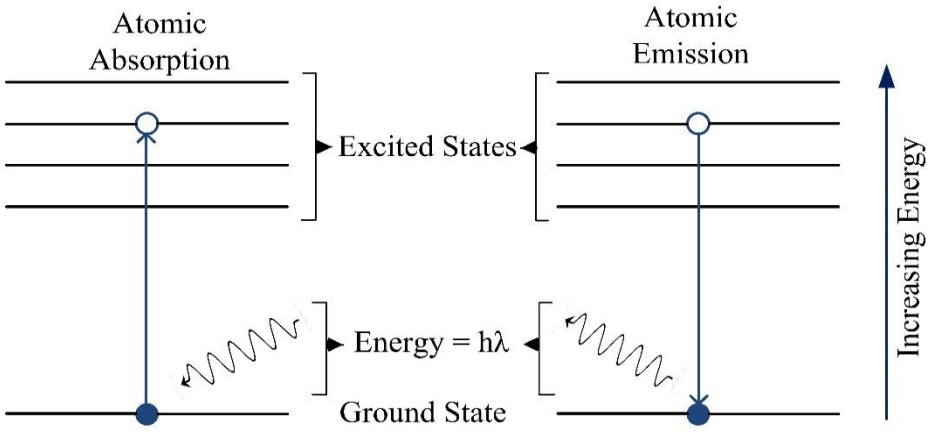

Figure 1.1: Diagram showing the release of energy by excited atoms.

Due to its small size and low power consumption, microplasma is not in thermodynamic equilibrium. In a non-equilibrium plasma, the variation among different kinds of temperatures is given by: $T_{excitation} > T_{electron} > T_{vibrational} > T_{rotational}$. When one or more of these four temperatures are not the same, the plasma is in non-equilibrium or partial local thermodynamic equilibrium [15]. The two main reasons for non-equilibrium are electron impact and high surface-area-to-volume ratio. In microplasma, the electrons exchange energy by collisions with radicals and neutral species. Plasma being confined to a small space increases electron collisions and average exchange of energy. Hence, the small size of microplasma makes the electron temperature, T_e, much higher than the gas temperature, T_g. Secondly, due to the high surface-area-to-volume ratio of the microplasma, the heat coupled from the power supply dissipates quickly. As a result, microplasma does not trap heat, and are called cold plasmas [16]

Different sample introduction techniques that have been coupled with microplasma are discussed in the following section.

1.3 Sample Introduction Techniques Used for Microplasma

1.3.1 Electrothermal Vapor Generation

The sample introduction technique currently being used for microplasma is electrothermal vapor generation (EVG). This technique requires a vaporization chamber which is connected to microplasma. This chamber has a tungsten or rhenium coil on a support rod which connects the coil to an external power supply [17]. A diagram of such a chamber can be found in Figure 1.2. In this sample introduction technique, a heated tungsten or rhenium coil is used to vaporize the analyte. If the sample is aqueous, it can be heated to about 100°C on the coil to evaporate water, before the introduction of analyte into the microplasma. The analyte is carried by the carrier gas

into the microplasma after applying a higher amount of current to the rhenium coil which raises its temperature, vaporizing the analyte [18]. This method has been used for detection of Ag, Cd, Cu, Hg, Pb, Sb, Sn, Zn, Na, Li, K, Mn, and Mg [6,18] and is usually used for elements that are not volatile or form volatile compounds. Using EVG for analysis of volatile elements like arsenic and mercury in water introduces error in quantification because these elements vaporize during the drying step meant for vaporization of the solvent. Hence, EVG can only be used for analysis of samples for non-volatile elements.

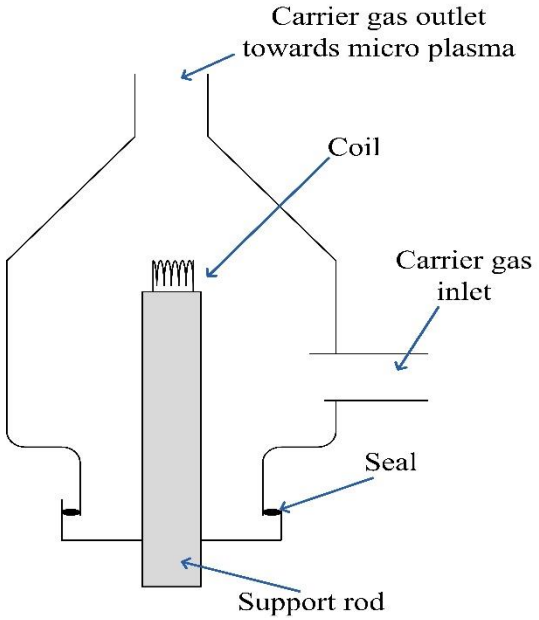

Figure 1.2: Diagram of vaporization chamber used for EVG.

1.3.2 Chemical Vapor Generation

Chemical vapor generation eliminates the problem caused by EVG in the analysis of liquid samples of volatile elements like arsenic and mercury, since this sampling technique does not require heating the sample. Chemical vapor generation converts non-volatile elements and

compounds into volatile compounds which can be transported into microplasma with the help of a carrier gas. CVG alleviates matrix interference, improves sampling efficiency, and improves sensitivity as it volatilizes the analyte, isolating it from its matrix [19]. CVG has been used for the analysis of As, Bi, Ge, Hg, Pb, Sb, Se, Sn, Te, and Hg [20,21,22]. Chemical vapor generation can be carried out by three methods: hydride generation, cold vapor generation, and photochemical vapor generation.

1.3.2.1 Hydride Generation

Hydride generation was introduced in 1970 for the analysis of samples for arsenic and Selenium by flame atomic absorption spectroscopy [23]. In this technique, an acidic solution of the analyte is reacted with a basic solution of a reducing agent, typically sodium borohydride ($NaBH_4$). This reducing agent reduces the metals to their volatile hydrides. The equation for reduction of metal E is [23]:

$$NaBH_4 + 3H_2O + HCl \rightarrow B(OH)_3 + NaCl + 8H \xrightarrow{E^{m+}} EH_n + H_2(\text{excess})$$

Here, m might or might not be equal to n [23].

The volatile hydrides from the reaction are then carried to the ICP, microplasma, etc. for detection. For microplasma, the setup for chemical vapor generation consists of a peristaltic pump, a reaction coil, and a gas liquid separator, as illustrated in Figure 1.3. The acidic solution of the analyte metal is reacted with a basic solution of the reducing agent, sodium borohydride ($NaBH_4$) or potassium borohydride (KBH_4), in a reaction coil. The volatile metal hydrides formed from the reaction are segregated from the liquid reaction mixture by a gas liquid separator (GLS), and then carried towards the microplasma by a carrier gas. The residual moisture in the carrier gas at the exit of the GLS can be removed by a desiccant such as concentrated sulfuric acid (H_2SO_4) [21], or

two stage drying with magnesium perchlorate ($Mg(ClO_4)_2.xH_2O$), followed by concentrated sulfuric acid [24,25]. Two-stage drying by two gas-liquid separators has also been used to remove water vapors [20]. The efficiency of hydride generation depends on the concentration of $NaBH_4$, the type and concentration of acid used as reaction medium and dynamics of mixing reagents [26]. Therefore, the concentration of $NaBH_4$ should be adjusted to get the maximum intensity of the analytical signal.

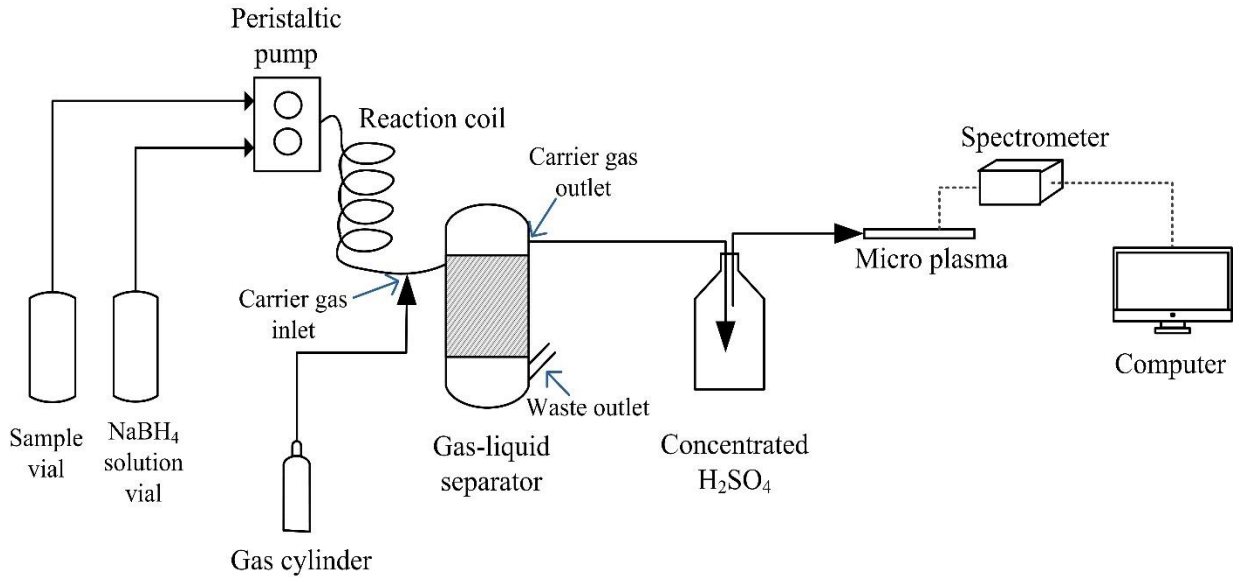

Figure 1.3: Diagram of the instrumental setup used for hydride generation. Concentrated H_2SO_4 has been shown as a desiccant, instead of a second gas-liquid separator.

Hydride generation offers advantages in terms of selectivity, detection limits, and elimination of matrix effects. The detection limit for arsenic using this sample introduction technique has been in the range of parts per billion, that is 0.2 – 4.8 µg/L [21,27]. Using hydride generation, arsenic species present in both organic and inorganic forms can be reduced, which makes this sample introduction technique very specific [28]. Inorganic arsenic, monomethyl arsenic acid (MMA),

dimethyl arsenic acid (DMA) and trimethyl arsine oxide (TMAO) are reduced to AsH_3, CH_3AsH_2, $(CH_3)_2AsH$ and $(CH_3)_3As$, respectively [28]. Hydride generation also eliminates the matrix effects caused by easily ionizable elements like calcium, magnesium, sodium, and potassium as these elements do not form hydrides [29]. These easily ionizable elements dismantle free electron equilibria of microplasma, disrupting and reducing the analytical signal [29]. Hydride generation prevents their introduction into microplasma, hence their presence in the sample does not impact the result.

There are problems associated with hydride generation as well, which include interference from transition metals, production of hydrogen as a by-product and memory effect. Transition metals like Ni, Co, Cu and Fe in high concentration can suppress the release of metal hydrides from the liquid solution [30]. These ions should be removed from the sample by ion exchange chromatography before analysis of the sample by the hydride generation. The other problem caused by this sample introduction technique is production of a large amount of hydrogen as a by-product. Hydrogen lessens the analytical signal in dielectric barrier discharge (DBD) microplasma [31] and compromises the background of the emission spectrum [32]. Lastly, hydride generation also has a problem of causing memory effects caused by previously run sample [24] which occurs due to the presence of unreacted element and due to the partial solubility of arsine, the volatile metal hydride formed in HG, in water (solubility of arsine is 28 mg/100 mL of water at 20˚C) [33]. Cleaning the instrument components with HNO_3, or ultrapure water to clear the memory usually consumes time, making analysis of a high number of samples strenuous.

1.3.2.2 Cold Vapor Generation

Cold vapor generation is a sample introduction technique, very similar to hydride generation. It uses stannous chloride ($SnCl_2$) as a reducing agent, instead of $NaBH_4$. Stannous chloride dihydrate

is soluble in water and reduces Hg^{2+} to Hg^0 which is volatilized. The chemical equation describing this process is [34]:

$$HgCl_2 + SnCl_2.H_2O \rightarrow Hg^0(g) + 2Cl^- + SnO_2(s) + 4Cl^- + 2H_2O$$

In this equation, mercury chloride is mentioned as a source of mercury in water [34].

$SnCl_2$ is a milder reducing agent as compared to $NaBH_4$ but is very selective for mercury. Hence, it can only be used for the detection of mercury, as it prevents spectral interferences from other hydride forming elements [30]. This sample introduction technique uses the same equipment as that used for hydride generation. One big advantage offered by cold vapor generation is the lack of production of hydrogen. Hydrogen, as mentioned earlier, diminishes the intensity of the analytical signal [32]. Since cold vapor generation does not produce hydrogen, it can be easily coupled to DBD microplasma [32].

Cold vapor generation usually uses the same equipment as that used for hydride generation and has very good detection limit for mercury. Yuan et al. used a gold filament preconcentrating trap to adsorb mercury which was then released from the trap for detection, by heating the trap. Carrier gas, argon, carries the mercury released from cold vapor generation towards the gold trap, and afterwards carries the thermally desorbed mercury from the gold trap towards the microplasma for detection [35]. The mercury sample is acidified with 0.5% (v/v) HCl and reacted with 10% (m/v) $SnCl_2$ solution which is prepared in 10% (v/v) HCl [35]. This preconcentration step allowed the use of higher amount of sample solution (100 mL) [35], as the water vapors released from the reaction solution passed through the discharge chamber before the collection of the emission signal. Water vapors usually disturb or extinguish the microplasma, therefore, the emission signal cannot be collected when the microplasma is turned off. In another source, the solution made in

5% (v/v) HCl solution is reacted with 5% (m/v) $SnCl_2$ solution made in 5% (v/v) HCl solution [24]. In this study, only 300 µL of sample volume was used to get the desired signal and there was no preconcentration step involved [24]. For cold vapor generation, the concentration of the reagents should be optimized to get a signal with high intensity and a small-time domain. Cold vapor generation has very low detection limit and has very low requirement for the amounts of sample and reagent needed for analysis. The detection limit for cold vapor generation has been reported to be in the range of parts per trillion [24,35]. However, just like hydride generation, the memory from previously run samples can become an issue [24].

1.3.2.3 Photo Chemical Vapor Generation

Photochemical vapor generation uses free radicals generated by photoredox reactions in the presence of low molecular weight organic compounds as reductants which volatilize the analyte elements [30]. In addition to expanding the range of elements that can be analyzed, photochemical vapor generation also provides the benefit of simpler reactions, less interference, and elimination of the reducing agent [31].

The instrumentation for photochemical vapor generation consists of a photoreactor with a low-pressure Hg lamp, along with a peristaltic pump and a gas-liquid separator. The volatile analytes are carried by a carrier gas, argon, to the microplasma for detection [31]. The instrumental set-up for dielectric barrier discharge microplasma coupled to photochemical vapor generation as a sample introduction technique is given in Figure 1.4. In this set-up, the peristaltic pump is used to transfer the sample solution and formic acid solution into a flow-through photochemical reactor. The products from this reactor are introduced into the gas-liquid separator from where they are carried to the microplasma with the help of a carrier gas. The analyte elements are detected with the help of optical emission spectroscopy [31]. PVG has been used as a sample introduction

technique for the analysis of samples for As, Co, Hg, Ni, Fe, Se, Bi, Sb, Cd, As, Os, I, Br, and Te in ICP [30,36,37]. For microplasma, it has only been used for detection of Fe, Co, Ni, Se, and Hg [31,38,39].

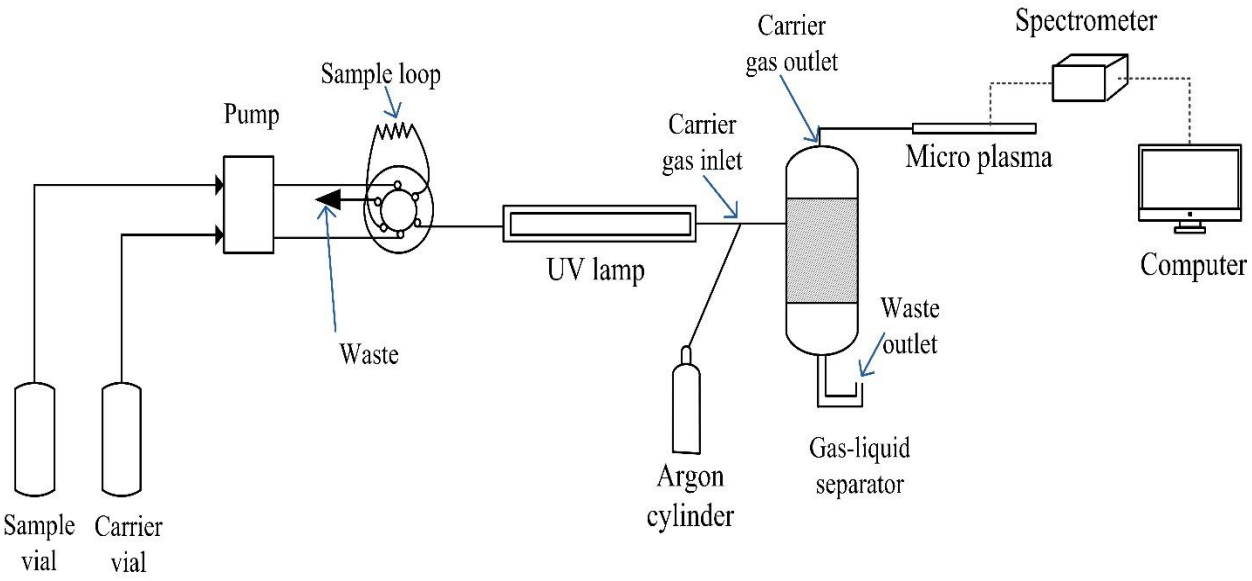

Figure 1.4: Instrumental setup used for photochemical vapor generation.

1.4 Description of Project

Developing hydride generation as a sample introduction technique for microplasma was the aim of this research project. Since arsenic contamination is an issue in many parts of the world and poses a hazard to millions of people, the target element for analysis for this research was also arsenic in water samples.

For coupling hydride generation (chemical vapor generation) as a sample introduction technique with microplasma, two kinds of equipment designs were tested, a batch and a discrete flow system. Afterwards, the spectral response of microplasma towards water vapors and hydrogen released from the hydride generation reaction was assessed, while the microplasma was being operated in

three different carrier gases (helium, argon, and mixture of argon – 1000 ppm hydrogen). In the end, the method for running the arsenic reaction trial was determined, and detection limit for arsenic in helium and argon microplasma was estimated.

Chapter 2

Instrumentation

2.1 Outline

- Explanation of the setup used to generate microplasma and the spectrometer used for recording emission spectra.
- Two kinds of equipment were tested for hydride generation – the batch system and the discrete flow system.
- Description of different components of the equipment for the discrete flow system and the reason for using glass as the fabrication material.

2.2 Construction of the Microplasma Device

In this work, a microplasma was powered by HVAC power supply (model PVM-12, Information Unlimited, Amherst, NH 03031-0716 USA). This power supply converted DC input into high voltage AC power output. This HVAC power supply was supplied with DC current by another DC power supply which had an adjustable output. Hence, changing the DC output changed the output by the HVAC power supply as well [40]. By turning on the HVAC power supply, microplasma was generated between two stainless steel electrodes, each of which was glued to an end of a quartz glass tube with an inner diameter 1 mm, wall thickness 0.66 mm and length about 11.5 cm. The distance between the tips of the two electrodes inside the glass tube was 4.7 cm. The HVAC power supply had an adjustable frequency output. Changing the frequency would impact the stability of the microplasma, making it more ‘diffuse’ or ‘string like’.

The detector used for all the experimentation was a portable fiber-optic spectrometer with an integrating 2048-pixel, linear Photo Diode Array (PDA) detector. It covers the wavelength range

from 190 nm to 850 nm. The fiber optic cable had a diameter of 600 µm, and a length of 2 m [41] (labelled as F600-UV-VIS-SR).

2.2.1 Data Collection by the Spectrometer

The spectrometer can collect spectral data in two forms: static shot and episodic data. The static shot is a single emission spectrum collected at a set integration time, with wavelength (in nm) on the x-axis and intensity (in A.U) on the y-axis. Integration time is the amount of time the detector keeps electrons trapped in the pixel wells before reading them. The integration time should be chosen to maximize the counts without saturating the detector [42]. It is measured in unit of time, millisecond. Episodic data is the spectral data collected by spectrometer over time. It displays a series of emission spectra collected over time in 3D form. Each emission spectrum in the episodic data, collected at a specific time, is called an episode [43]. In this research project, episodic data was collected for reaction trials, that is for reaction of $NaBH_4$ solution with 9% (v/v) HCl solution or arsenic solution.

2.3 Equipment for Hydride Generation

The equipment for hydride generation was separately made and tested for results. The purpose of this equipment is to mix the reagent solution and sample solution to generate volatile hydrides which are then carried by the carrier gas towards the microplasma. Two kinds of equipment were tested for chemical vapor generation: Batch system and discrete flow system. Afterwards, the discrete flow system was chosen for further experimentation because of its reproducible and more efficient mixing. The description of both types of equipment can be found in sections 2.3.1 and 2.3.2.

2.3.1 Batch System

The batch system consists of a vessel in which a known amount of reagent and sample are introduced. The mixing of the reagent and the sample occurs by diffusion and convection. Convection occurs by mixing the reagent and sample by agitation (random turbulence) [44].

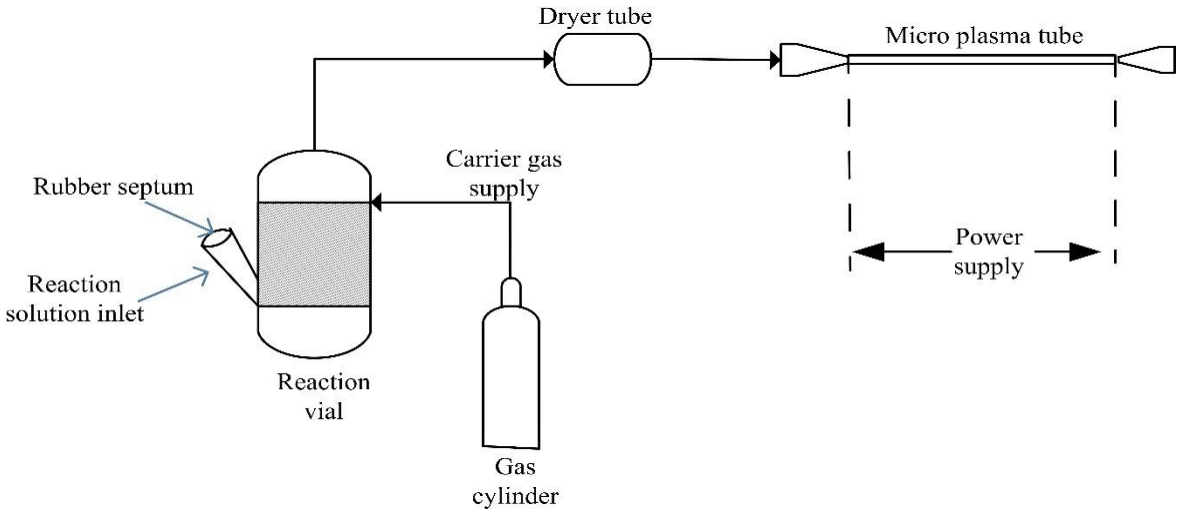

Figure 2.1: Diagram showing the equipment for batch system coupled to microplasma.

In Figure 2.1, the vessel has an inlet and an outlet for the carrier gas. It also has an inlet for the reagent and the sample solution. A syringe was used to introduce a known amount of sample solution (100 µL) and reagent solution (also 100 µL) into the vessel, through the reaction solution inlet which had the opening covered by a rubber septum. The sample solution was injected first. The reagent solution was injected only after the collection of episodic data started. Without the stir bar, the mixing of the reagent and the sample solution was too slow. Afterwards, a stir bar was added to the vessel to aid in mixing the sample solution and the reagent solution. Batch system proved that a very small amount of reaction solution, that is 200 µl, was needed to generate the analytical signal.

Although the batch system got rid of the peristaltic pump, it introduced other problems. Without the stir bar, the reaction between the reagent solution and the sample solution was too slow and yielded only a small amount of arsine at a time, leading to a very low intensity signal. After adding the stir bar, the agitation became too turbulent, leading to non-reproducibility in the signal generated. Moreover, injecting the reagent and sample solution into the vessel from outside also introduced atmospheric gases into the system. The rubber septum too was permeable to air. Microplasma is very sensitive to atmospheric gases as they take up its energy. Therefore, the discrete flow system was chosen for hydride generation.

2.3.2 Discrete Flow System

The equipment for the discrete flow system for chemical vapor generation consists of two peristaltic pumps, a high-vacuum three-way valve, a reaction coil, a high vacuum 2-way valve, a gas-liquid separator (GLS), and a cold trap. This setup is portrayed in Figure 2.2.

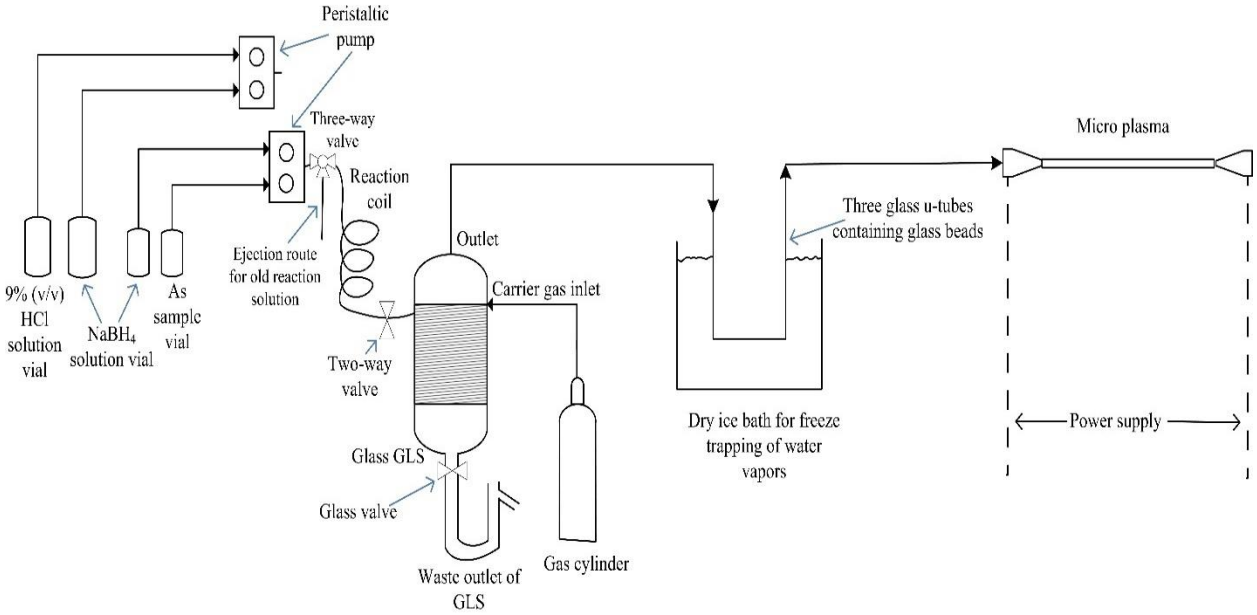

Figure 2.2: Diagram of discrete flow system equipment used for hydride generation.

One of the peristaltic pumps transports the sample reaction mixture, and the other pumps the blank reaction mixture to clean up all the memory. Running the blank reaction solution after each arsenic reaction trial is important because of the unreacted analyte and dissolved hydride present in the solution droplets from the prior trial [45]. The peristaltic pump for sample reaction draws the sample solution and $NaBH_4$ solution from their respective vials and mixes both solutions in a tee piece. Similarly, the pump for the blank reaction solution also mixes the 9% (v/v) HCl solution and $NaBH_4$ solution in a tee piece. At a particular time, only one pump is connected to the three-way valve of the equipment, therefore only one of the two reaction solutions passes through the three-way valve. Both these reaction solutions pass through the same inlet of the three-way valve. From the three-way valve, the reaction solution enters the reaction coil. The purpose of the reaction coil is to increase the mixing of the two solutions by inducing a secondary flow. This secondary flow occurs due to centrifugal forces in the coil [44]. The exact mechanism and optimized conditions for the secondary flow are not clear [44]. From the reaction coil, the reaction solution falls into the GLS, through a two-way valve. In the GLS, a carrier gas is introduced which mixes with the arsine, hydrogen and water vapors released from the reaction solution, and carries them into the microplasma, through a cold trap. The cold trap is used to remove water vapors from the carrier gas by condensing and freezing them. The equipment for the chemical vapor generation/hydride generation is designed to introduce a minimum amount of water vapors in the microplasma.

2.3.2.1 Purpose of valves

As mentioned in the paragraph above, two kinds of valves are used in the apparatus, one being a three-way valve and the other being a two-way valve. The reaction solution enters the reaction coil through a three-way valve, and it enters the GLS through a 2-way valve. Both valves are designed

by the supplier to tolerate high gas pressure without leakage. A vacuum seal was also applied to both valves to further prevent any leakage of gas.

2.3.2.2 Two-way Valve

The 2-way valve is meant to control the amount of reaction solution entering the GLS. The 2-way valve ensures reproducibility in the amount of reaction solution being introduced in the GLS for each trial, since the amount of arsine carried to the microplasma (and hence the intensity of arsenic signal) depends on the amount of reaction solution in the GLS. In the reaction coil, arsine and hydrogen are present in the form of bubbles which push the liquid reaction solution forward into the GLS. Therefore, as the peristaltic pump stops pumping more sample and reagent solutions, movement of the reaction solution in the reaction coil does not stop. Microplasma is very sensitive to hydrogen. Therefore, it dims after the reaction solution enters the GLS but afterwards, regains its initial power. Dimming of the microplasma over a time-period decreases its power and hence reduces its sensitivity over this period. More liquid moving into the GLS from the reaction coil means that most of the GLS is filled with the reaction solution, leading to microplasma remaining dim for longer duration of time. Moreover, arsenic signal also keeps on appearing for a longer duration of time, as arsine is being released from the reaction solution entering the GLS. This rate of entrance of reaction solution into the GLS, after the pump is turned off is not reproducible, making the arsine signal non-reproducible. To avoid this problem, the two-way valve is immediately closed after the peristaltic pump turns off, allowing less than 1 mL solution to enter the GLS for each trial. Hence, the two-way valve tolerates pressure from both sides after it is turned off. On one side, it tolerates pressure of the carrier gas (which is ~3 atm) introduced in the GLS, and on the other side, it tolerates pressure due to release of arsine and hydrogen from the reaction solution in reaction coil. By closing the 2-way valve immediately after turning off the pump, the

microplasma remains dim for only about 4-6 seconds, while the arsenic signal appears for about 1-2 minutes in the emission spectrum. In short, a two-way valve is required to lessen the dimming period of the microplasma and keep the time domain of the signal short.

2.3.2.3 Three-Way Valve

After the signal for trial has been collected, it is time to discard the reaction solution from the previous trial. This is done by the help of the valve in the GLS which is opened to eject the reaction mixture in the GLS. The reaction mixture from the reaction coil is ejected by the help of the three-way valve.

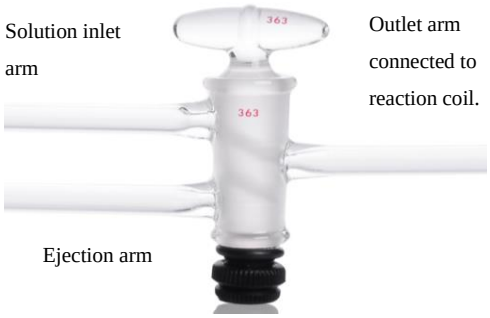

Figure 2.3: Photo of a three-way valve with oblique bores, and three arms.

The purpose of the three-way valve is to discard the old reaction solution from the reaction coil. The three way-valve has oblique bores, as displayed in Figure 2.3. Therefore, at a time only one of the two inlet arms of the valve are connected to the arm for outlet (arm which is connected to the reaction coil). One of the two arms (called the solution inlet arm) on the left side of the valve is connected to the tee piece from which the reaction solution enters the valve. While the other arm (called the ejection arm) is connected to an empty glass tube whose other end is dipped in water to prevent the backflow of atmospheric gases into the system by diffusion. During the reaction

trial, the solution inlet arm is connected to the outlet arm with the help of an oblique bore, allowing the reaction solution to pass into the reaction coil and then into the GLS. After the data collection has stopped, the outlet arm is connected to the ejection arm and the two-way valve is opened. The pressure of the carrier gas moving from GLS into the reaction coil derives the reaction solution in it, towards the ejection arm of the 3-way valve, hence discarding the old reaction solution from the coil. This ejection continues for about 6 minutes (time-period set arbitrarily). Afterwards, the plug in 3-way valve is rotated to connect the solution inlet arm to the outlet arm of the valve. And the system is then allowed to equilibrate for about 1 to 3 minutes (time-period set arbitrarily) before the next trial or the cleaning cycle. When the solution inlet arm is connected to the outlet arm of the valve, the valve tolerates pressure due to the release of arsine and hydrogen from the reaction solution in the reaction coil, after the two-way valve is closed. Hence, the purpose of a three-way valve is to ensure that only fresh reaction solution enters the GLS for each trial.

2.3.2.4 Gas Liquid Separator (GLS)

The purpose of a gas liquid separator is to separate the liquid reaction mixture from the gaseous products, that is the hydride of the analyte element and the hydrogen gas.

The gas liquid separator has four different glass channels connected to it (as represented in Figure 2.4), one is an inlet for the carrier gas, one is an inlet for the reaction solution, one is an outlet for the carrier gas mixed with the hydrides and hydrogen, and the last one at the bottom is a waste outlet, guarded by a valve. The carrier gas inlet is attached in a tangential manner to the body of the GLS (as shown in Figure 2.5). This tangential inlet allows the gas to move in a spiral fashion inside the chamber, exerting more pressure on the walls of the GLS [17]. In this way, as the reaction solution enters the GLS from another inlet on its wall, the carrier gas mixes thoroughly with the reaction solution. The solution inlet and gas inlet were made separately on the GLS,

instead of introducing both the solution and carrier gas together. This was done because mixing the carrier gas with reaction solution outside of the GLS, before its introduction in the GLS, resulted in the carrier gas carrying higher amounts of water vapors, making the desiccant too wet if a drying tube was used or clogging the cold trap too quickly if this was being used. The volatile hydrides mix with the carrier gas and are carried to the microplasma, through a cold trap, for detection. After collecting the data for the reaction trial, the valve at the bottom of the GLS is opened to expel the reaction solution. The waste tube present below the valve is U-shaped. After ejection of the reaction solution from the GLS, it is filled with liquid waste which prevents the influx of atmospheric gases into the GLS through diffusion, every time the waste valve is opened. The total inner volume of the GLS is about 4 mL. A high carrier gas flow rate and a decreased surface area of tubing and GLS are meant to minimize the loss of hydrides due to sorption or decomposition [46]. A low inner volume is also meant to lessen the void volume of the GLS and help in decreasing the time domain of the signal. Moreover, microplasma is very sensitive towards ppm levels of analyte, and hence requires a very small amount of sample for analysis, making a 4 mL GLS appropriate for use.

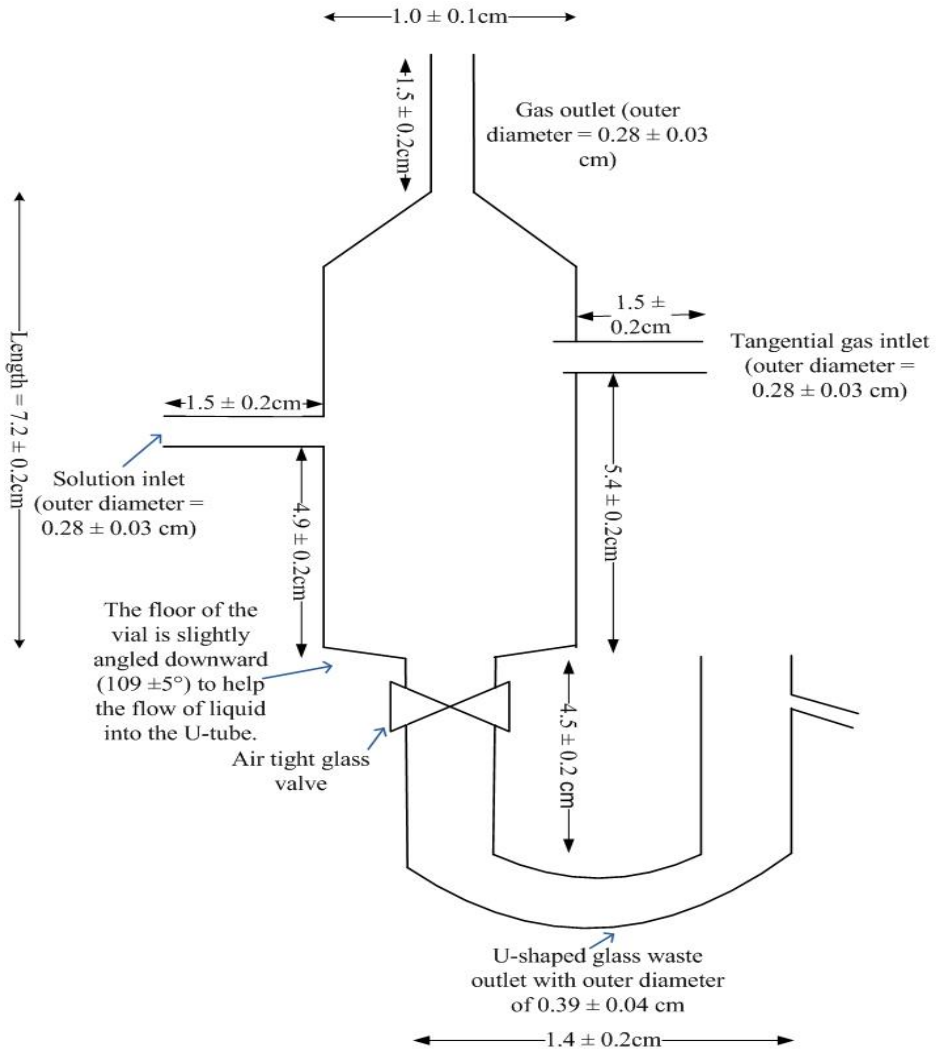

Figure 2.4: Diagram of gas-liquid separator used in the discrete flow system.

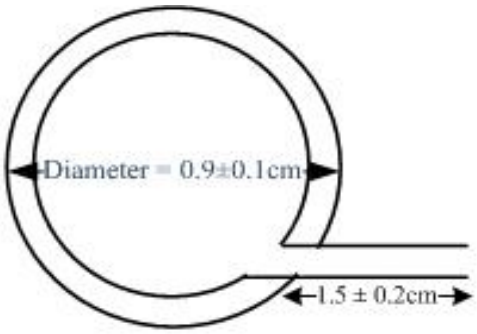

Figure 2.5: Cross section of GLS showing the tangential gas inlet only.

2.3.2.5 Water Vapors Trap

For removal of water vapors, two methods were tested, the drying tube containing a desiccant and a cold trap. Both the drying tube and cold trap were attached between the GLS and the microplasma for experiments, as water vapors came out of the GLS. Initially the Drierite desiccant was used to remove water vapors in the drying tube. However, over time, the desiccant gets used up and starts leaving more water vapors in the system, which is seen as an increasing OH peak (308 nm) intensity. Hence, its efficiency in removing water vapors depletes over time before it changes color, leading to non-reproducibility among different reaction trials. Therefore, the drying tube was replaced by the cold trap to remove water vapors because the efficiency of cold trap remains the same over time. However, after 10 – 20 runs of sample, the cooling tubes in the cold trap get clogged due to ice formation around the glass beads and must be replaced. Hence, the cold trap is more reliable as compared to the drying tube.

The cold trap consists of three u-shaped glass tubes containing glass beads, dipped in dry ice. The glass tubes which were 25 cm in length, inner diameter 0.34 cm and outer diameter 0.7 cm were bent into a U shape by heating on a Bunsen burner. These u-tubes were filled with 2 mm glass beads and connected to each other in sequence. Water vapors were removed from the carrier gas coming out of the GLS, due to contact with the cold glass beads in the tube.

A.

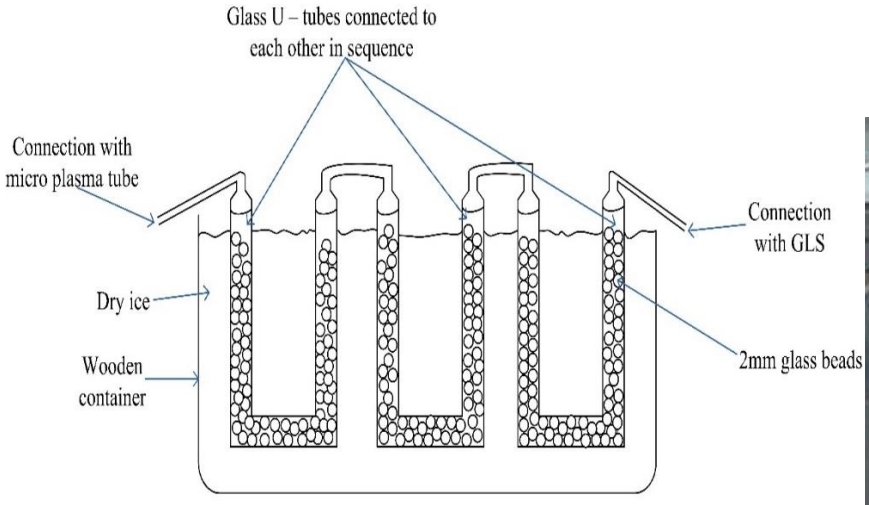

B.

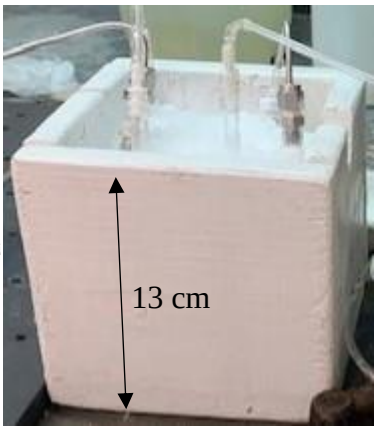

Figure 2.6: A. Diagram of cold trap. B. Photo of cold trap used in discrete flow system equipment.

2.4 Material Used to Make the Equipment

The equipment for hydride generation is made of glass because glass is impermeable to gas, unlike plastic, and is non-reactive to acids and bases, unlike metal. Apart from preventing the loss of hydrogen gas and volatile hydride, it also prevents the influx of atmospheric air into the system through diffusion, which is typically observed for plastic. Atmospheric gases not only consume energy from the microplasma, leaving lower power for the analyte, but also crowd the emission spectrum as the detector used in our device has a short focal length and low resolution. Moreover, arsine does not adsorb on glass, just like polyethylene, and polytetrafluoroethylene (PTFE, Teflon) [47].

2.5 Conclusion

A discrete flow system was chosen for hydride generation, with its equipment consisting of two peristaltic pumps, a three-way valve, a reaction coil, a two-way valve, a gas-liquid separator

(GLS), and a cold trap. All the equipment, except for the peristaltic pump and its tubes, was made of glass to prevent the influx of atmospheric air into the system.

Chapter 3

Experimentation with Different Carrier Gases

3.1 Outline

- Three kinds of experiments were conducted for microplasma operated in three different carrier gases, helium, argon, and mixture of argon – 1000 ppm hydrogen.
- The impact of water vapors on the emission spectra for different gases was studied and the reproducibility in the emission spectra and the power input of microplasma was evaluated.
- Impact of running carrier gas through the cold trap on the emission spectrum is discussed and the efficacy of the cold trap in removing water vapors is discussed.
- Response of microplasma operated in different carrier gases, towards hydrogen released from hydride generation reaction was also studied.

3.2 Reason for Following Experimentation

Since the hydride generation method releases hydrogen and water vapors, in addition to the release of volatile metal hydrides, it is important to observe the behavior of microplasma in the presence of hydrogen and water vapors in its carrier gas. And since cold traps are being used in the equipment to eliminate water vapors, it is also important to note if passing the carrier gas through a cooling tube impacts the emission spectra at all. Carrying out these experiments narrowed down the number of factors that may impact reproducibility of the experiment.

The microplasma can be operated in different carrier gases. Therefore, the impact of water vapors, cooling tubes, and hydrogen released from the hydride generation reaction on the microplasma operated in three different gases, namely UHP helium, BIP argon, argon-1000 ppm hydrogen was evaluated.

3.3 Labelled Emission Spectra for Microplasma Operated in Different Carrier Gases

Before showing the results for different experiments, it is important to label the peaks seen in emission spectra generated from the microplasma operated in carrier gases helium and argon. For collecting these spectra, the copper tube carrying the carrier gas was directly attached to the microplasma tube. Therefore, there was no influx of atmospheric gases into the system. Any species observed in the emission spectrum shows its presence in the gas cylinder. The Figures 3.1 and 3.2 show the fully labelled emission spectra of these gases:

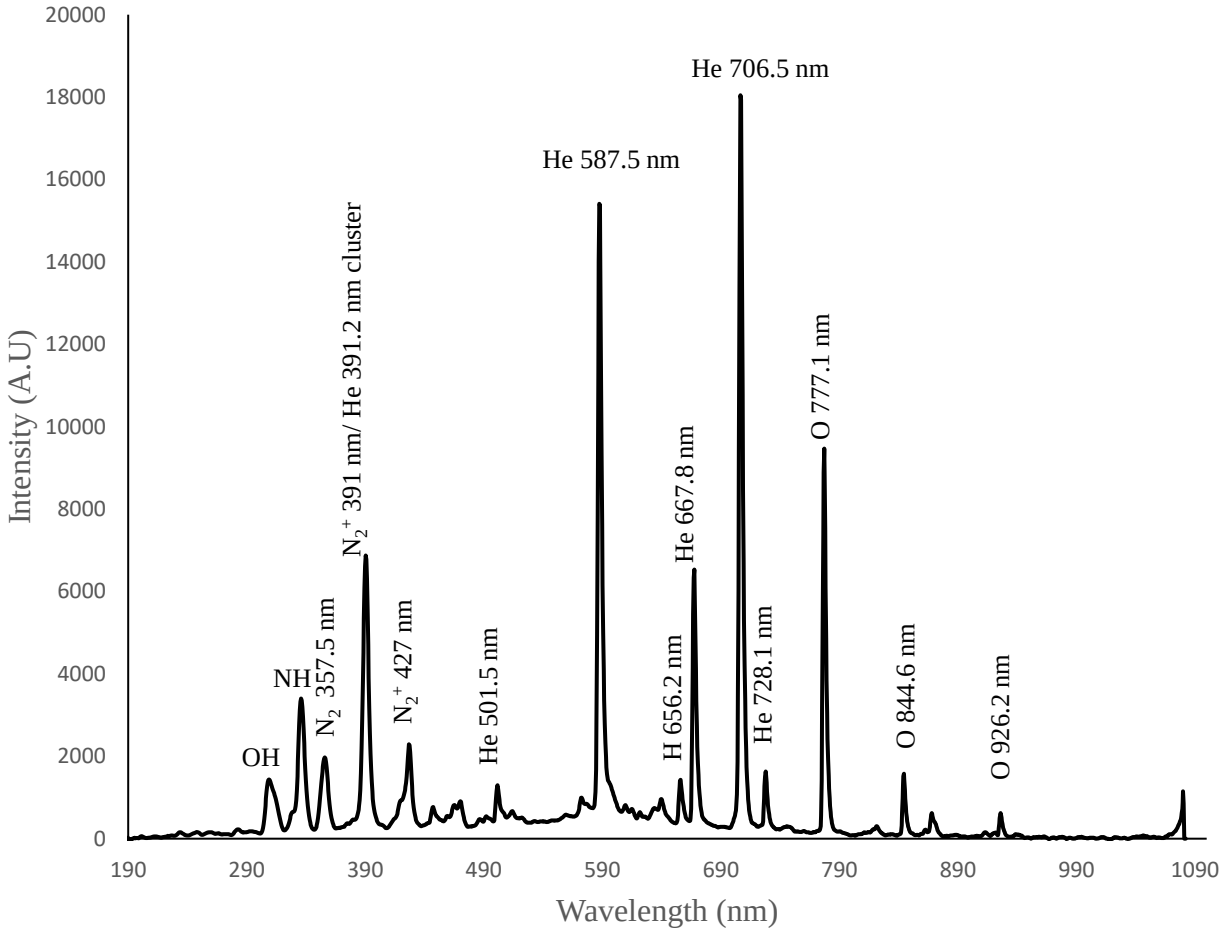

Figure 3.1: Emission spectrum for microplasma operated in ultra-high purity (UHP) helium.

In this emission spectrum, the line 357.5 nm is N_2 [48], and the lines 391 nm and 427 nm comprise the N_2^+ first negative system band [48,49,50]. The helium and oxygen peaks were labelled according to information available on National Institute of Standards and Technology (NIST) [51] and the journal article by Bashir et al., 2022 [50]. Similarly, the Oxygen lines seen at 777.7 nm, 844.6 nm and 926.2 nm are labelled according to NIST database [51].

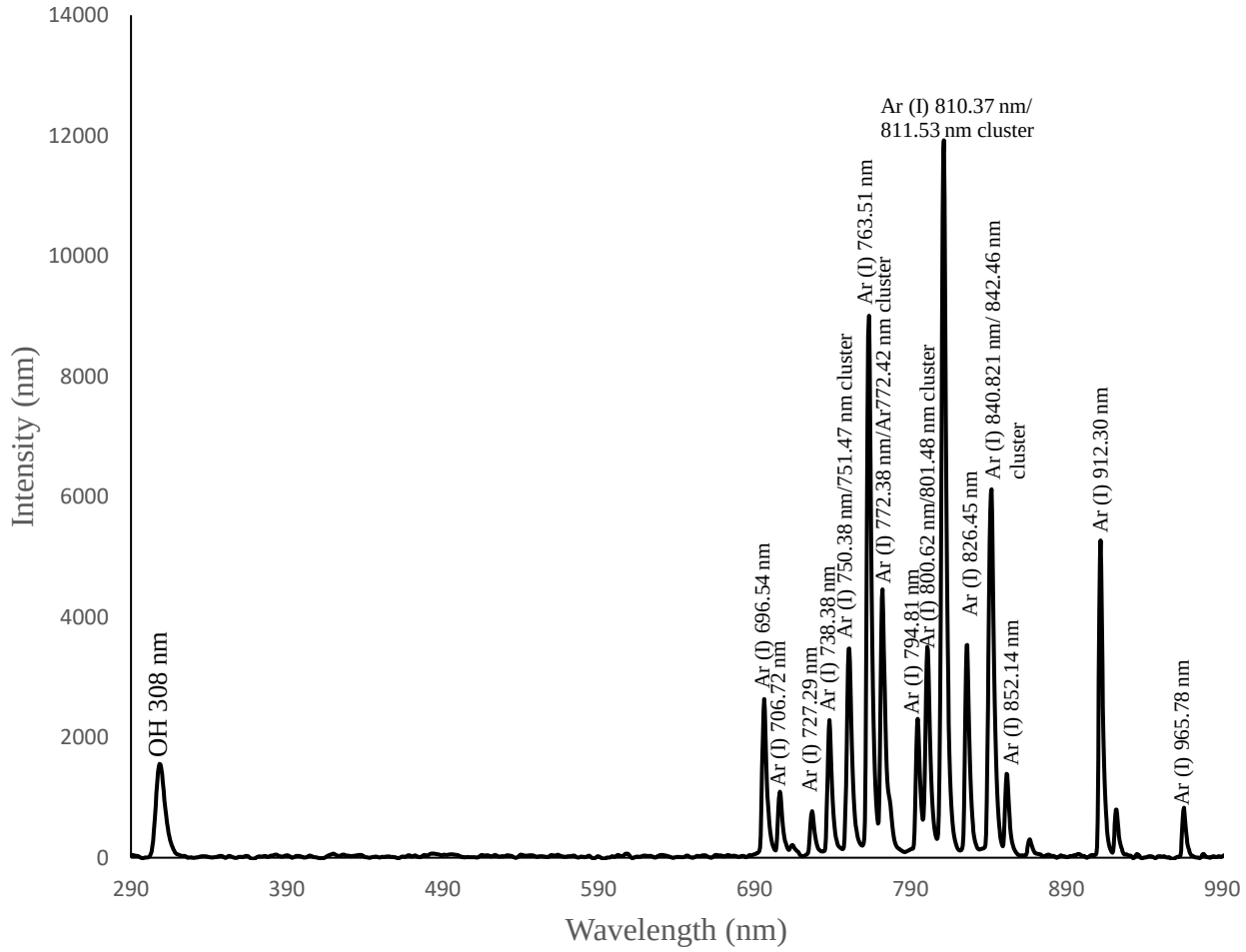

Figure 3.2: Emission spectrum for microplasma operated in BIP argon.

All the argon spectral lines are labelled in the spectrum according to information given by NIST database [52] and literature [6].

3.4 Impact of Water Vapors on Emission Spectrum

The purpose of this experiment was to observe the emission spectra generated for the microplasma operated in different carrier gases with water vapors and look for reproducibility and changes in the emission spectrum. For this purpose, one, two, three and four peristaltic pump tubes, made of PVC plastic, were connected between the microplasma tube and the copper tube carrying the carrier gas. The emission spectra were collected at IT 20ms and 100ms. PVC tubes were used under the assumption that diffusion of water vapors into the tubes would remain constant over time. And therefore, the amount of water vapors introduced in the microplasma would be the same for each trial. The setup with one PVC tube can be seen in Figure 3.3. The length of each peristaltic pump tube was 49.3 cm; its inner diameter was 2.79 mm and wall thickness was about 0.9 mm. The PVC tubes were connected by the help of glass tube connectors (glass tubes of outer diameter 4.4 mm, inner diameter 2.7 mm, and length around 3 – 4 cm), as represented in Figure 3.3. An increase in number of plastic peristaltic pump tubes between the microplasma tube and the copper tube carrying the carrier gas, resulted in a surge in the influx of water vapors and other atmospheric gases into the system because of permeability of the plastic. For each of the experimental conditions (different number of PVC tubes attached), the frequency of the power supply was adjusted to ensure stable power input for the microplasma and to get maximum intensity emission spectrum. Moreover, the increase in the amount of water vapors in the carrier gas changed its properties like its dielectric constant, thermal conductivity, etc., changing the properties of the microplasma generated and its power input requirements.

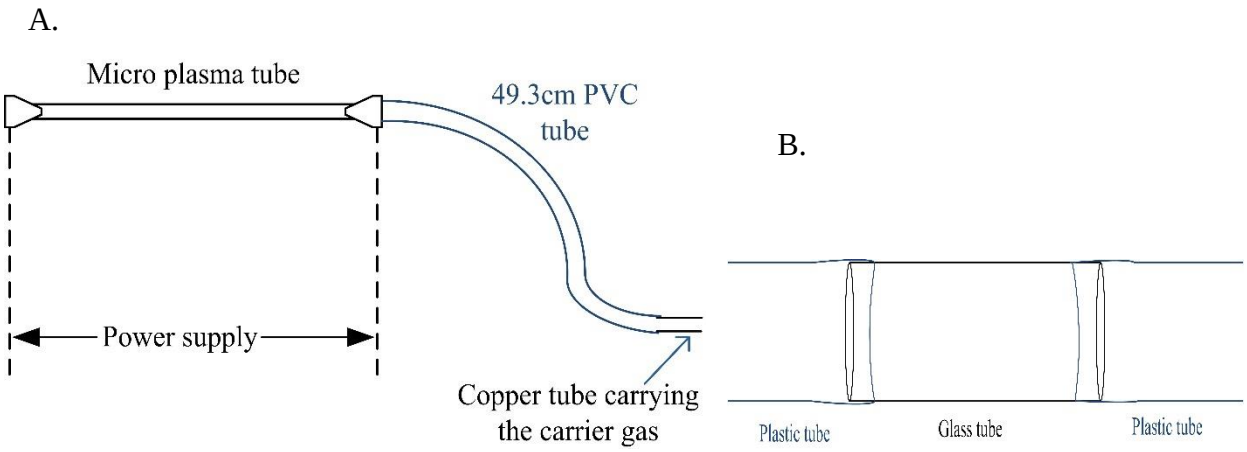

Figure 3.3: Diagram showing A. PVC tube attached between the microplasma tube and the copper tube carrying carrier gas. B. Plastic tubes connected to each other through a glass tube connector.

For all the experimental conditions, the emission spectra were collected after keeping the microplasma on for 1 minute. This is because the power input for microplasma became constant within one minute, and the emission spectrum produced also became constant. The experiments are named one PVC tube, two PVC tubes, three PVC tubes, and four PVC tubes, depending on the number of PVC pump tubes attached. For the Control experiment, the copper tube carrying the carrier gas was directly connected to the microplasma tube. The results obtained for all different experimental conditions were quite reproducible. This shows that even though water vapors diminished the power of the microplasma, the microplasma still produced precise results. This can be seen in the tables and figures in sections 3.4.1, 3.4.2, and 3.4.3:

3.4.1 Helium as a Carrier Gas

For a specific experimental setup, the power input remained quite stable, and the emission spectra generated by the microplasma were very reproducible. The power input and frequency of

microplasma in different experimental conditions are mentioned in Table 3.1. The average emission spectra for different experimental conditions were plotted for comparison in Figure 3.4.

Experiment	Average Voltage (Volts)	Average Current (Ampere)	Average Power (V*I) (Watt)	Relative Standard Deviation in Power	Average Frequency (Hz)	Relative Standard Deviation in Frequency
Control	10.72	1.30	13.99	0.69%	84964	0.045%
One PVC Tube	10.72	1.19	12.73	0.68%	86856	0.038%
Two PVC Tubes	8.41	1.38	11.60	2.20%	84808	0.045%
Three PVC Tubes	9.25	1.404	12.99	0.54%	85191	0.046%
Four PVC Tubes	9.28	1.404	13.04	0.32%	85219	0.038%

Table 3.1: Power input for helium microplasma in different experimental conditions.

The average frequency used for different experiments was 85380 Hz, and the relative standard deviation in the frequency was 0.87%. However, it was the power input that changed with an enhanced influx of water vapors in the microplasma, due to increase in number of PVC tubes attached between the micro plasma tube and the copper tube. The standard deviation in the power input was 6%.

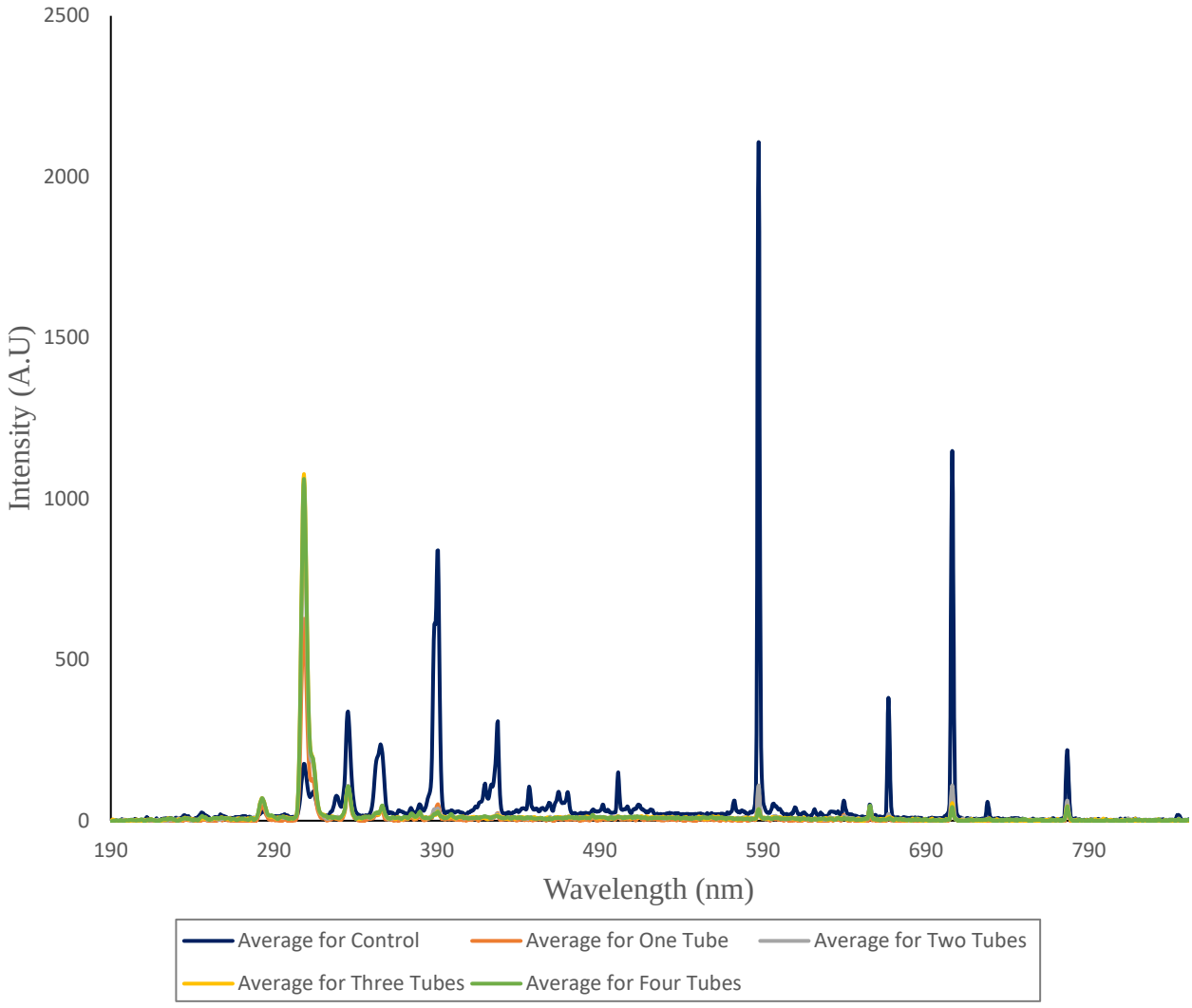

Figure 3.4: Average emission spectra of helium microplasma for different experimental conditions at integration time 20 ms.

In the emission spectrum, water vapors drastically impacted the intensity of the helium peaks. This shows that water vapors were taking up most of the power of the microplasma. The impact of the number of PVC tubes on the intensity of helium peaks was similar. Moreover, the OH peak was very close in intensity for the two-tubes, three-tubes and four tubes experiment, indicating that the influx of water vapors in the system was not linear with the increase in number of PVC tubes attached.

In the emission spectra, OH peak is higher in intensity as compared to the oxygen or nitrogen peaks, although, the air in the atmosphere has much higher percentage of nitrogen and oxygen as compared to water vapors. This is because the peristaltic pump tubes are made of PVC plastic which has far more permeability for water vapors as compared to oxygen. Permeability of PVC for oxygen is reported to be 0.7901×0^{7} mL mm^{-2} day^{-1} Pa^{-1} and that for water is reported to be 18.279×10^{14} g mm^{-2} s^{-1} Pa^{-1}, in the literature [53]. The seller does not give any information for permeability of the PVC peristaltic pump tubes. PVC also has slightly greater permeability for oxygen and CO_2, as compared to nitrogen [54]. High NH peak in the spectrum is due to greater concentration of nitrogen in the atmosphere as compared to the other two gases. Hence, the OH and NH peaks are higher than other atmospheric gases peaks due to higher permeability of PVC towards water vapors and because of high concentration of nitrogen in atmosphere.

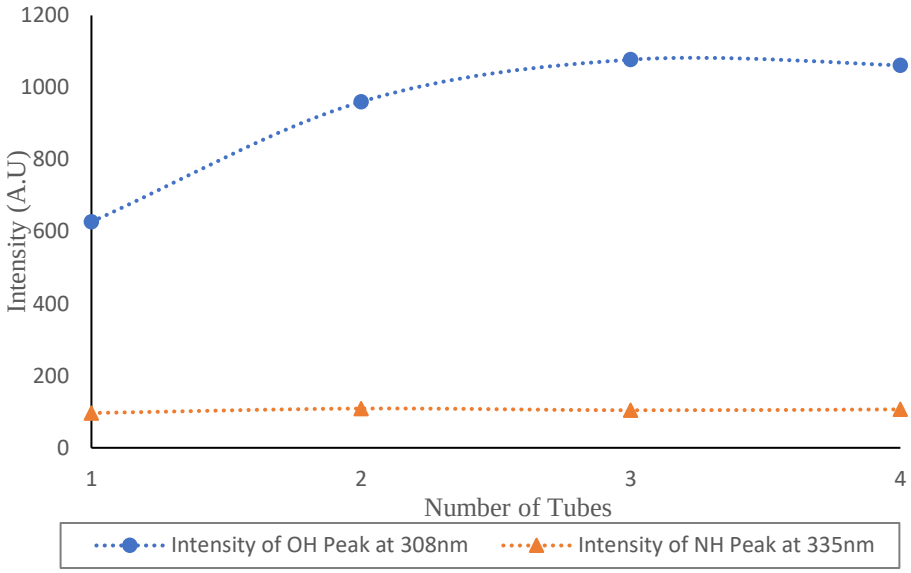

Figure 3.5: Change in intensity of the OH and NH peaks with an increase in the number of PVC tubes in setup for helium microplasma.

In Figures 3.5, the curve for the OH peak is non-linear, even though the frequency for all experimental conditions was similar. This is due to non-linear diffusion of water vapors and other gases. NH peak remains almost constant for different experiments. Diffusion through the plastic material occurs by pore effect, and solubility diffusion effect [53]. In the first case, the gases diffuse because of pores or ruptures in the material. And in the second case, the concentration gradient between two sides of the packaging material, and the solubility of gases in the corresponding material determine the transmission of gases across the material [53]. Diffusion across plastic due to its permeability depends on the structure of the plastic, its thickness, its permeability towards different gases, and the difference in pressure and concentration gradient [55]. The amount of water vapors in the environment may not be high enough to cause a considerable surge in water vapors in the system when more PVC tubes are attached, hence making the calibration curve non-linear. More water diffuses in from the first two tubes, leaving a

negligible concentration gradient for water in the next tubes. Hence, the diffusion of water vapors in the system does not rise linearly with the increase in number of plastic tubes.

3.4.2 BIP Argon as Carrier Gas

PVC tube experiment was also conducted for microplasma operated in BIP argon. Just like the helium microplasma, the results obtained for this carrier gas were quite reproducible, although, the impact of water vapors on the argon microplasma was quite less as compared to that on helium microplasma.

Experiment	Average Voltage (Volts)	Average Current (Ampere)	Average Power (V*I) (Watt)	Relative Standard Deviation in Power	Average Frequency (Hz)	Relative Standard Deviation in Frequency
Control	11.33	0.510	5.78	0.80%	87291	0.04%
One PVC Tube	11.33	0.572	6.48	0.97%	83955	0.2%
Two PVC Tubes	11.33	0.611	6.92	0.93%	84179	0.03%
Three PVC Tubes	11.33	0.613	6.95	0.81%	84167	0.07%
Four PVC Tubes	11.33	0.628	7.12	0.72%	84177	0.03%

Table 3.2: Power input for argon microplasma in different experimental conditions.

Table 3.2 shows that with the influx of water vapors in the system, the power input needed to generate stable microplasma remained similar. The relative standard deviation among power input for different experimental conditions was 8.13% and relative standard deviation in

frequency for different experimental conditions was 1.68%. The results were reproducible, although water vapors influenced the microplasma negatively.

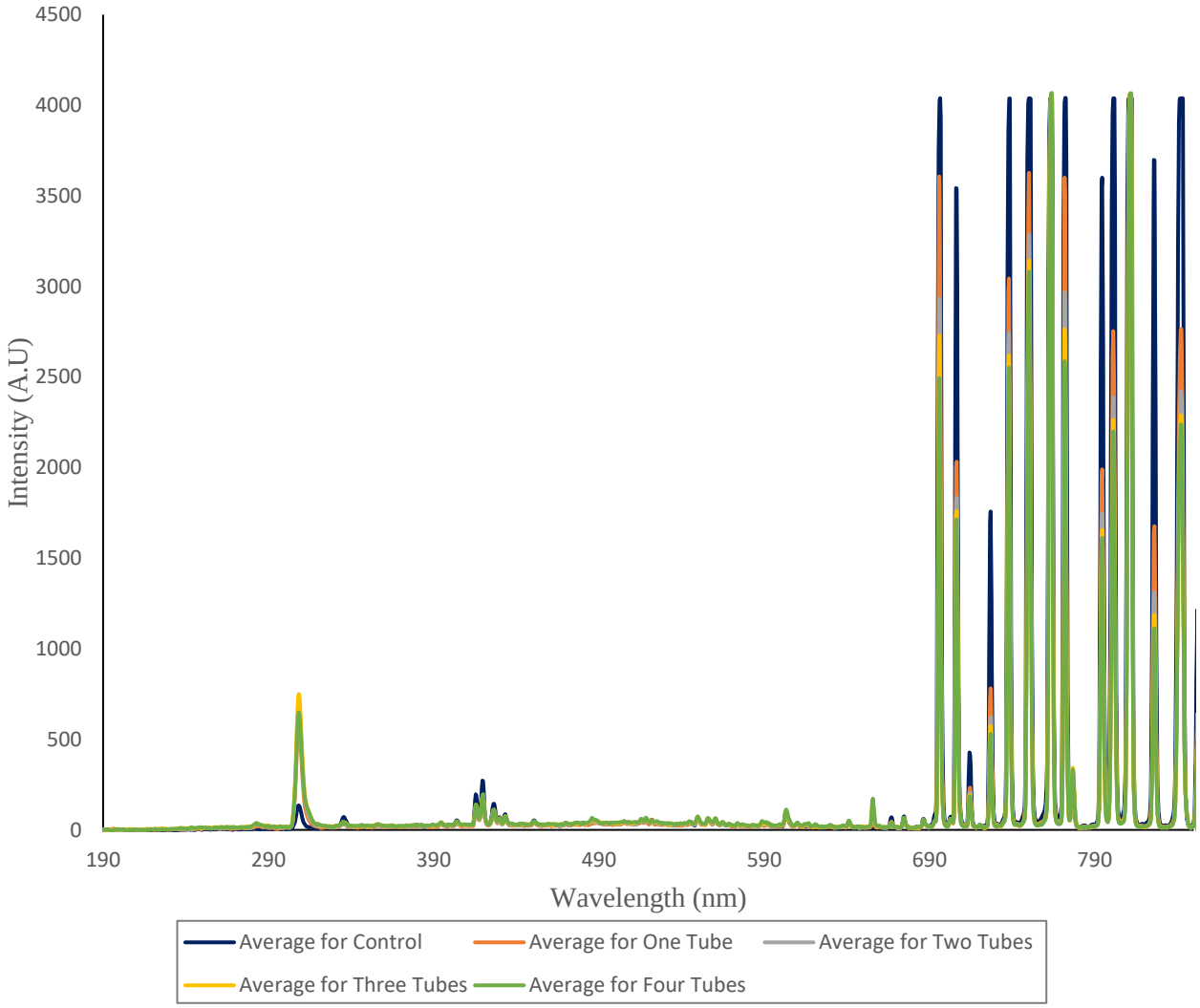

Figure 3.6: Emission spectra collected for argon microplasma after passing the carrier gas through a different number of PVC tubes, IT =20 ms.

Similarly, the curve showing change in intensity of OH with a change in number of PVC tubes attached was also like that obtained for helium.

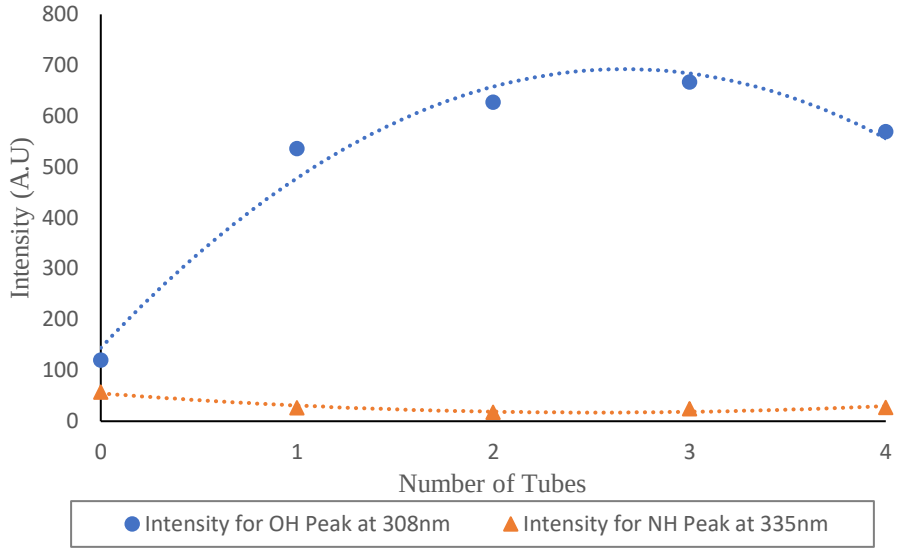

Figure 3.7: Change in intensity of the OH and NH peaks with an increase in the number of PVC tubes in the setup for an argon microplasma.

3.4.3 Argon – 1000 ppm Hydrogen as Carrier Gas

The microplasma operated in argon – 1000 ppm hydrogen behaved differently as compared to that operated in pure helium and pure argon. It was observed that the water vapors did not impact the microplasma power. The emission intensities of argon peaks remained the same with the influx of water vapors in the microplasma. Moreover, the water vapors did not impact the reproducibility of microplasma as well.

Experiment	Average Voltage (Volts)	Average Current (Ampere)	Average Power (V*I) (Watt)	Relative Standard Deviation in Power	Average Frequency (Hz)	Relative Standard Deviation in Frequency
Control	11.24	0.596	6.70	0.36%	84617	0.03%
One PVC Tube	11.24	0.609	6.85	0.31%	87239	0.17%
Two PVC Tubes	11.24	0.636	7.14	0.19%	83036	0.01%
Three PVC Tubes	11.24	0.633	7.12	0.64%	86883	0.019%
Four PVC Tubes	11.24	0.672	7.55	0.38%	82346	0.05%

Table 3.3: Power input for the argon – 1000 ppm hydrogen microplasma in different experimental conditions.

The information in Table 3.3 reveals that the power input and frequency remained about the same for different experimental conditions. The relative standard deviation in power among different experimental conditions is 3.9% and relative standard deviation in frequency among different experimental conditions is 2.5%.

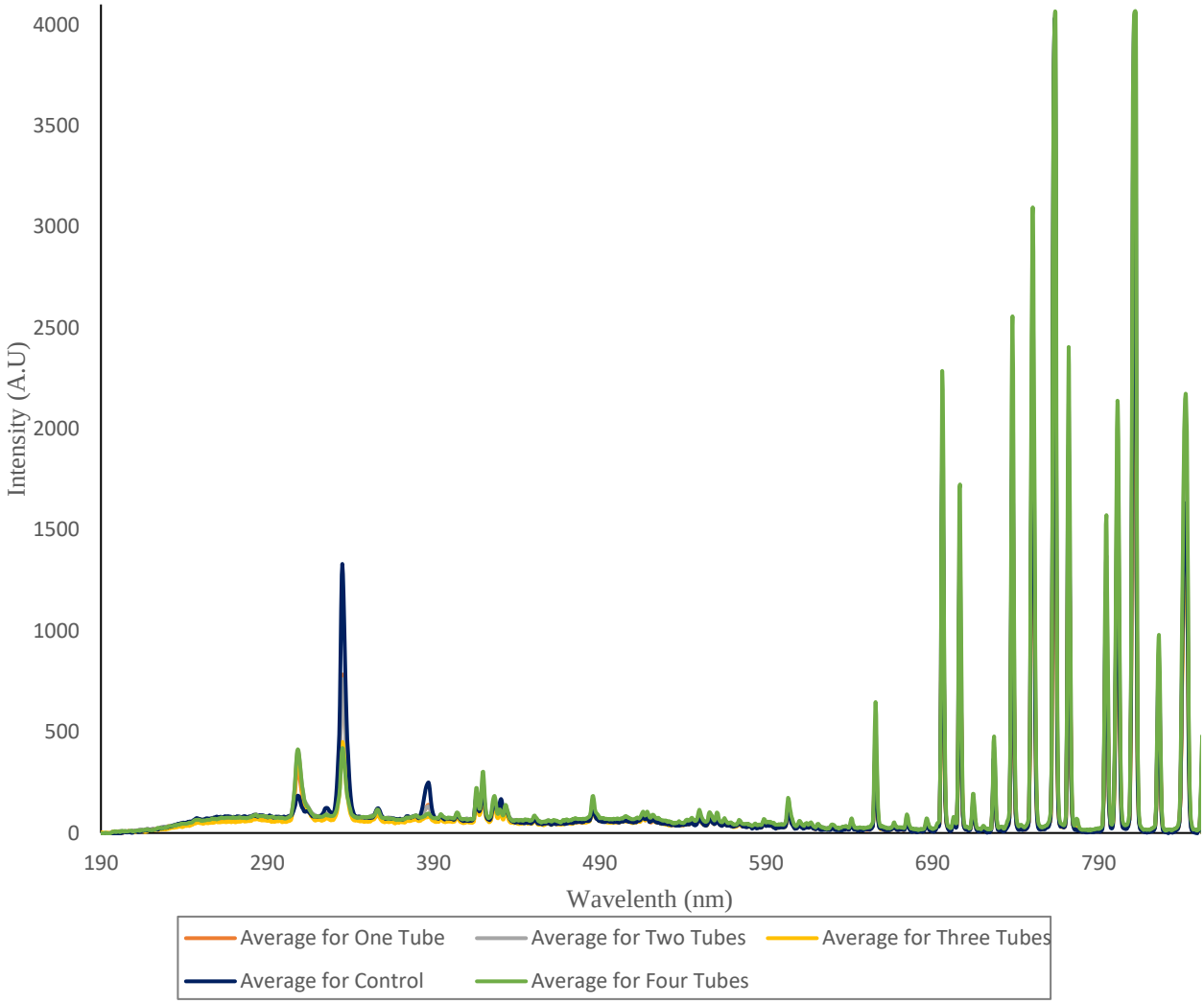

Figure 3.8: Average emission spectra of the argon – 1000 ppm hydrogen microplasma for different number of PVC tubes in the setup, collected at IT = 20 ms.

It was seen that with the rise in number of peristaltic pump tubes between the carrier gas carrying copper tube and the microplasma tube, the OH peak intensified but the NH peak decreased in intensity. This reduction in intensity may be due to a lower excitation of NH molecules due to the influx of water vapors. The change in intensity of the OH and NH peaks with increase in the number of PVC tubes attached is graphed in Figure 3.9:

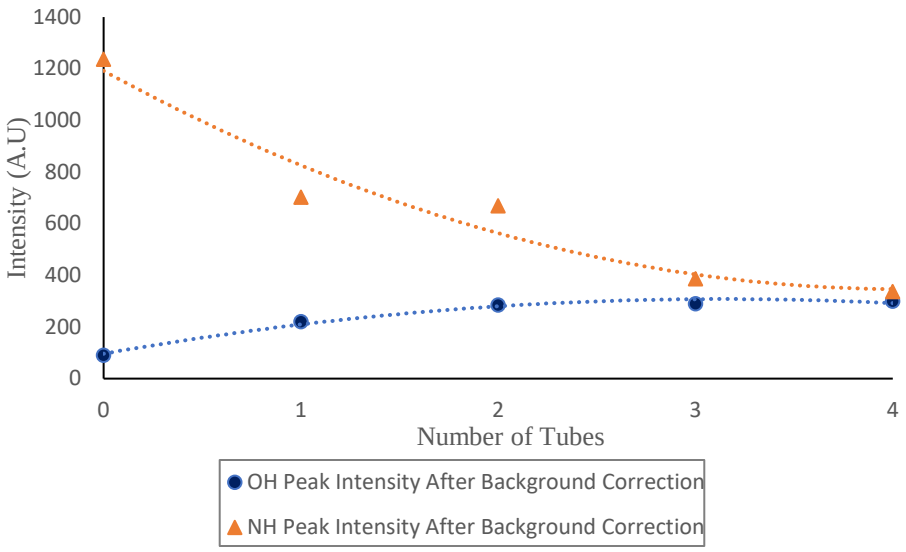

Figure 3.9: Change in intensity of the OH and NH peaks with an increase in the number of PVC tubes in the setup for argon – 1000 ppm hydrogen microplasma.

The microplasma operated in argon – 1000 ppm hydrogen was the least impacted by the water vapors. In fact, the impact of water vapors on the emission intensities of argon peaks was negligible. This suggests that if argon – 1000 ppm hydrogen is used as a carrier gas, the equipment attached to the microplasma for hydride generation (discrete flow system) can be constructed from plastic. However, since the microplasma operated in helium and argon was negatively impacted by the influx of water vapors, the equipment was made of glass to prevent any influx of water vapors into the system from the environment.

3.5 Impact of Passing the Carrier Gas through Cold Metal Coils:

3.5.1 Any Changes in the Emission Spectrum of the Microplasma

Microplasmas are low temperature and low power plasmas [56]. Therefore, it is important to note if passing the carrier gas through a cold trap impacts the emission spectrum at all. To see if cooling the carrier gas impacted the microplasma, the carrier gas was passed through two metal tube coils

dipped in dry ice. The metal tubes used to make the coils had an outer diameter of 3.14 mm, inner diameter 1.67 mm and lengths 41 cm and 32.5 cm, respectively. These metal tubes were coiled manually and were connected to each other by a connecting plastic tube of length 2 – 3 cm. Both these metal coils were dipped in dry ice. The copper tube carrying the carrier gas was connected to one of the coils. Whereas the other end of the second coil was connected to the microplasma tube. The emission spectra were collected at integration times of 20 ms and 100 ms. The Control emission spectra were collected by attaching the copper tube carrying the carrier gas directly to the microplasma tube.

Microplasma operated in none of the three gases tested was negatively impacted by the cold metal coils. For argon and helium, only the OH (308 nm) and NH (335 nm) peaks diminished slightly in intensity after these carrier gases were passed through the cold metal coil. All other peaks remained almost the same. No visible impact of the cold coils was seen on the emission spectrum generated for argon – 1000 ppm hydrogen. This can be seen in the emission spectra in Figures 3.10, 3.11, 3.12. All these emission spectra were collected at integration time of 20 ms.

3.5.1.1 Helium Microplasma

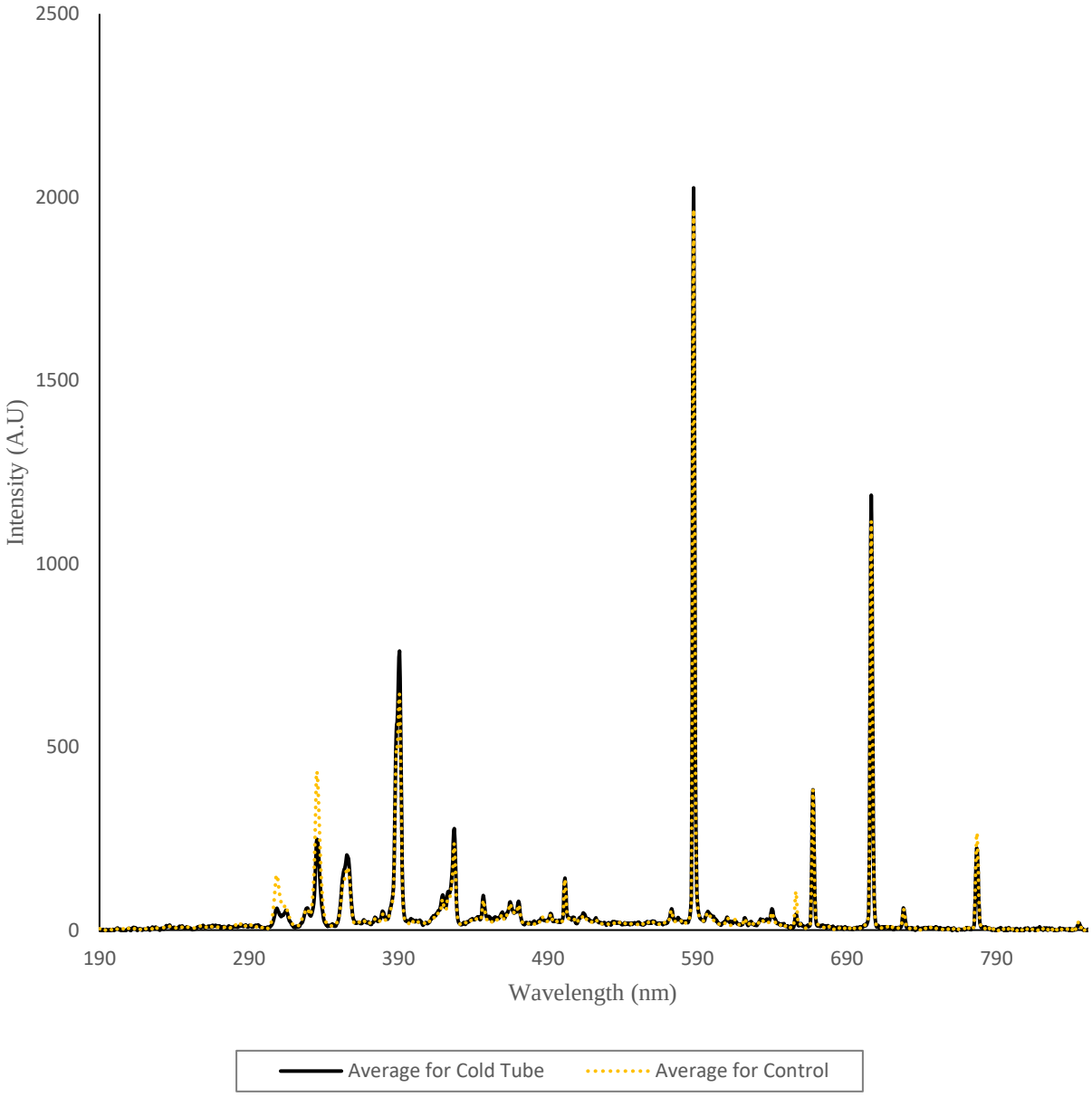

Figure 3.10: Overlapping emission spectra for the control and cold tube experiment for the helium microplasma.

3.5.1.2 Argon Microplasma

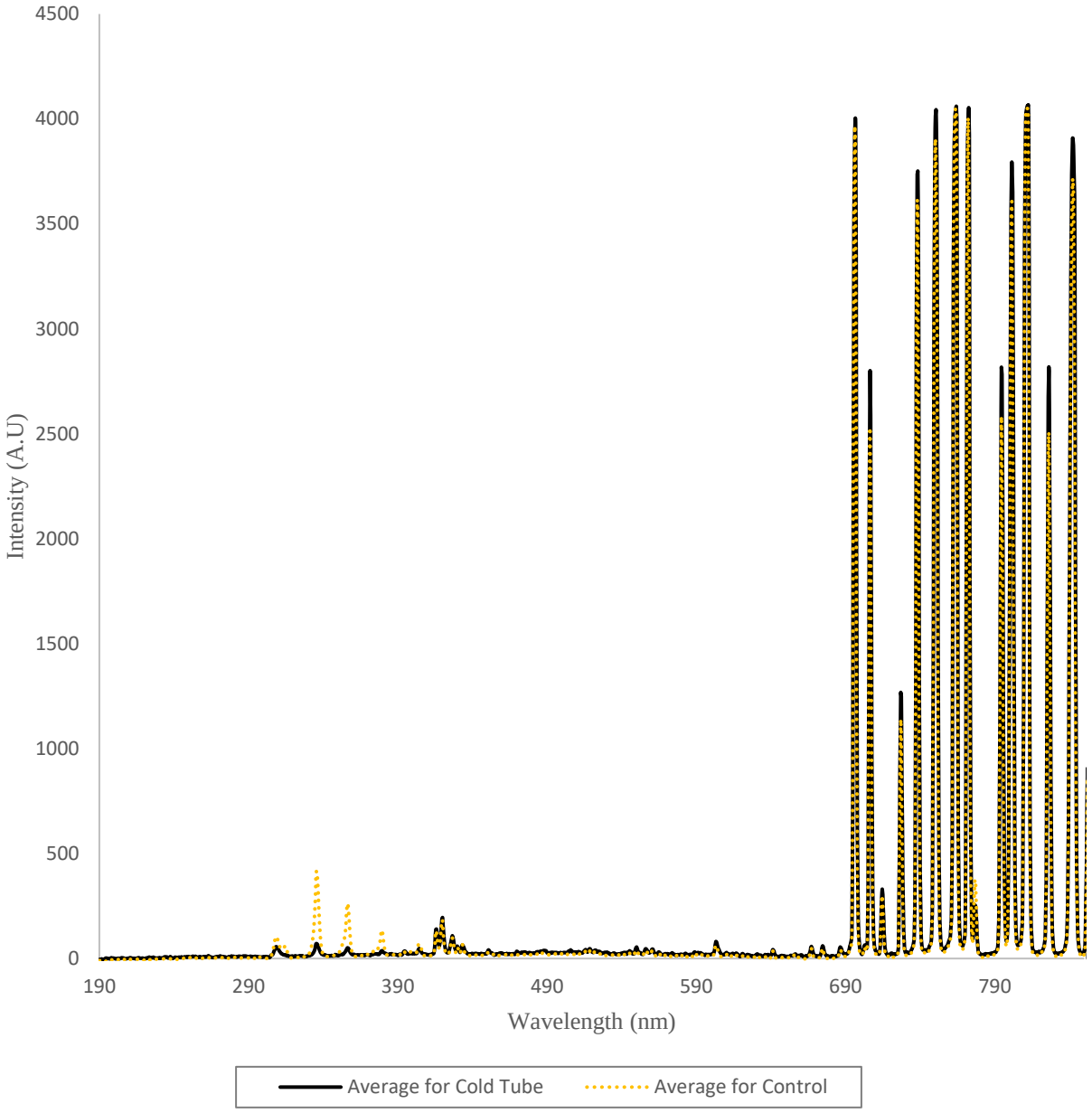

Figure 3.11: Overlapping emission spectra for the control and cold tube experiment for the argon microplasma.

3.5.1.3 Argon – 1000 ppm Hydrogen Microplasma

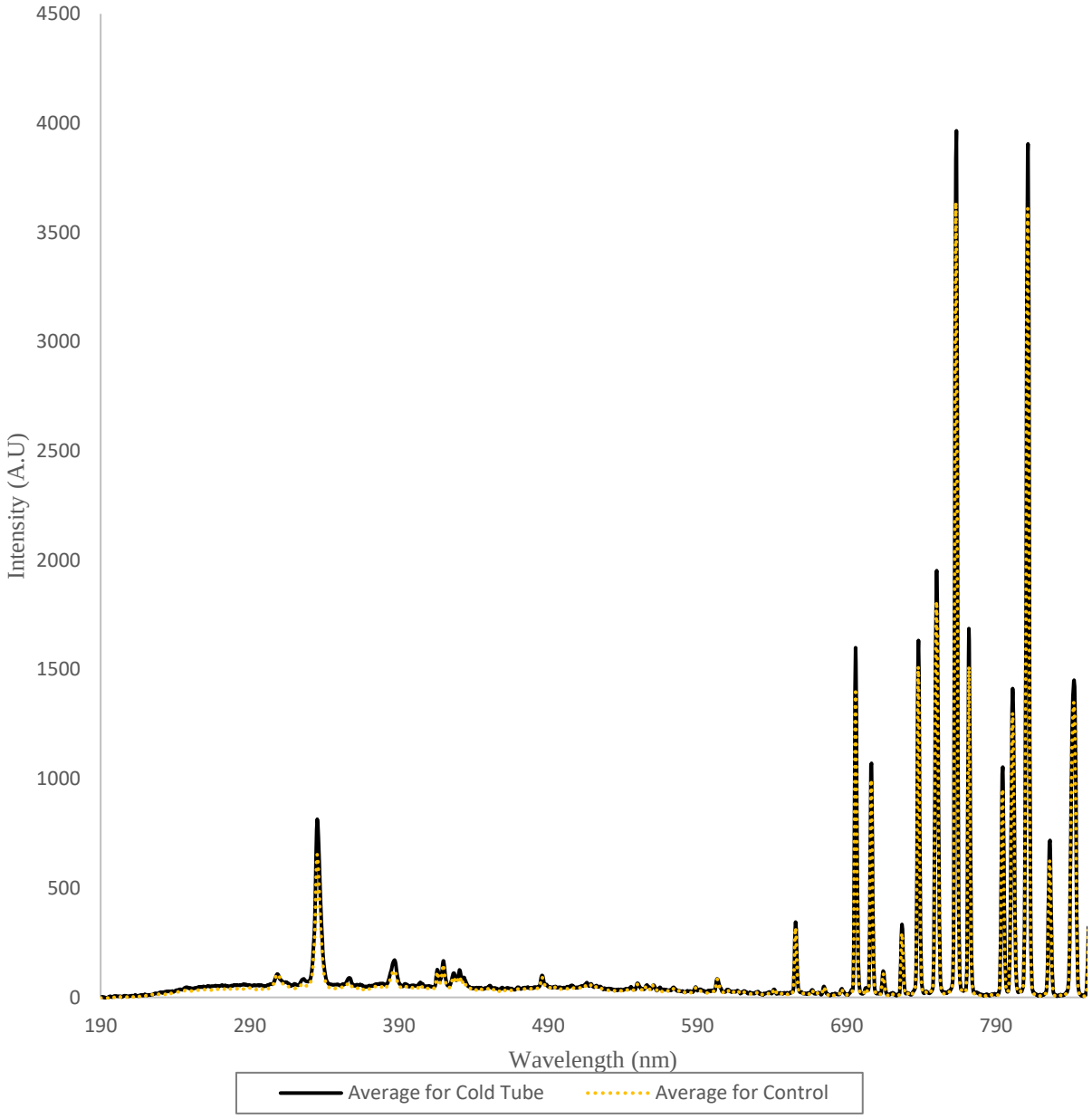

Figure 3.12: Overlapping emission spectra for the control and cold tube experiment for the argon – 1000 ppm hydrogen microplasma.

3.5.2 Testing the Efficiency of the Cold Trap

It is important to remove all the water vapors generated from the reaction solution in the GLS as water vapors dim the helium microplasma drastically. For removing water vapors, a cold trap (as described in Chapter 2, section 2.3.2.5) was used, and its efficiency was tested by using two different experimental setups. In the first experimental setup, the equipment for chemical vapor generation was set up as described in Chapter 2 – section 2.3.2. However, instead of using a $NaBH_4$ solution and an acidic solution, milli Q water was added to both the reagent vial and the sample vial. Afterward, in the next experimental setup, one end of the GLS was closed by attaching it to a closed-ended glass tube. The carrier gas was mixed with water in a plastic tee piece before its introduction into the GLS through a tangential inlet. This was done to ensure better mixing of water with the carrier gas, generate finer water droplets, and force the carrier gas to carry more water vapor. After exiting the GLS, the carrier gas with water vapors passed through the cold trap before entering the microplasma tube.

The introduction of ultrapure water into the GLS did not cause dimming of helium microplasma at all. For the experimental setup, in which ultra-pure water and carrier gas were introduced separately in the GLS (as illustrated in Figure 2.2 in Chapter 2), only a slight increase in the OH peak intensity was seen (episodic data displayed in Figure 3.13A). This could be because only a small amount of water vapor was taken up by the carrier gas from the GLS. For the experimental setup in which the carrier gas was mixed with water before its introduction into GLS, a higher intensity of the OH peak was seen over a few episodes. This is because the carrier gas was forced to carry more water by allowing the water, being pumped through the reaction coil and 2-way valve, to mix with carrier gas, helium, in a plastic tee connector before its introduction in the GLS. The episodic data for this experiment can be seen in Figure 3.13B. Higher intensity peaks formed

from atmospheric gases, in the region 200 nm to 300 nm, are due to the permeability of the plastic tee connector and due to dissolved gases present in the milli Q water. Peaks from atmospheric gases can also be seen in Figure 3.13A due to the presence of dissolved gases in milli Q water. Although the helium microplasma dims in the presence of water vapors, as observed in section 3.4, it remained stable for this experiment. This experiment proves that the cold trap was efficient in removing most of the water vapors and that it can be used in discrete flow system equipment.

A.

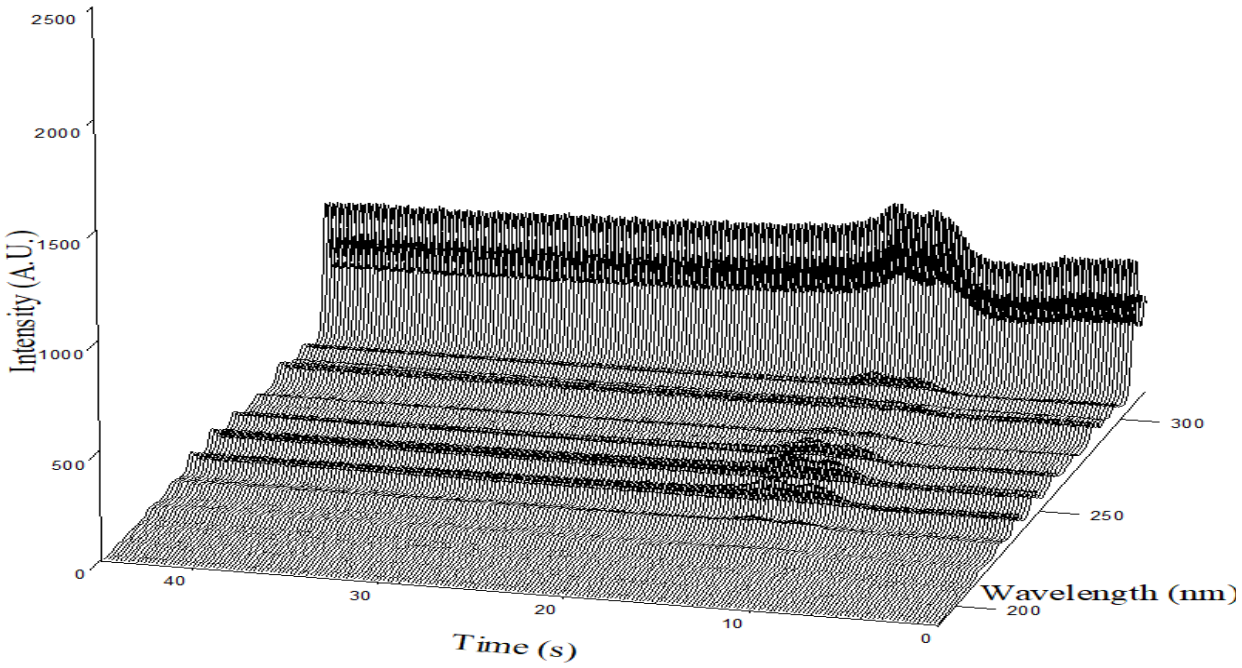

B.

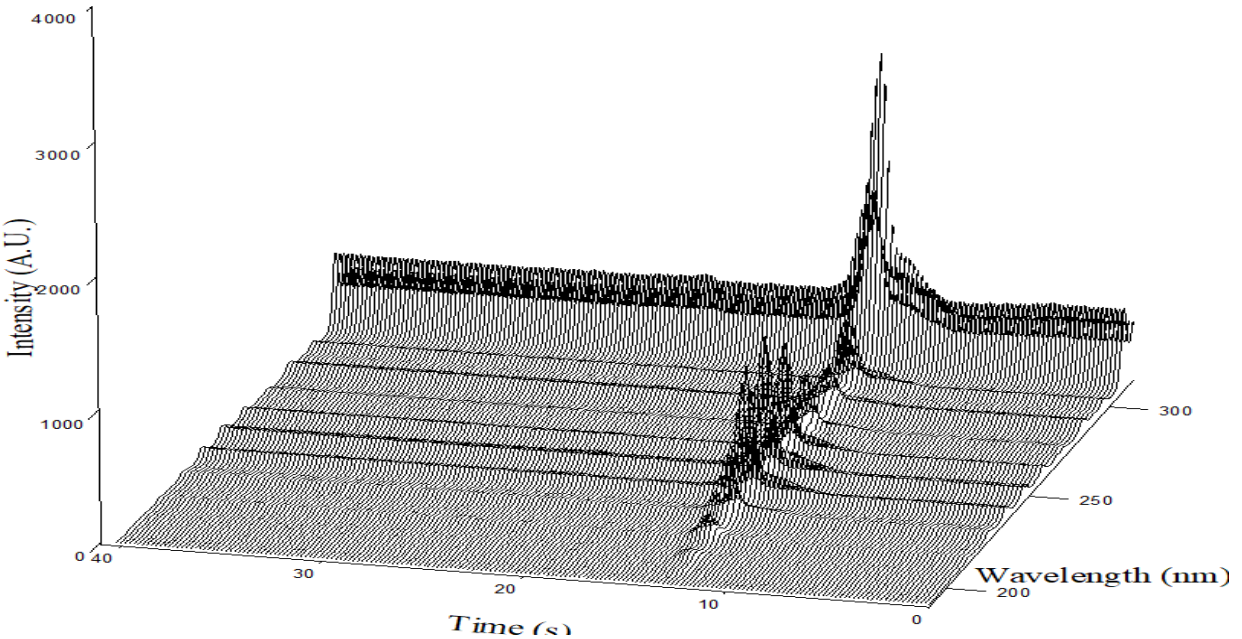

Figure 3.13: Episodic data collected for A. trial in which milli Q water was mixed with water in the GLS and B. trial in which milli Q water was mixed with carrier gas, helium, in a plastic tee connector before its introduction in the GLS.

3.6 Impact of Hydrogen Released from the Reaction Solution

As explained in Chapter 1, the $NaBH_4$ solution releases nascent hydrogen in an acidic solution which then reacts with the hydride forming element, like arsenic, to produce its volatile hydride (arsine). Nascent hydrogen is produced in excess which enters the microplasma along with the volatile hydride and water vapors. Hydrogen changes the thermal process in the microplasma as it has higher thermal conductivity than most gases, including argon and helium. Moreover, it also has relatively higher dissociation temperature [26]. Therefore, with hydride generation, a new problem was seen. Hydrogen released from the reaction solution would momentarily dim the microplasma. Changing the carrier gas had a small impact on the dimming problem of the microplasma caused by nascent hydrogen released from the reaction solution.

For observing the impact of $NaBH_4$ concentration on the dimming of microplasma, the equipment for hydride generation (discrete flow system) was set up as described in Chapter 2 – section 2.3.2. A 9% (v/v) HCl solution was used as a sample solution and reacted with varying concentrations of the $NaBH_4$ solution made in 0.5% (w/v) NaOH solution. Different concentrations of $NaBH_4$ solutions used were around 0.05% (m/v), 0.1% (m/v), 0.2% (m/v) and 0.4% (m/v). This experiment was repeated for three carrier gases, helium, argon, and argon – 1000 ppm hydrogen. For each reaction trial, episodic data was collected by the spectrometer for about 1 – 2 minutes. The results for different carrier gases can be found in sections 3.6.1, 3.6.2, 3.6.3:

3.6.1 For Microplasma Operated in Helium with Input Power of 14.8 watts

The helium microplasma was negatively impacted by the hydrogen released from the reaction solution but there was a very small change in the background of its emission spectrum. The helium microplasma, operated at a power around 14.8 watts, was very sensitive to hydrogen released from the reaction solution. Hydrogen diminishes the emission intensities of almost all spectral lines

momentarily. Afterwards, as the amount of hydrogen released from the reaction solution in the GLS decreases over time, the helium microplasma starts regaining its initial power which is seen as increasing emission intensities of different spectral lines, as seen in Figure 3.14. The emission spectrum for microplasma operated in UHP helium had a very low background, as compared to that from BIP argon and argon-1000 ppm hydrogen. Even introduction of hydrogen into the microplasma from the reaction solution caused a small increase in background.

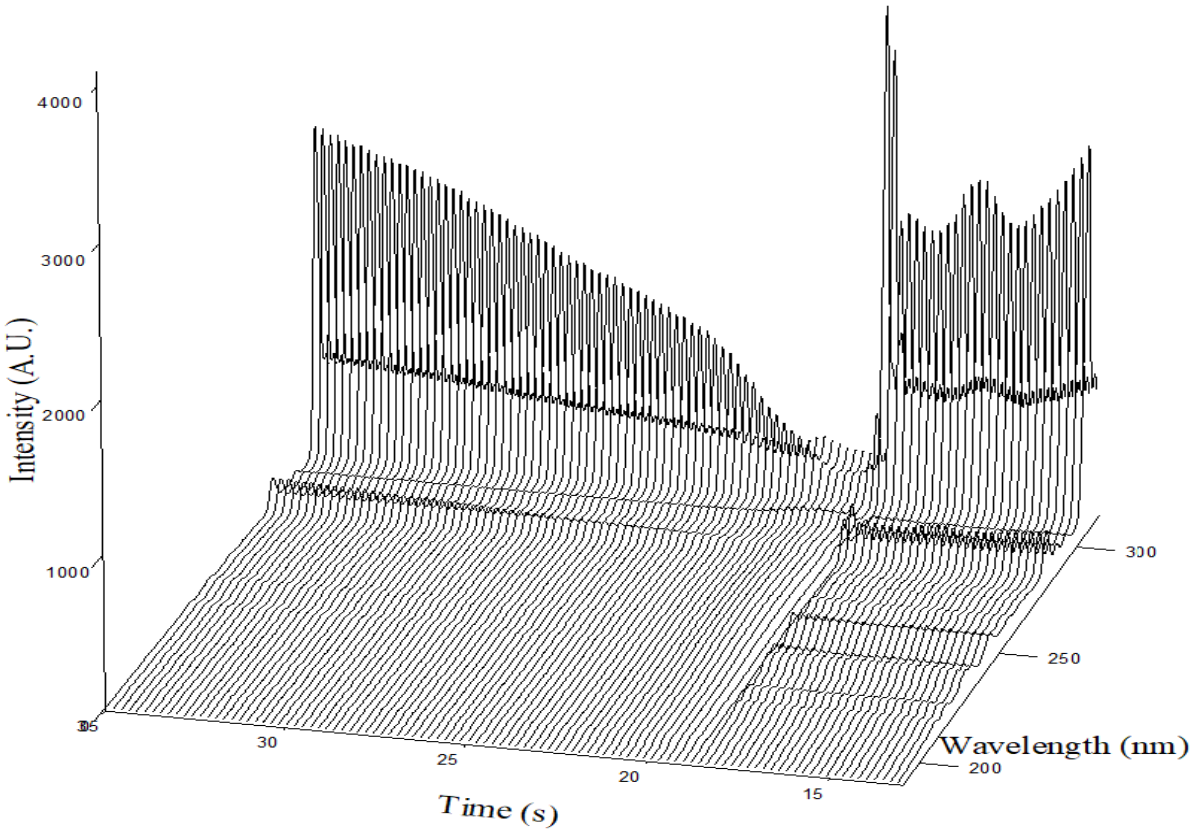

Figure 3.14: Episodic data for blank reaction of 0.0514% (m/v) $NaBH_4$ with 9%(v/v) HCl for helium microplasma.

In Figure 3.14, wavelength range of only 190 nm to 320 nm is shown, although, data for the wavelength range up to 850 nm is also present. In this part of the emission spectrum, the OH peak at 308 nm is the highest peak. The presence of hydrogen momentarily lowers the emission intensity of the OH peak at 308 nm. Afterwards, as the hydrogen released from the reaction solution becomes negligible, the microplasma starts regaining its power, which is seen in the OH peak regaining its emission intensity over time in the episodic data. This slow increase in intensity of OH peak is because the helium microplasma takes time to regain its power.

Increasing the concentration of the $NaBH_4$ further caused the microplasma to dim momentarily when the amount of hydrogen in the carrier gas is maximum. During this dimming moment, the signal to noise ratio almost drops to ~0 as the microplasma is extinguished. This can be seen in Figure 3.15 which shows the reaction trial for 0.104% (m/v) $NaBH_4$ solution.

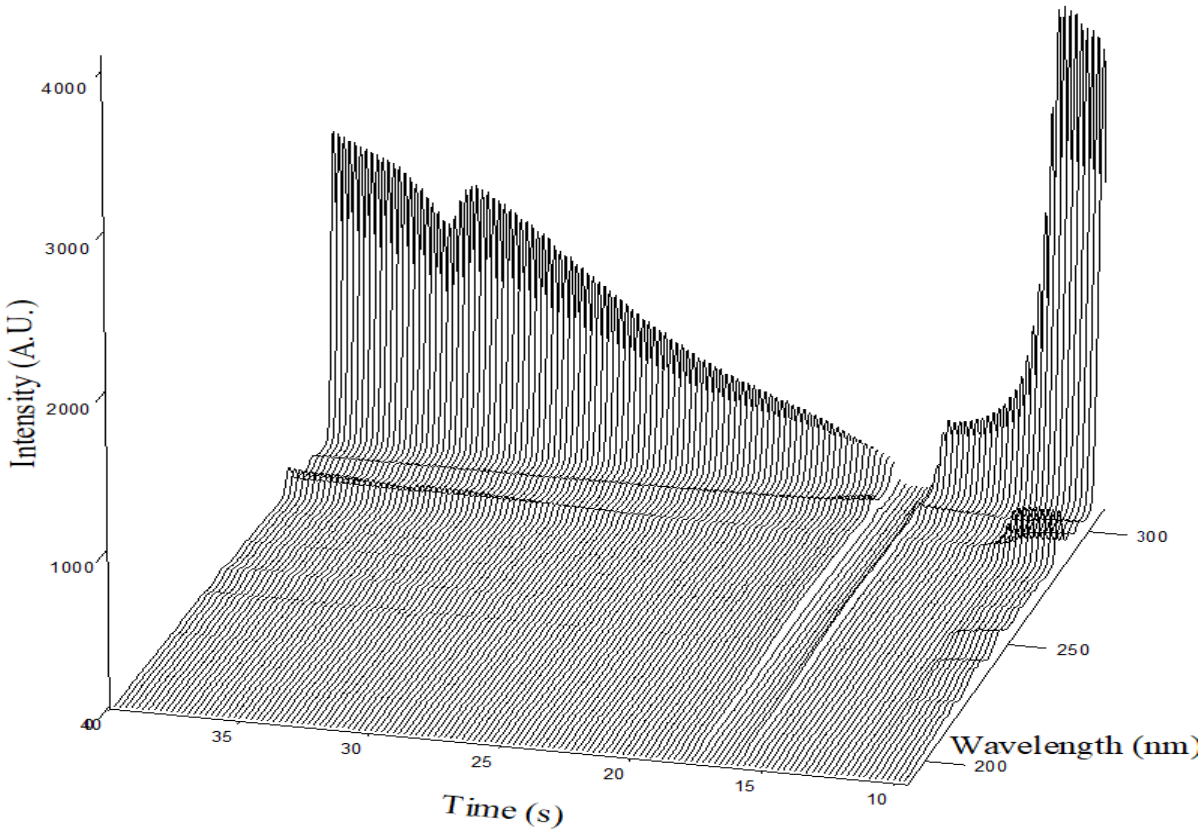

Figure 3.15: Episodic data for blank reaction of 0.104% (m/v) $NaBH_4$ with 9%(v/v) HCl in helium microplasma.

In Figure 3.15, microplasma can be seen dimming during the time duration 15.5 to 18 seconds on the time axis. As the concentration of $NaBH_4$ is increased, the microplasma is dimmed for a longer duration of time and takes longer to regain its initial power, as observed in Figure 3.16:

A.

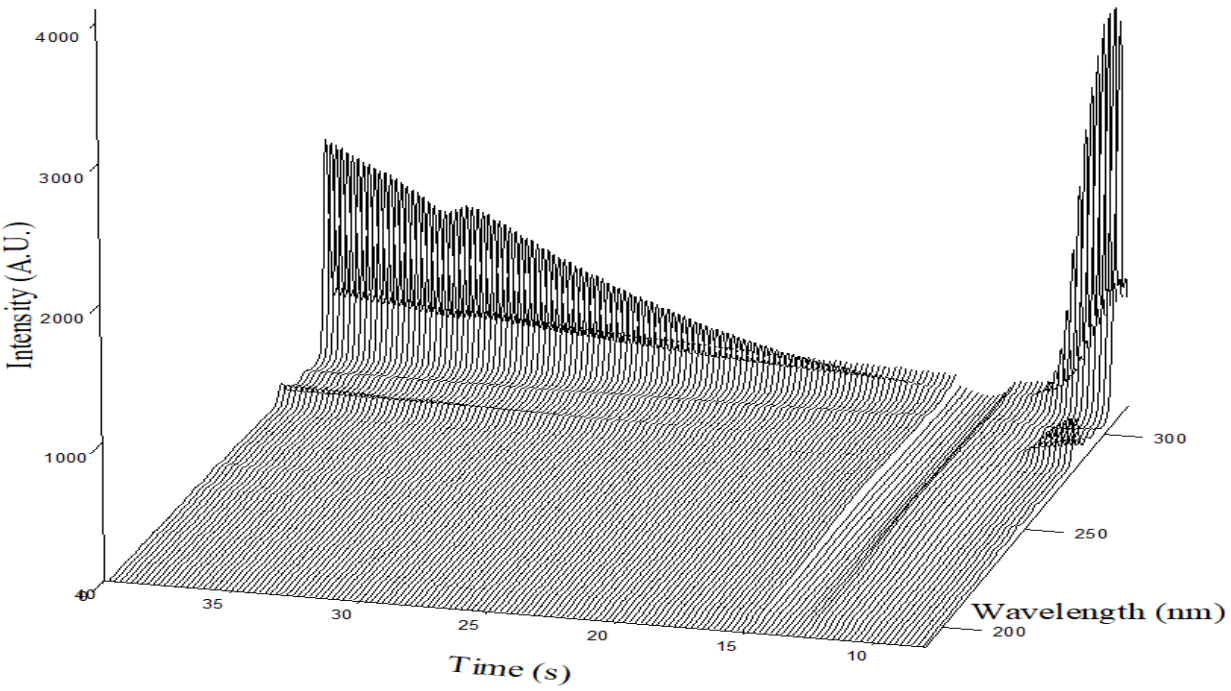

B.

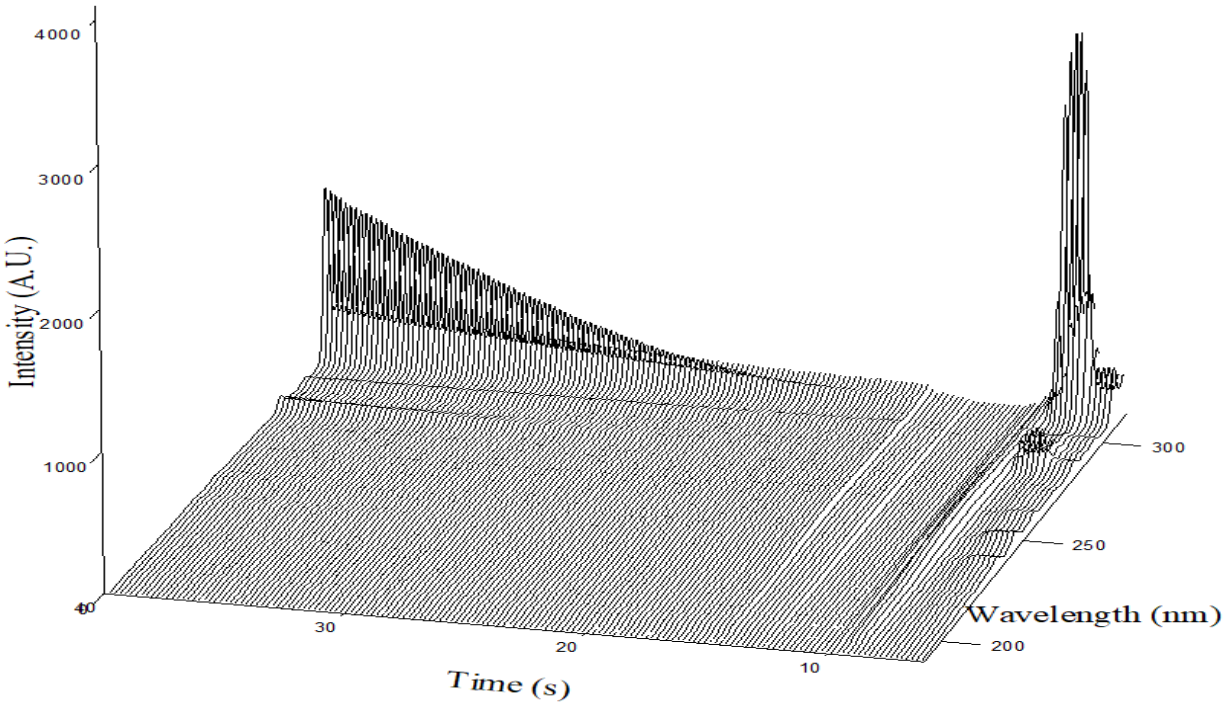

Figure 3.16: Episodic data for reaction trials with A. 0.208% (m/v) $NaBH_4$ and B. 0.415% (m/v) $NaBH_4$ solutions for microplasma operated in helium.

3.6.2 For Microplasma Operated in Argon with Input Power of 5.9 watts.

Similarly, for BIP argon, the only concentration of $NaBH_4$ solution that did not extinguish the microplasma was 0.05% (m/v). With a rise in concentration of $NaBH_4$, the time for which the microplasma remained dim increased. However, after turning off momentarily, the microplasma turned on again on its own and regained its initial power quite quicker, as compared to helium microplasma. It was also observed that for argon, hydrogen raised the background of the emission spectrum. This disturbance in background was greater than that seen for helium.

Episodic data for blank reaction trials, with varying concentrations of $NaBH_4$, conducted with argon as carrier gas are displayed in Figure 3.17, which is extended over two pages:

A.

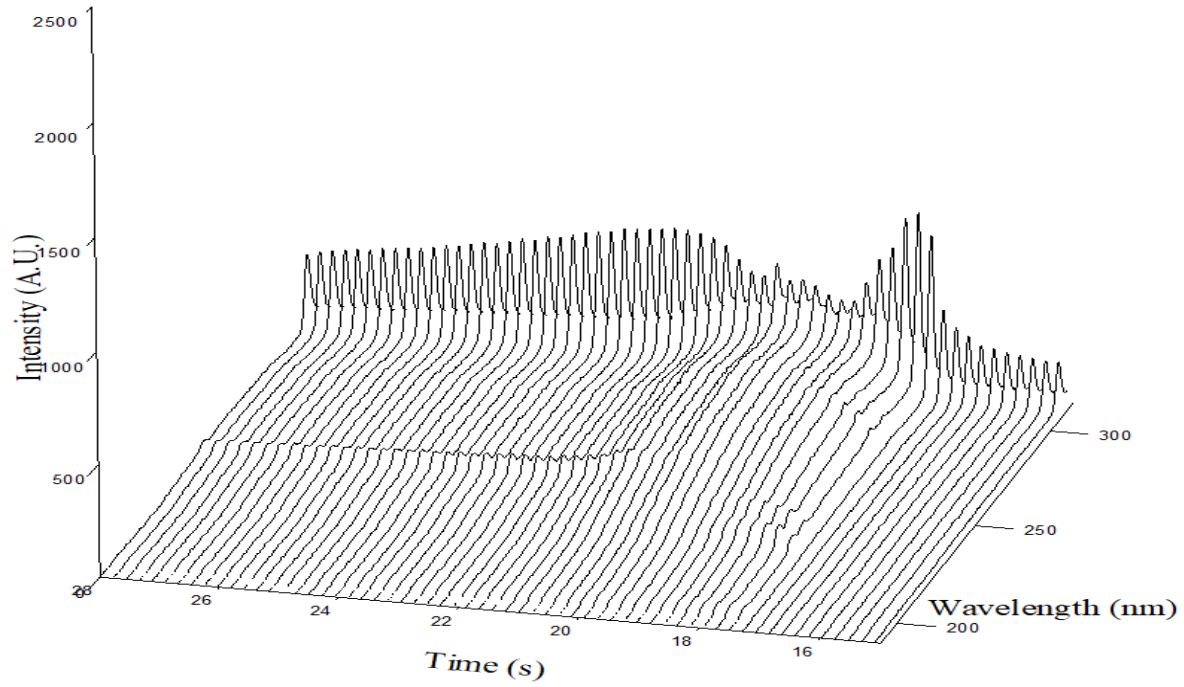
2500
2000
1500
1000
500
Intensity (A.U.)
28
26
24
22
20
18
16
Time (s)
300
250
200
Wavelength (nm)

B.

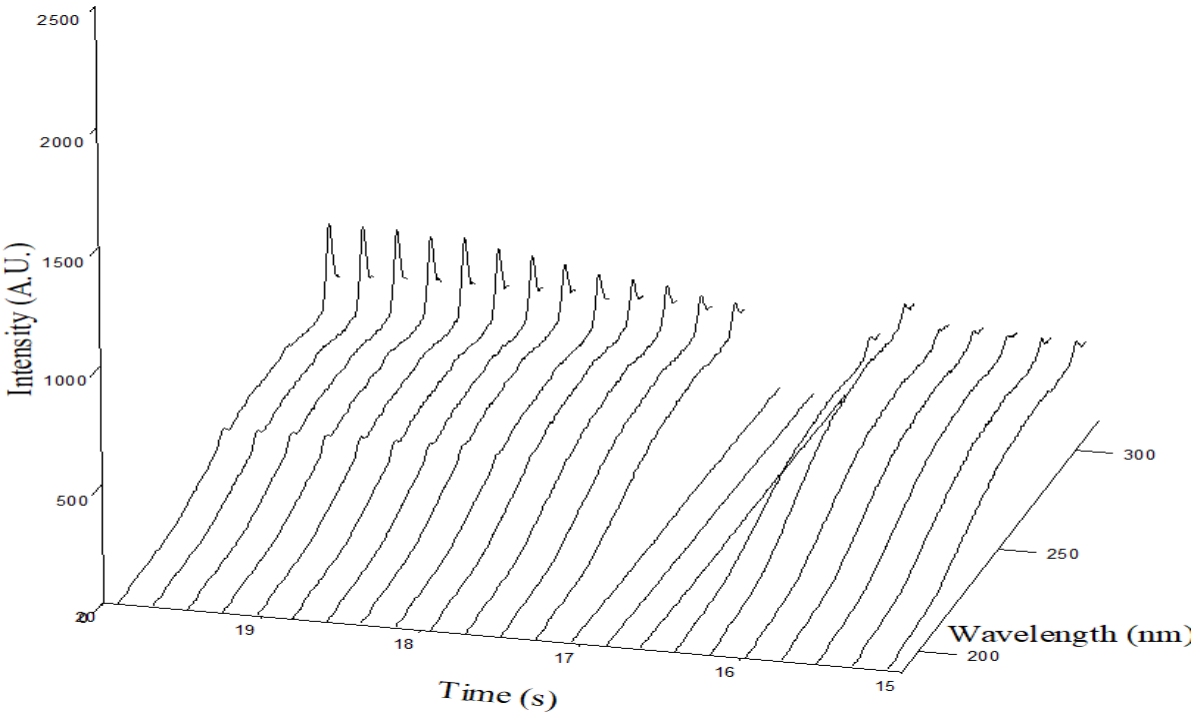
2500
2000
1500
1000
500
Intensity (A.U.)
20
19
18
17
16
15
Time (s)
300
250
200
Wavelength (nm)

C.

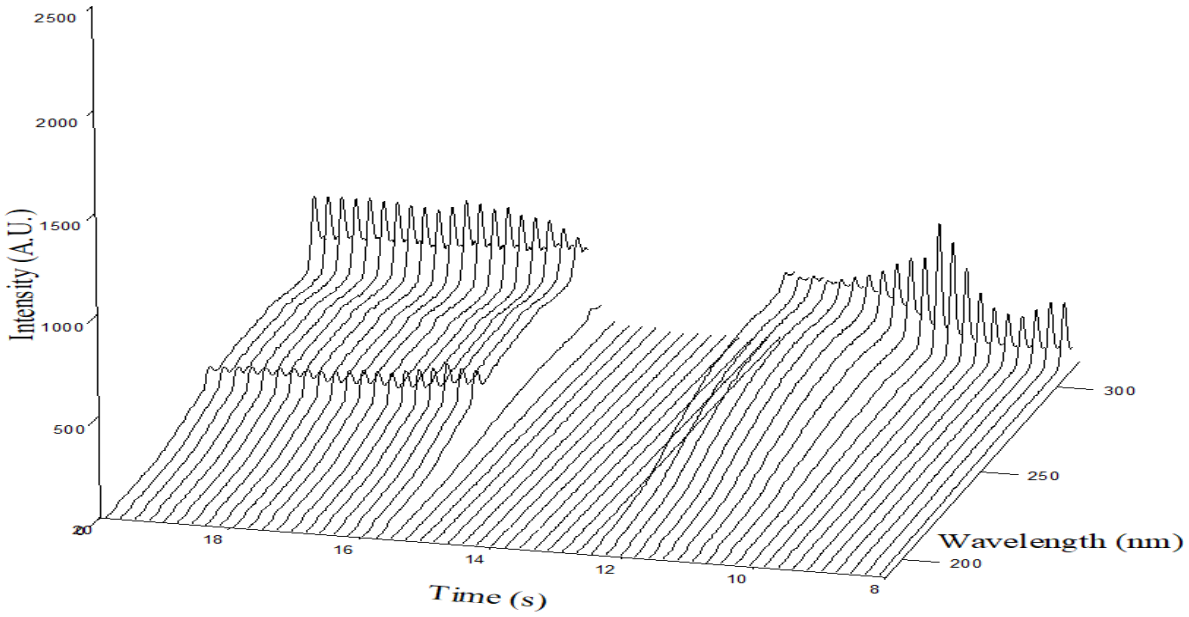

D.

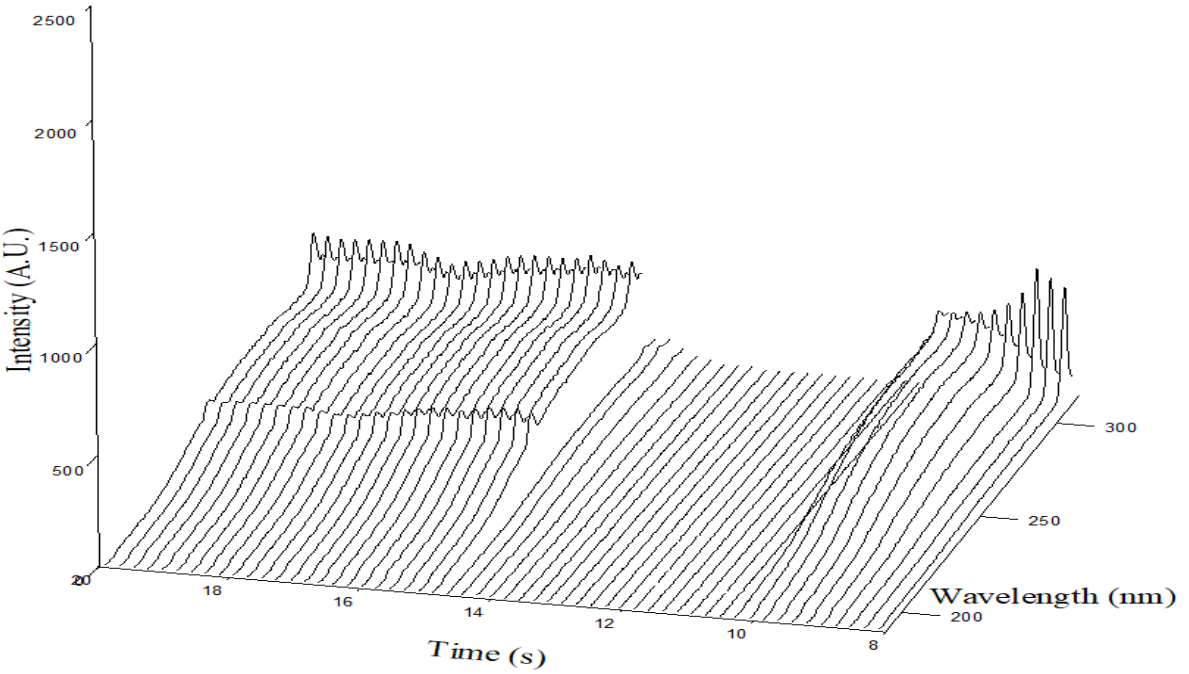

Figure 3.17: Episodic data for blank reaction trials conducted with A. 0.05% (m/v) $NaBH_4$, B. 0.1% (m/v) $NaBH_4$, C. 0.2% (m/v) $NaBH_4$, and D. 0.4% (m/v) $NaBH_4$, when microplasma was being operated in BIP argon. Only part of episodic data collected before, during and after dimming of microplasma is shown.

For emission spectra obtained from Argon micro plasma, the background shifts with influx of hydrogen from the reaction solution. This shift in background increases with increase in amount of hydrogen introduced in the micro plasma. Afterwards, as the amount of hydrogen released from the reaction solution reduces, the intensity of background also decreases.

3.6.3 For Microplasma Operated in Argon – 1000 ppm Hydrogen with Input Power of 6.5 watts.

In the end, the carrier gas mixture argon – 1000 ppm hydrogen was tested to see changes in the background of its emission spectrum, caused by hydrogen. Secondly, the other purpose of testing this carrier gas was to see if a microplasma operated in this gas mixture could tolerate hydrogen released from the reaction solution. Since the carrier gas already had hydrogen in it, it was assumed that the microplasma was being operated at frequency and power input conditions at which it would be better able to tolerate hydrogen. When the microplasma was operated in a mixture of argon – 1000 ppm hydrogen, even hydrogen released from a 0.05% (m/v) $NaBH_4$ reaction solution would disturb the microplasma momentarily. However, after dimming momentarily, the microplasma would turn on and regain its initial power very quickly. This can be deduced by comparing the episodes before and after dimming. The episodic data collected for blank reaction trials with varying concentrations of $NaBH_4$ are shown in Figure 3.18, which is extended over two pages.

A.

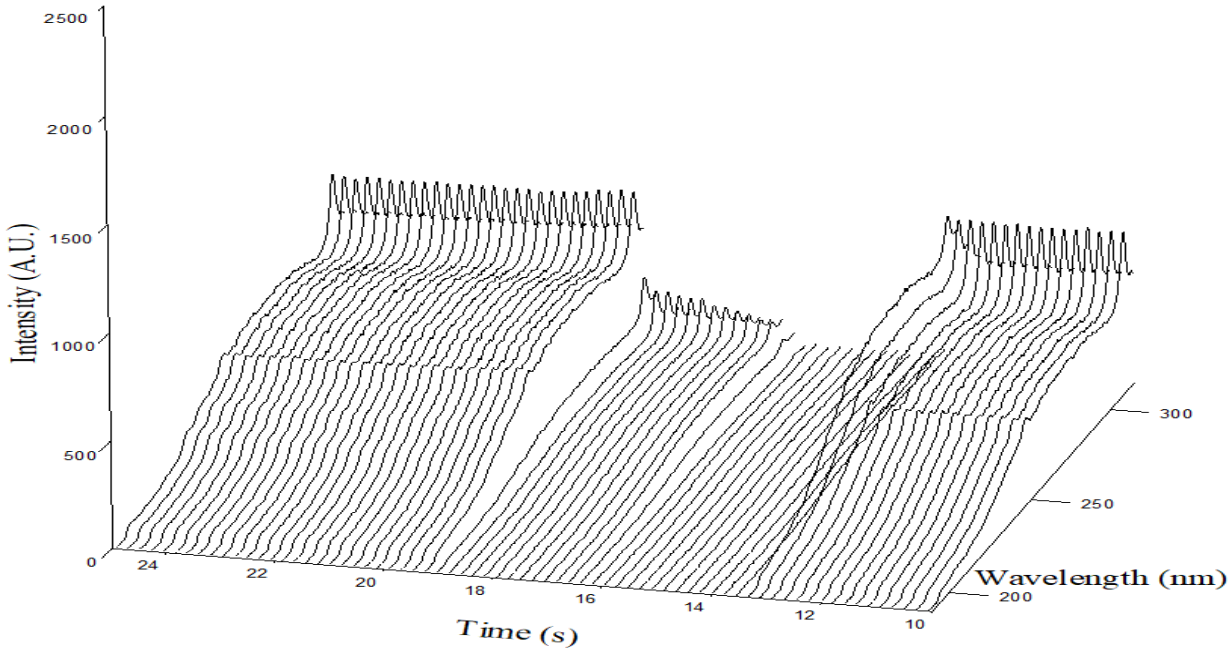
2500
2000
1500
1000
500
0
Intensity (A.U.)
24
22
20
18
16
14
12
10
Time (s)
300
250
200
Wavelength (nm)

B.

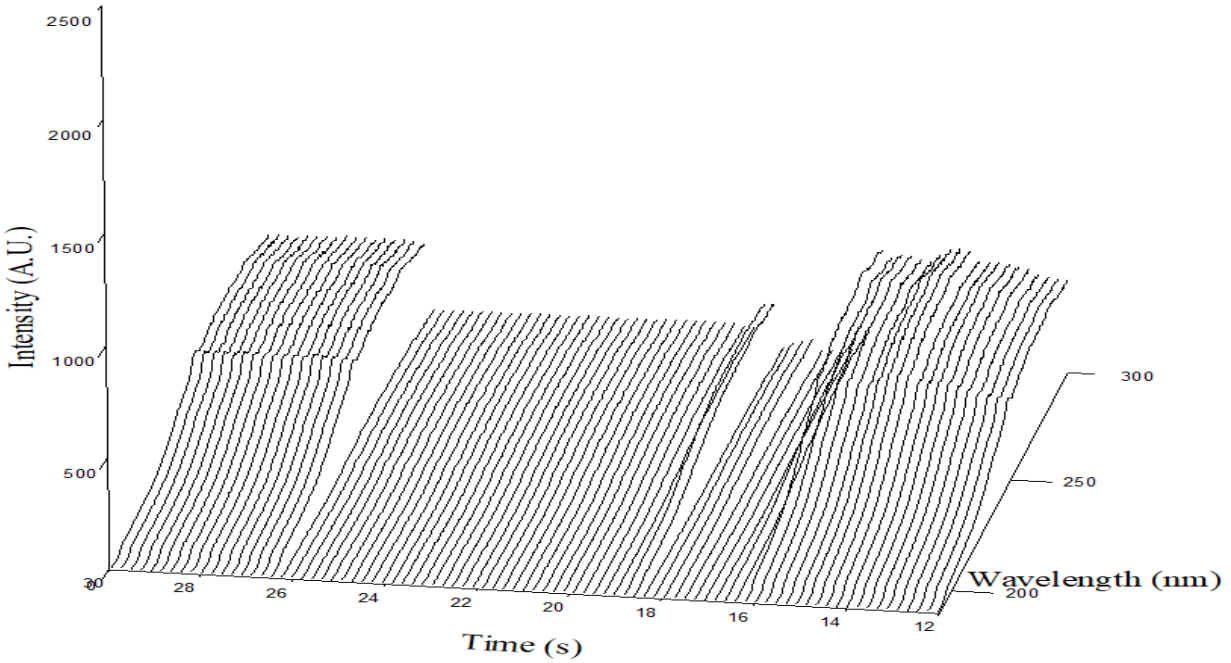
2500
2000
1500
1000
500
0
Intensity (A.U.)
30
28
26
24
22
20
18
16
14
12
Time (s)
300
250
200
Wavelength (nm)

C.

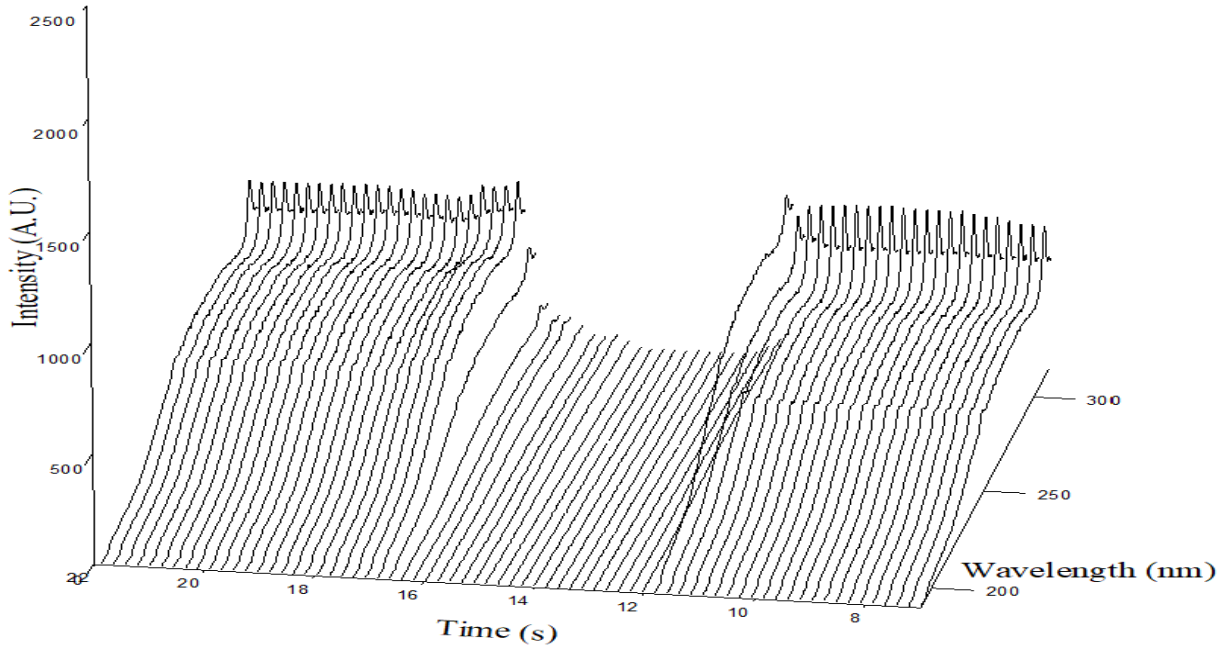

D.

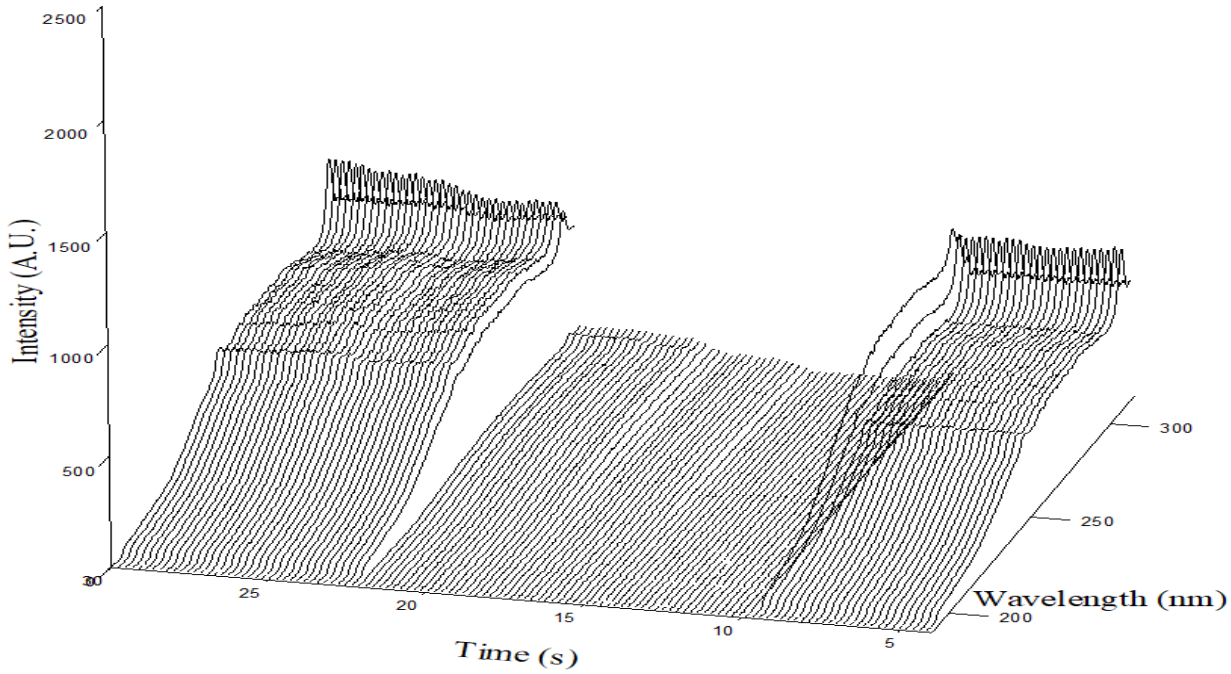

Figure 3.18: Episodic data for blank reaction trials conducted with A. 0.05% (m/v) $NaBH_4$, B. 0.1% (m/v) $NaBH_4$, C. 0.24% (m/v) $NaBH_4$, D. 0.49% (m/v) $NaBH_4$ for argon – 1000 ppm hydrogen microplasma. Only part of episodic data collected before, during and after dimming of microplasma is shown.

Just like the microplasma operated in other carrier gases, the hydrogen released from the reaction solution disturbs the microplasma operated in argon – 1000 ppm hydrogen as well. For $NaBH_4$ concentrations of 0.05% and 0.1% (m/v), the hydrogen released from reaction solution decreases the background, along with diminishing the argon peak intensities (argon peaks are not shown in Figure 3.18). This dimming of microplasma proves that presence of hydrogen in the carrier gas cannot stabilize the microplasma towards the hydrogen released from the reaction solution. There is no frequency or power input combination that prevents the dimming of microplasma caused by the hydrogen released from the reaction solution.

3.6.4 Impact of Microplasma Dimming

As seen in Figures 3.14 to 3.18, when the microplasma is dimmed for a few moments due to an influx of hydrogen, the signal to noise ratio reduces to 0 when the concentration of $NaBH_4$ used in the reaction trials is more than 0.05% (m/v). The volatile hydride, arsine, and hydrogen are released from the reaction solution at the same time. Therefore, dimming of microplasma results in a loss of the emission signal from the analyte. Moreover, this loss of signal is not reproducible for each trial. Sometimes, the analytical signal is lost when it is supposed to have the highest intensity, and sometimes, it is lost before or after the peak of the signal has been recorded. Hence, reproducibility in dimming does not mean reproducibility in the recorded analytical signal.

Effort was made to reduce or eliminate the dimming of microplasma due to hydrogen, by trying a two-step water vapor trap and by using higher flow rates of carrier gas (helium). Two-step water vapor traps, introduced after the GLS, were used under the assumption that removing more water vapors from the carrier gas might reduce the dimming time of helium microplasma as helium microplasma is more sensitive to water vapors as compared to argon microplasma and argon – 1000 ppm hydrogen microplasma. However, the two-step water trap after GLS had no impact on

the dimming time of microplasma. The flow rate of the carrier gas was changed for the blank reaction trials, using the discrete flow system as equipment, because flow rate of carrier gas changes the residence time of a species in the microplasma. It was assumed that the dimming period of the microplasma would also decrease due to an enhanced flow rate of carrier gas, helium. Although the increase in flow rate of the carrier gas changed the signal intensities of the OH (308 nm) and NH (335 nm) peaks, it could not resolve or reduce the dimming issue of microplasma. In conclusion, both experiments failed to produce desirable results.

3.7 Conclusion

In this chapter, the impact of water vapors, cold trap and hydrogen released from the blank reaction solution on the microplasma operated in three different carrier gases, helium, argon, and a mixture of argon-1000 ppm hydrogen was evaluated. The reaction mixture from hydride generation emits water vapors and hydrogen gas which are carried by the carrier gas towards the microplasma. Similarly, the impact of the cold trap on the emission spectrum was studied and its efficacy in removing water vapors was also evaluated. These experiments helped in deciding the amount of $NaBH_4$ that can be used in reaction trials and helped in narrowing down the list of factors that may impact precision of the results.

In the first experiment, the impact of water vapors on the emission spectra collected for a microplasma operated in three different gases was observed and efficiency of the cold trap in removing water vapors was assessed. For this experiment, PVC tubes were attached between the microplasma tube and the copper tube carrying the carrier gas. PVC is much more permeable to water vapors as compared to atmospheric gases like nitrogen and oxygen. These PVC tubes allowed the influx of water vapors in the system. It was observed that when the amount of water

vapors introduced in the carrier gas was constant, the microplasma yielded reproducible results. The change in power input of the microplasma with an increase in the number of PVC tubes in the setup was also very small. The helium microplasma was most drastically impacted by water vapors in the system. The reduction in emission intensities of the argon peaks due to influx of water vapors in argon microplasma was only about 50 – 55%. No negative impact of water vapors was seen on the emission spectrum for argon – 1000 ppm hydrogen. Passing the carrier gas through the cold trap did not impact the emission spectrum of any carrier gas negatively, indicating that the cold trap can be used in the equipment. It was also found that the cold trap was very effective in removing most of the water vapors released from the solution in the GLS. This experiment proved that microplasma could yield reproducible results with water vapors present in the system and that the cold trap was helpful in removing water vapors released from solution in the GLS.

Afterwards, different concentrations of $NaBH_4$ were tested in blank reaction trials with the discrete flow system equipment coupled to the microplasma operated in three different gases, helium, argon, and mixture of argon-1000 ppm hydrogen. Hydrogen released from the hydride generation reaction destabilizes the microplasma and dims it momentarily if it is present in high amount. For helium and argon as carrier gases, it was only the 0.05% (m/v) $NaBH_4$ concentration that did not dim the microplasma. Reaction trials with higher concentration of $NaBH_4$ extinguish the microplasma momentarily due to release of more amount of hydrogen from the reaction mixture in the GLS. The time for which the microplasma remains dim rises with the increase in $NaBH_4$ concentration. Subsequently, as the amount of hydrogen released from the reaction solution present in the GLS decreases, the microplasma regains its initial power. Argon microplasma takes much less time to regain its power as compared to helium microplasma. This is because argon has lower ionization potential of 15.8 eV [57] as compared helium which is 24.6

eV [52]. Hence, argon gas is easier to ionize as argon ions are easier to produce because of the smaller energy gap between the atom's ground state and its first excited state [58]. The third gas, argon – 1000 ppm hydrogen mixture, was also used as a carrier gas for the microplasma with hydride generation as a sample introduction technique. The purpose of using this gas was to see if there was a power input or frequency for mixture of argon and hydrogen that would make the microplasma stable to hydrogen released from reaction solution, and if there was any impact of hydrogen released from the hydride generation reaction on the spectral background. Any influx of hydrogen generated from the hydride generation reaction disturbed the microplasma too much, decreasing the signal to noise ratio of the emission lines for argon and other species, also decreasing the spectral background seen in the emission spectrum, due to dimming of the microplasma. Even 0.05% (m/v) $NaBH_4$ released too much hydrogen which disturbed the microplasma operated in this gas mixture. However, just like pure argon, as the amount of hydrogen released from the reaction solution decreased, the microplasma regained its initial power very quickly. Since the helium and argon microplasma were able to tolerate hydrogen released from the 0.05% (m/v) $NaBH_4$ solution in the reaction mixture, this concentration of $NaBH_4$ was used in the next experiments which included the reaction of $NaBH_4$ solution with arsenic solution.

In conclusion, these experiments showed the impact of water vapors and hydrogen on the microplasma operated in three different carrier gases. These experiments proved that if the amount of water vapors introduced in the microplasma is constant, the microplasma yields precise results, although its emission intensity can be impacted, depending on the carrier gas used. The cold trap was efficient in removing most of the water vapor. The hydrogen released from the reaction solution can momentarily dim the microplasma. The concentration of $NaBH_4$ that should be used in the reaction trials is 0.05% (m/v).

Chapter 4

Detecting Arsenic in Helium and Argon Microplasma

4.1 Outline

- Discussion of the procedure for cleaning the equipment used for hydride generation and the reagents used in hydride generation.
- Explanation of arsenic emission peaks seen in the emission spectrum of the argon and helium microplasma.
- Method for clearing all the memory caused by the previously run arsenic sample.
- The best observation position over the microplasma tube to get the most intense arsenic signal in both helium and argon microplasma.
- Difference in the arsenic signal intensity collected from the helium and argon microplasma.
- Estimating the detection limit of arsenic in helium and argon microplasma.
- Changes in the equipment design are needed to improve the reproducibility of the arsenic reaction trials.

4.2 Procedure for the Cleaning Equipment

The equipment used for hydride generation was thoroughly cleaned before its use in the experiment. All the glass equipment was soaked in detergent solution overnight to remove the vacuum seal on the valves. Afterwards, this equipment was washed with DI water to get rid of the soap and then dipped in dilute nitric acid or dilute HCl solution for at least one day. This glass equipment was then rinsed with DI water three times and with milli Q water three times before

being dried in a clean room. The peristaltic pump tubes used for carrying the $NaBH_4$ solution and the HCl solution were soaked in a dilute nitric acid solution for two days before being rinsed by DI water and milli Q water three times each. The peristaltic pump tube used for carrying the arsenic solution was submerged in detergent solution overnight. Afterwards, it was rinsed with DI water to get rid of the soap and then soaked in the dilute nitric acid solution for at least one day. Similarly, the vials which contained the reagent solution were first washed with neutral detergent and then drenched in dilute nitric acid for at least two days. After taking the vials out of the dilute nitric acid solution, the vials were washed with DI water and milli Q water three times each, before being dried in a clean room. The equipment was cleaned to prevent any memory or interference caused by contamination of the equipment.

4.3 Reagents

All reagents used in this experiment were of analytical grade and Milli Q water, obtained from a Milli Q system (Catalogue number: QTUM000EX), was used as a diluent. For all the experiments mentioned earlier and, in this chapter, the 9% HCl solution was made by diluting a 37% hydrochloric acid aqueous solution (Sigma Aldrich, Cas number: 7647-01-0). A 0.5% (m/v) NaOH solution was made by dissolving sodium hydroxide (Sigma Aldrich, 97% purity, Cas number: 1310-73-2) in milli Q water. The arsenic solution was made by diluting the stock As (III) solution (Inorganic Ventures, 1001 ± 5µg/L) with 9% (v/v) HCl solution. The $NaBH_4$ solution was made by dissolving sodium borohydride (Sigma Aldrich, 99% purity, Cas number: 16940-66-2) in 0.5% (m/v) NaOH solution.

All the solutions made for experimentation were sonicated for at least 10 minutes to remove dissolved atmospheric gases. This is because the peaks from the dissolved gases interfere with the

analytical signal due to low spectral resolution. Moreover, dissolved gases also hinder the smooth flow of a liquid through the peristaltic pump tubing.

4.4 Arsenic Lines

This research was mainly focused on the detection of arsenic in water samples by hydride generation because arsenic contamination of water poses a health hazard towards millions of people worldwide. The maximum acceptable concentration of arsenic in drinking water is 10 µg/L (10 ppb) according to a report released by Health Canada [59] and guidelines provided by the UN [60]. Although arsenic can also be present in water in the form of organic compounds, only inorganic arsenic (As^{3+}) was used for experimentation in this project.

For hydride generation, the inorganic arsenic present in an acidic sample is reacted with sodium tetrahydroborate, $NaBH_4$, to generate arsine gas (AsH_3). The equation for this reaction that forms the hydride, AsH_n from As with oxidation state m+, is [61]:

$$NaBH_4 + 3H_2O + HCl \rightarrow H_3BO_3 + NaCl + 8H$$

$$As^{m+} + 8H \rightarrow AsH_n + H_2\ (excess)$$

In this research, arsenic with oxidation state +3 was used. Therefore, As (III) was converted to AsH_3 during hydride generation reaction. According to this reaction equation, for every 0.4 mL reaction solution consisting of 0.2 mL of 30 ppm As solution and 0.2 mL of 0.05% (m/v) $NaBH_4$ solution, 8×10^{-8} moles of arsine and 6.41×10^{-6} moles of hydrogen are released (assuming all reactants are converted to products).

Using argon and helium as carrier gases, the equipment for hydride generation (discrete flow system) was coupled with microplasma. The concentration of arsenic was raised from 30 ppm to 50 ppm to identify its emission lines, as the arsenic emission lines would increase in intensity due

to increasing concentration of As^{3+} in the sample. The emission spectra obtained after introduction of arsenic into the helium and argon microplasma are exhibited in Figures 4.1 and 4.2:

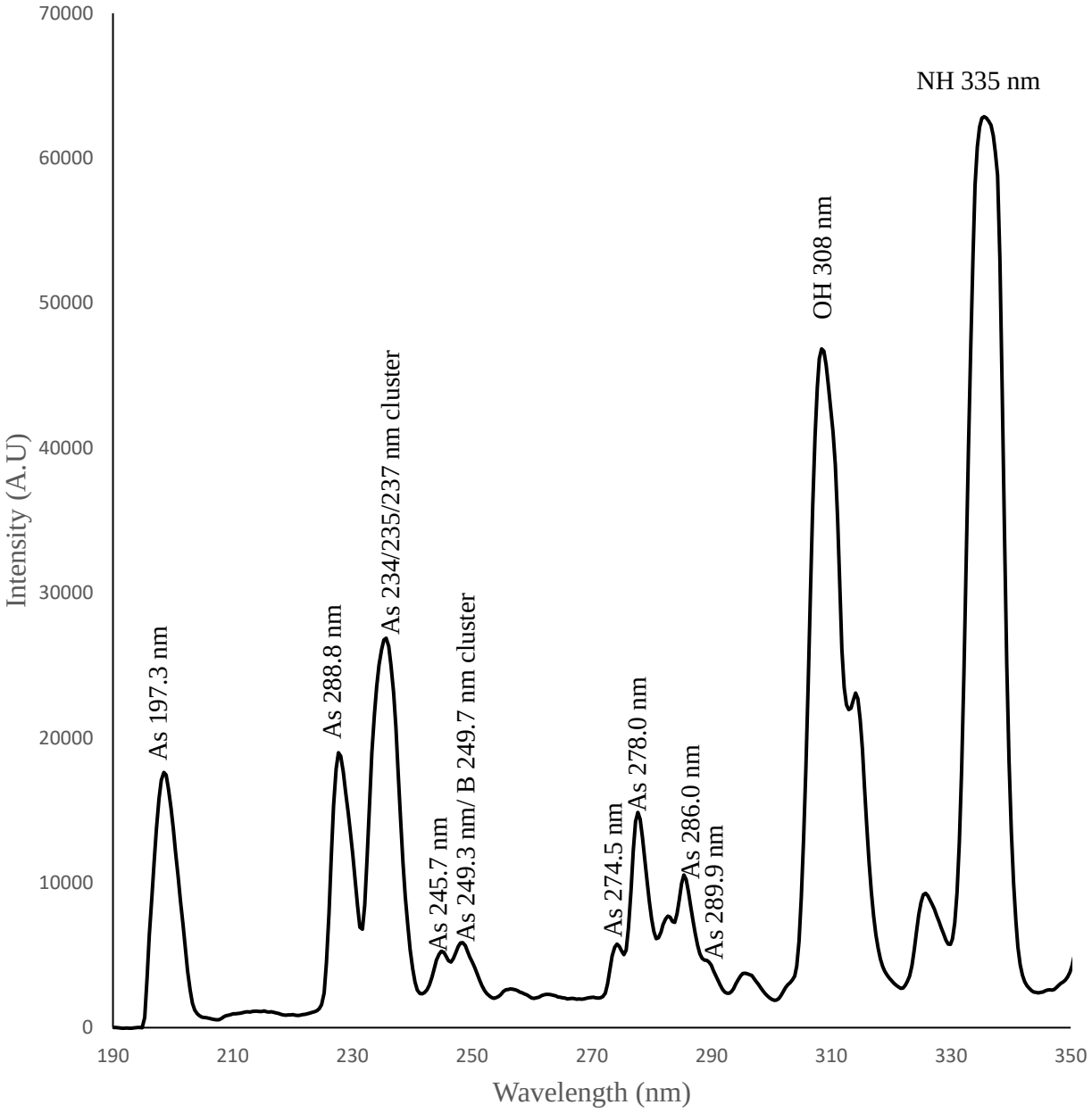

Figure 4.1: Emission spectrum of arsenic in helium microplasma. Episodes showing the arsenic signal were added to make this spectrum.

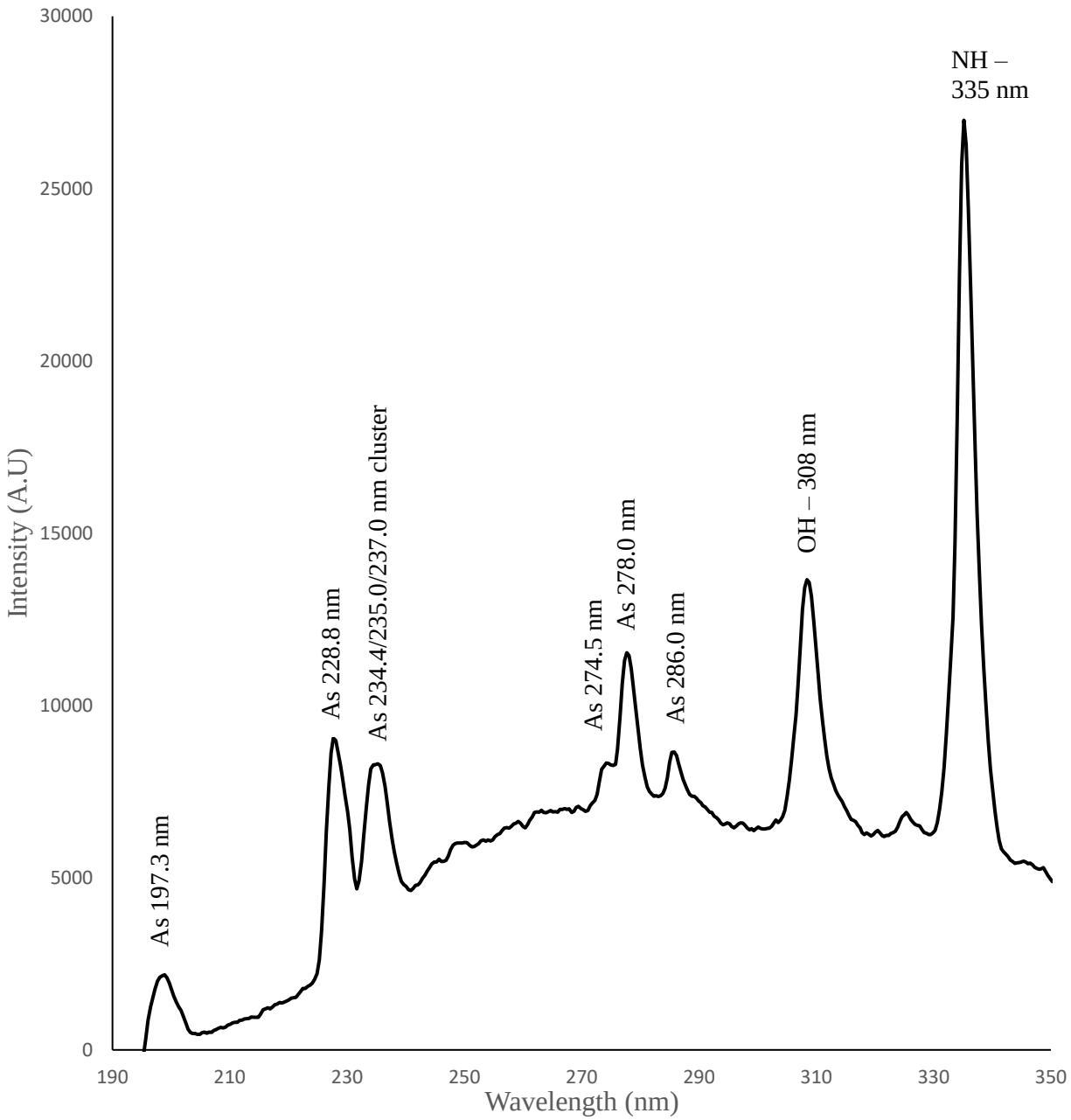

Figure 4.2: Emission spectrum of arsenic in argon microplasma. Episodes showing the arsenic signal were added to make this spectrum.

Figures 4.1 and 4.2 show the emission spectra with wavelength range of 190 nm to 350 nm because the arsenic peaks appear in this region of the spectrum only. In this spectrum, all the arsenic peaks are labeled (197.3 nm, 228.8 nm, 234.4/235.0/237.0 nm cluster, 245.6 nm, 249.2

nm, 274.5 nm, 278.0 nm, 286.0 nm, and 289.9 nm) according to information stated by NIST [51] and other literature sources [20,62,63]. The values of the transition probabilities and the excitation energy of different spectral lines mentioned in the emission spectrum are in Table 4.1. Out of these nine arsenic peaks, the peaks at 274.5 nm, 278.0 nm, and 286.0 nm are very weak peaks with low intensity. They appear on the high spectral background caused by hydrogen in the emission spectrum collected from argon microplasma. Helium microplasma being more sensitive towards As also shows the peaks at 245.6 nm, 249.2 nm and has a lower background. It also shows a weak peak at 289.9 nm, which forms a cluster with neighboring peak at 286.0 nm. The first three arsenic peaks at 197.3 nm, 228.8 nm and 234.4/235.0/237.0 nm are usually seen in the emission spectrum and out of these three peaks, the peak at 197 nm is the least impacted by the hydrogen background. This peak appears to have a lower intensity as compared to 228 nm and 234.4/235.0/237.0 nm, in argon microplasma. But the intensity of As peak at 197.3 nm is comparable to As peak at 228 nm in helium microplasma. It should be noted that the As peaks appear in the UV region, and the optical fibers often have reduced transmission of UV light [64]. Secondly, oxygen gas present in the spectrometer/atmosphere also absorbs FUV light (120 nm – 200 nm) [65]. Since the arsenic peak at 197.3 nm lies in the FUV region, it is more negatively impacted by signal loss due to optical fiber and atmospheric absorption.

Arsenic reaction trial was also conducted for the argon – 1000 ppm hydrogen microplasma. The signal for arsenic in the microplasma operated in this gas was very weak due to dimming of the microplasma caused by hydrogen released from the reaction solution, and due to the high background of its emission spectrum (which is because of the presence of hydrogen in the carrier gas itself). The emission spectrum for arsenic collected in argon – 1000 ppm hydrogen microplasma is not produced in this chapter due to low sensitivity of this microplasma for arsenic.

Similarly, other experiments with hydride generation as a sample introduction technique for arsenic were not conducted for the microplasma operated in this carrier gas mixture for the same reason, that is low sensitivity.

Element	Wavelength (nm)	Relative Intensity	Transition Probability A_{ki} (s^{-1})	Energy Levels E_i (eV) – E_k (eV)
As I	193.759	800r	2.19×10^{8}	0.00000 - 6.39885
As I	197.262	585r	2.02×10^{8}	0.00000 - 6.28523
As I	199.035	170r	Not given	1.31330 - 7.54255
As I	199.113	100r	Not given	1.31330 - 7.54010
As I	199.543	100r	Not given	2.25479 - 8.46820
As I	200.334	230r	Not given	1.35324 - 7.54010
As I	200.919	100r	Not given	2.31200 - 8.48085
As I	201.332	100r	Not given	2.31200 - 8.46820
As I	211.299	100	Not given	2.25479 - 8.12064
As I	214.408	100	Not given	2.25479 - 8.03560
As I	216.552	135	Not given	2.31200 - 8.03560
As I	228.812	350r	2.8×10^{8}	1.35324 - 6.77019
As I	234.403	35	3.5×10^{7}	2.25479 - 7.54255
As I	234.984	350r	3.1×10^{8}	1.31330 - 6.58797
As I	236.967	6r	6.0×10^{7}	2.31200 - 7.54255
As I	237.077	100r	4.2×10^{7}	2.31200 - 7.54010
As I	238.118	135r	Not given	1.35324 - 6.55850
As I	245.653	170r	7.2×10^{6}	1.35324 - 6.39885
As I	249.291	40	1.2×10^{7}	1.31330 - 6.28523
As I	274.500	40r	2.6×10^{7}	2.25479 - 6.77019
As I	278.022	170r	7.8×10^{7}	2.31200 - 6.77019
As I	286.044	100r	5.5×10^{7}	2.25479 - 6.58797
As I	289.871	50r	9.9×10^{6}	2.31200 - 6.58797
As I	506.898	100	Not given	6.55850 - 9.00377
As I	512.134	100	Not given	6.39885 - 8.81912
As I	540.813	100	Not given	6.58797 - 8.87992
As I	545.132	135	Not given	6.77019 - 9.04395
B I	249.67687	110	8.40×10^{7}	0.0000000 - 4.9642890
B I	249.77224	210	1.68×10^{8}	0.0018953 - 4.9642890
B I	286.11	20 (intensity shared by many lines)	9.9×10^{5}	6.7903466 - 11.12244

Table 4.1: Transition probabilities and energy levels of different arsenic and boron lines, as published by NIST [51].

To compare the spectral lines observed in the emission spectrum to the information available on NIST, the relative intensity, transition probability and excitation energy of the atomic levels is considered. Transition probability translates the intensity of atomic or molecular absorption or emission lines into a population of a particular species in the initial level of the transition [66]. Hence, A_{ki} is the probability per second that an atom in state k spontaneously emits light in a random direction and is de-excited to state i [67]. The E_i and E_k are the lower and upper energy levels of a line, respectively. The maximum excitation energy observed in the argon-hydrogen microplasma is 9.3 eV [68]. And the excitation energy of helium lines seen in the microplasma is 19 eV to 23.1 eV (indicating higher excitation energy of helium microplasma as compared to argon microplasma). All the arsenic lines indicated in Table 4.1 have excitation energy below 9.1 eV. This means that these lines can be easily excited by both argon and helium microplasma. The arsenic line at 193.759 nm does not appear in the spectrum due to FUV light absorbance by oxygen in the spectrometer/atmosphere or loss of the UV emission signal by the optical fiber, whereas the lines 199.053 nm to 201.332 nm may form a cluster with line 197.262 nm due to low spectral resolution. The arsenic lines between 211 nm to 216 nm do not appear in the emission spectrum obtained in this lab and have also not been observed in the emission spectra obtained from microplasma in studies done by other people [20,21]. The arsenic lines in the range 234 nm to 237 nm have a good transition probability and a good relative intensity. They are all likely to be excited by the microplasma, but they form a cluster in the emission spectrum due to low spectral resolution. The line 238.118 nm has a good relative intensity, but its transition probability is not mentioned, hence this line cannot be mentioned in the emission spectrum. The arsenic peaks 245.653 nm and 249.291 nm also appear in the emission spectrum, out of which the peak 245.653 nm is a weak line due to its lower transition probability and As 249.291 nm overlaps with Boron 249.7 nm line.

Boron (present in the form of H_3BO_3 after HG reaction) is carried by the carrier gas into the microplasma and its emission line 249.7 nm often appears for the blank reaction solution as well, when no arsine is generated and detected. The peaks 274.500 nm, 278.022 nm and 286.044 nm also appear in the emission spectrum but have lower intensity as compared to 197 nm, 228 nm, and 235 nm due to their lower transition probabilities. The peaks 274.5 nm and 278.0 nm overlap in the emission spectrum due to low spectral resolution. Arsenic line 289.871 nm has a very low transition probability (9.9×10^6) as compared to other arsenic lines. Therefore, this peak has the least intensity as compared to other As lines in the emission spectrum. Arsenic lines above 500 nm are also not seen in the emission spectrum and their transition probability has not been stated by the NIST database. The Boron line at 286.11 nm is not likely to appear and hence, not likely to interfere with arsenic 286.044 nm line due to its very low transition probability (9.9×10^5). Even the relative intensity of this line stated by NIST is too low.

4.5 Experiment for Clearing Memory

Memory effect is defined as the persistence of the analytical signal after analysis of the sample and reasonable rinse time [69]. Memory effect usually occurs due to the presence of unreacted sample and due to the partial solubility of arsine in water (as droplets of previously run reaction solution remain in the discrete flow system equipment even after the previously run reaction solution has been ejected). Memory effects for hydride generation have also been reported in the literature when this sample introduction technique is coupled to ICP [70,71]. It is important to eliminate the memory effect since it can result in biased outcomes and compromised results.

In this project, a blank reaction solution was used to clear the memory. This means that after running the arsenic reaction trial, a separate peristaltic pump was used to pass a 9% (v/v) HCl and

0.05% (m/v) $NaBH_4$ reaction solution through the equipment used for hydride generation. To determine the number of cleaning cycles needed to clear the memory, the episodic data was first collected for 3 ppm arsenic reaction trials. Afterwards, blank reaction solutions were run through the equipment and their episodic data was collected to see if there were any arsenic peaks in the data. The presence of arsenic peaks in the episodic data of the cleaning cycle would show that memory had not been cleared. Similarly, absence of arsenic peaks in the episodic data of the cleaning run would suggest that all the memory had been cleared from the equipment, and no memory effect would be seen in the next arsenic reaction trials.

It was observed that after running the arsenic reaction trials with the 3 ppm arsenic solution, the arsenic signal appeared in a maximum of 3 cleaning cycles only. Afterwards, no arsenic signal was seen in the next cleaning run. This indicates that 3 cleaning cycles are enough to clear the memory for a 3 ppm arsenic reaction trial. The episodic data collected for arsenic reaction trial and cleaning cycles can be found in Figures 4.3 and 4.4, respectively.

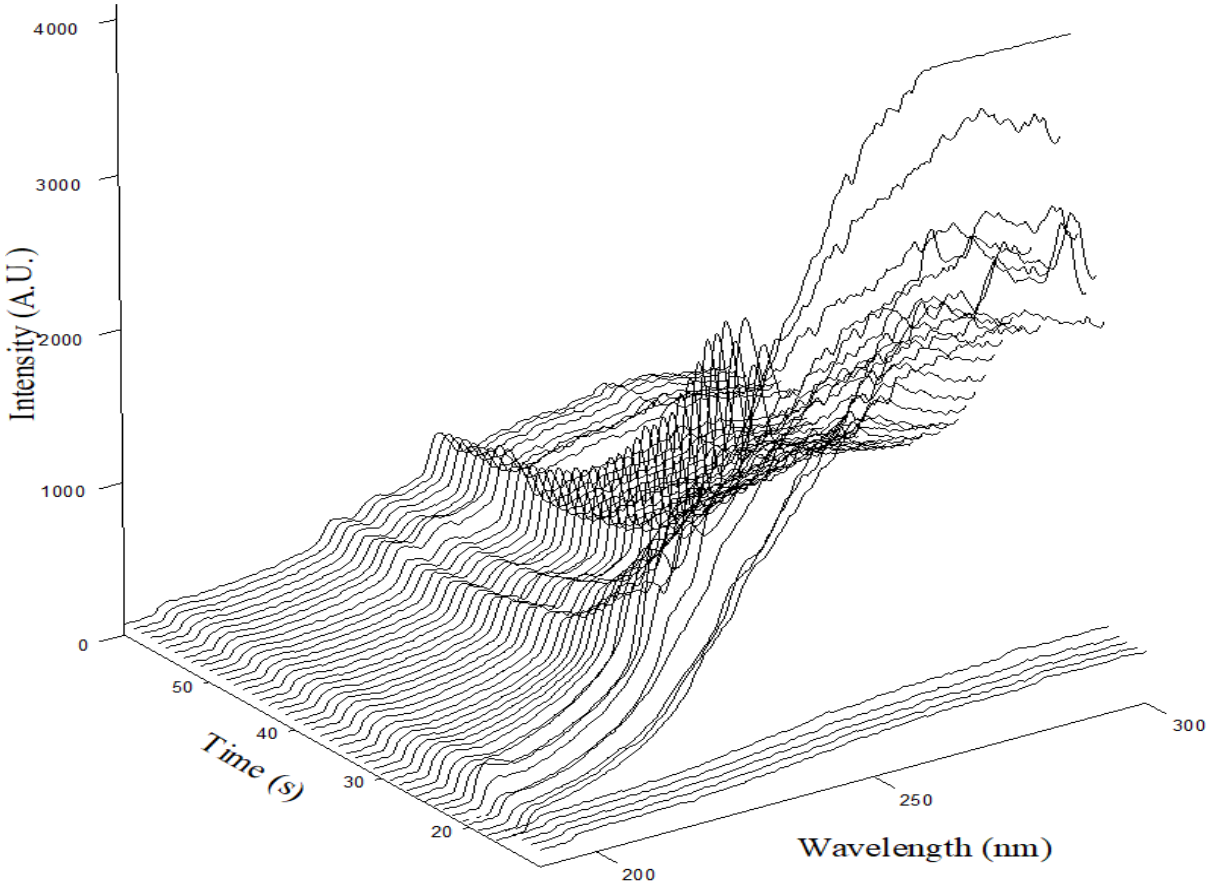

Figure 4.3: Episodic data for a 3 ppm arsenic reaction trial at integration time 500 ms.

A.

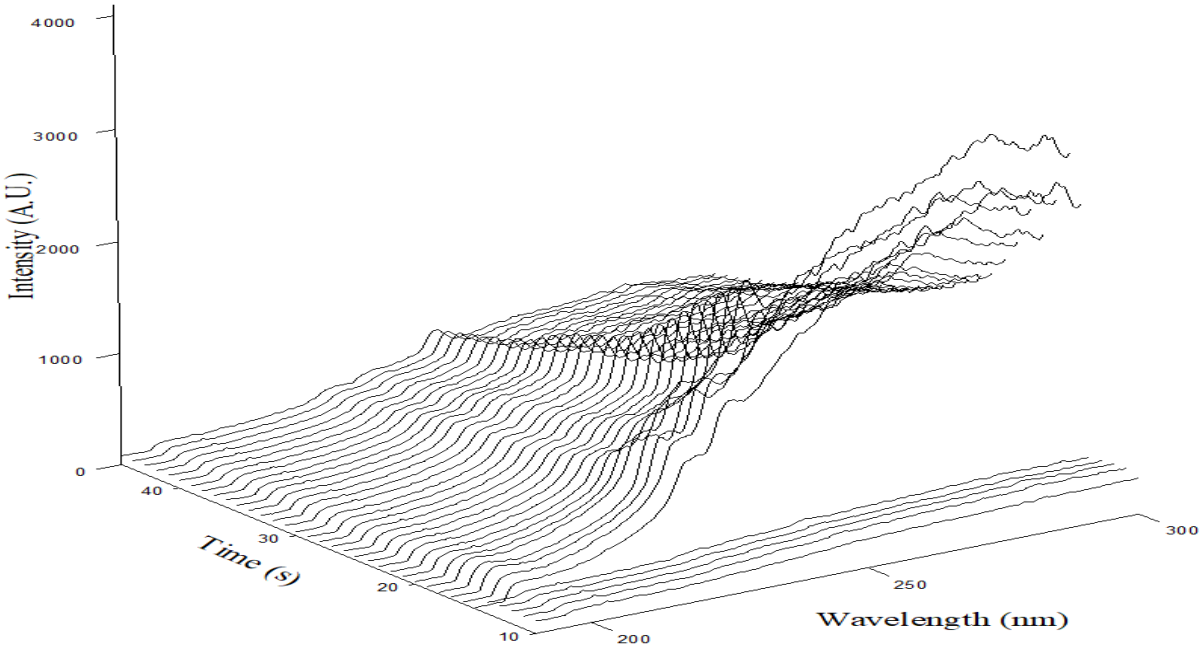
4000
3000
2000
1000
0
Intensity (A.U.)
40
30
20
10
Time (s)
200
250
300
Wavelength (nm)

B.

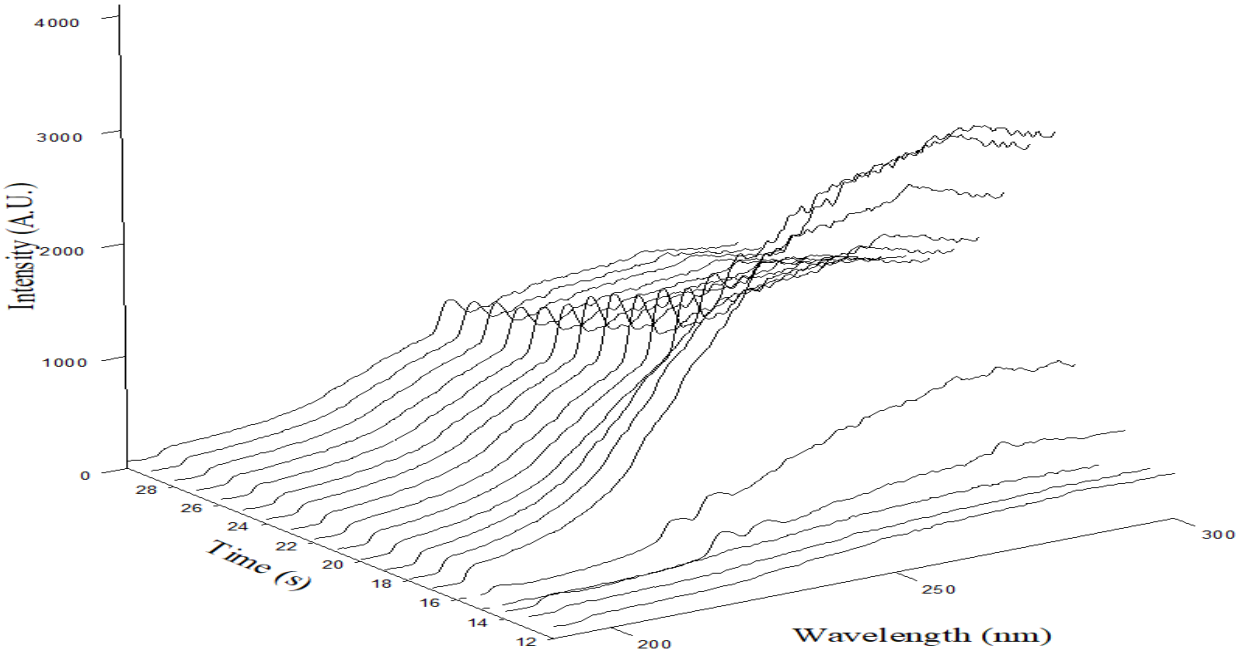
4000
3000
2000
1000
0
Intensity (A.U.)
28
26
24
22
20
18
16
14
12
Time (s)
200
250
300
Wavelength (nm)

C.

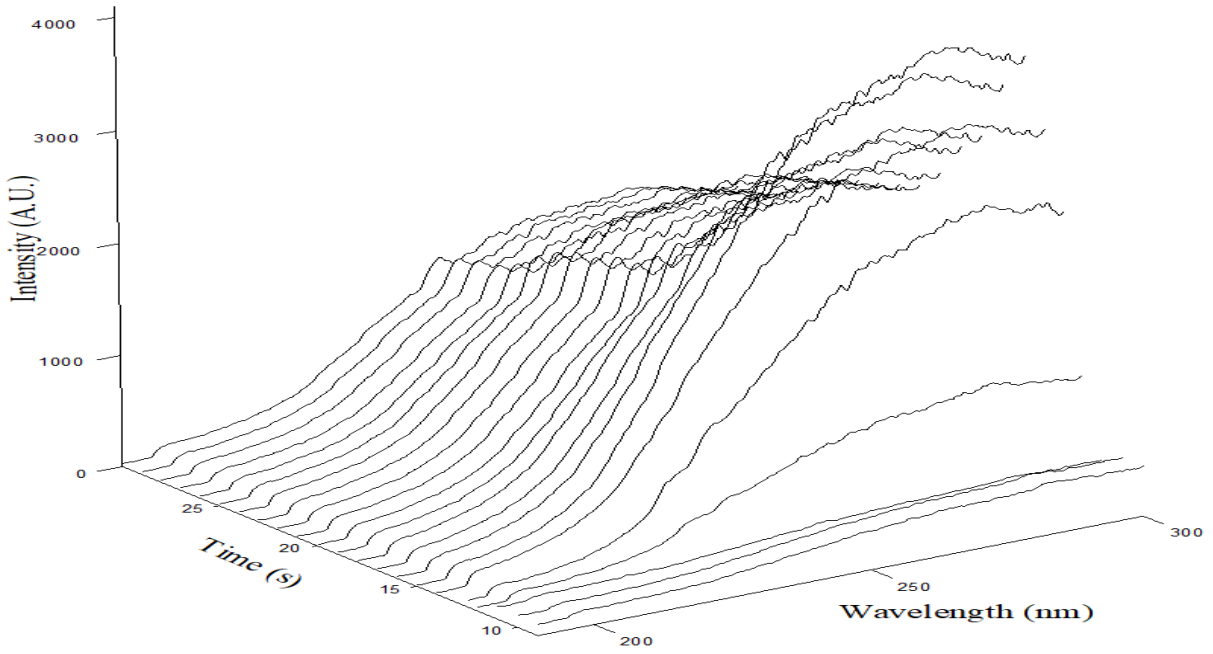

D.

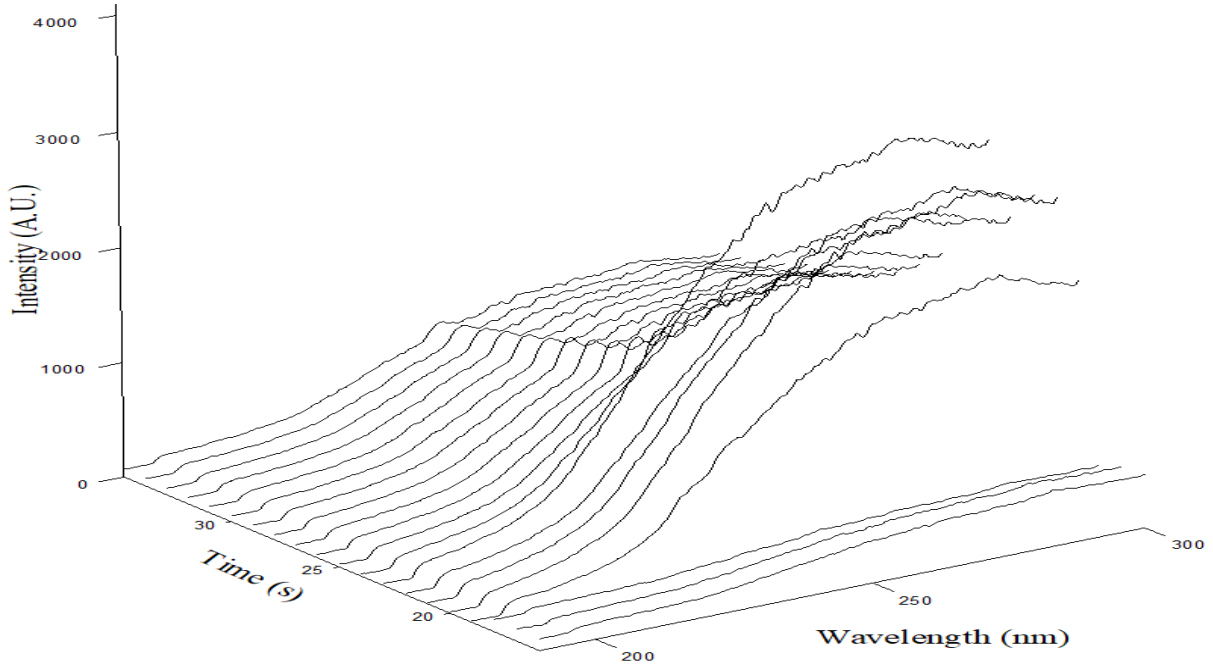

Figure 4.4: Episodic data for A. first cleaning run, B. second cleaning run, C. third cleaning run, and D. fourth cleaning run, after arsenic reaction trial. The integration time for these episodes was 500 ms.

The signal intensity of arsenic in arsenic reaction trial (Figure 4.3) is low due to low spectral sensitivity and low concentration of the arsenic sample (3 ppm). Episodes with high background show a low intensity arsenic signal which tails even when the background decreases in subsequent episodes. The signal intensity of arsenic in the first cleaning run is lower as compared to that in arsenic reaction trial. In the second cleaning run, there are only two episodes which show the arsenic signal. Whereas the arsenic signal in the third cleaning run has a very low intensity in the first two episodes, close to being negligible. The signal for the arsenic peaks in the third cleaning cycle was better than the one shown above for only a few trials. For other trials, this signal was negligible in the 3^{rd} cleaning cycle. Similarly, the 4^{th} cleaning run does not show any arsenic peak. Hence, it was assumed that three cleaning cycles are enough to clear all the memory.

The same experiment was conducted for 30 ppm arsenic sample, since 30 ppm As sample was used for finding the best observation position for arsenic over the microplasma tube – experiment discussed in section 4.6. It was found that when the concentration of arsenic was 30 ppm in the sample, 5 cleaning runs were required to clear all the memory.

4.6 Best Observation Position for Arsenic Emission Signal Over the Microplasma Tube

The intensity of the analytical signal and the spectral background of the emission spectrum observed in the microplasma depends on the observation position [6]. Therefore, it is important to find the best observation position for arsenic signal over the microplasma for the purpose of recording a high intensity emission from the analyte. The observation position was varied by changing the position of the optical fiber cable over the microplasma tube by moving the optical fiber cable away from one front electrode (electrode through which the analyte and carrier gas

were introduced) towards the other, as represented in Figure 4.5. This experiment was conducted for both carrier gases, argon, and helium.

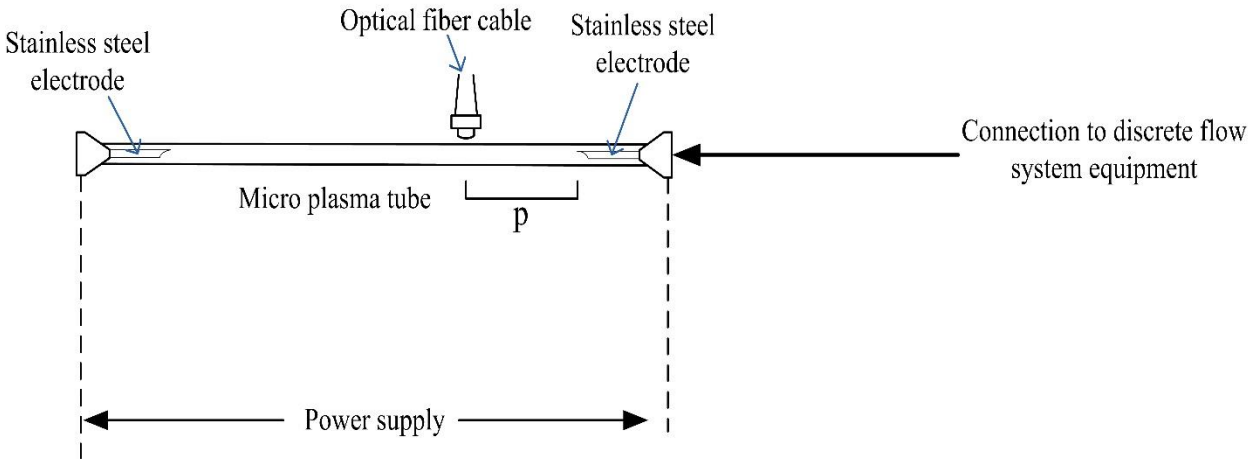

- p is the distance between the stainless steel electrode and the optical fiber cable

Figure 4.5: Diagram showing the position of optical fiber cable over the microplasma tube. The distance between the optical fiber cable and the electrode, p, was changed for different trials.

4.6.1 Equipment and Reagents

For this experiment, the equipment for the discrete flow system, as described in Chapter 2 – section 2.3.2, was used to collect data for arsenic reaction trials. The sample solution consisted of 30 ppm As (III) made in a 9% (v/v) HCl solution and the reagent solution consisted of a 0.05% (m/v) $NaBH_4$ solution made in a 0.5% (m/v) NaOH solution.

4.6.2 Method for Running the Reaction Trials

For the arsenic reaction trials conducted at different optical fiber positions to be comparable, it is important to make sure that all other experimental conditions were the same. This includes the flow rate of the carrier gas, the flow rate of the reaction solution which is pushed by the peristaltic

pump and the amount of reaction solution in the GLS for each trial. The flow rate of the carrier gas and the pump speed of the peristaltic pump were kept constant for the reaction trials. However, it was hard to control the amount of reaction solution in the GLS for each trial. This is because it is not only the peristaltic pump that pushes the reaction solution through the reaction coil, hydrogen gas produced in the reaction coil also pushes the reaction solution forward. As the amount of reaction solution introduced in the GLS changes, the amount of arsine and hydrogen gas carried towards the microplasma also changes, introducing variability in the intensity of arsenic signals. The amount of reaction solution in the GLS was measured by a vernier caliper as distance between the lower meniscus of the reaction solution and the valve of the GLS. Therefore, for this experiment, the arsenic reaction trials with same amount of reaction solution in the GLS were compared.

The arsenic reaction trials were run to collect episodic data for arsenic signal, followed by clearing the memory by passing a blank reaction solution. The microplasma was turned on for 30 – 40 seconds before running the trial. Afterwards, the episodic data collection at an integration time 100 ms, was started about 4 seconds before the peristaltic pump turned was on. As the peristaltic pump turned off after running for a desired amount of time, the two-way valve between the GLS and the reaction coil was quickly closed to prevent further movement of reaction solution into the GLS. The episodic data collection was stopped only after arsenic peaks seemed to disappear or became very low in intensity in the emission spectrum seen on the computer. After running the arsenic reaction trials, the blank reaction solution was run through the system 5 times to clear all the memory. Afterwards, the blank reaction solution was ejected from the reaction coil by opening the three-way valve towards the ejection route for 7 minutes. After this, the plug of the

three-way valve was turned towards the solution inlet route and allowed to equilibrate for about 1.5 - 3 minutes before starting a new arsenic reaction trial.

4.6.3 Background Correction of Spectral Data

Background correction was applied to all the emission spectra collected in this experiment, because the influx of hydrogen from the reaction solution into the micro plasma shifted the spectral background. For emission spectra collected from both helium and argon micro plasma, a polynomial fitting method was used to correct the baseline, using the OriginPro 2023b software. This software has been used for graphing and analysis by several papers published in literature. In this software, the Adjacent-Averaging smoothing is used with a window size set at 3 and a threshold set at 0.05.

Polynomial fitting method is widely used for baseline correction of different kinds of spectra, due to its simplicity and efficiency [72,73]. It uses the least square method to fit the spectral baseline [74]. Polynomial order allows the user to fit the estimated background over the parts of spectrum that may be considered background by the user. It allows the user to adjust the estimated background smoothness [75]. The recommended range of polynomial orders for background fitting is 4 – 6 [72]. Similarly, the coefficients of the polynomial are changed to approach the shape of actual baseline. Therefore, the calculated polynomial function form is closer to actual baseline [74].

4.6.3.1 Processing Episodic Data Collected from Helium Microplasma

The episodic data collected from Helium microplasma was also processed in OriginPro 2023b for background removal. For episodic data collected from arsenic reaction trials in helium microplasma, only 10 episodes (starting from the episodes that began to show the As signal) were

added and plotted against the wavelength (nm). Spectral data in the wavelength range of 190 nm to 302 nm was imported into OriginPro 2023b for further processing. Since the background in spectral data generated from helium micro plasma was already low, 6 – 7 anchor points were used to generate a 4^{th} order polynomial fit. The anchor points were generated by using the 2^{nd} Derivative (zeroes) method but were manually replaced to generate a matching baseline. For emission spectra collected at positions 0 cm and 0.34 cm, 7 anchor points (at 194 nm, 206 nm, 222 nm, 241 nm, 256 nm, 272 nm, and 301 nm) were used to generate baseline because spectral background at these observation positions was higher. Whereas, for emission spectra collected at other three observation positions, 6 anchor points (at 194 nm, 207 nm, 222 nm, 253 nm, 271 nm, and 301 nm) were used to generate a baseline. Afterwards, this baseline was subtracted from the raw spectral data to apply background correction.

A.

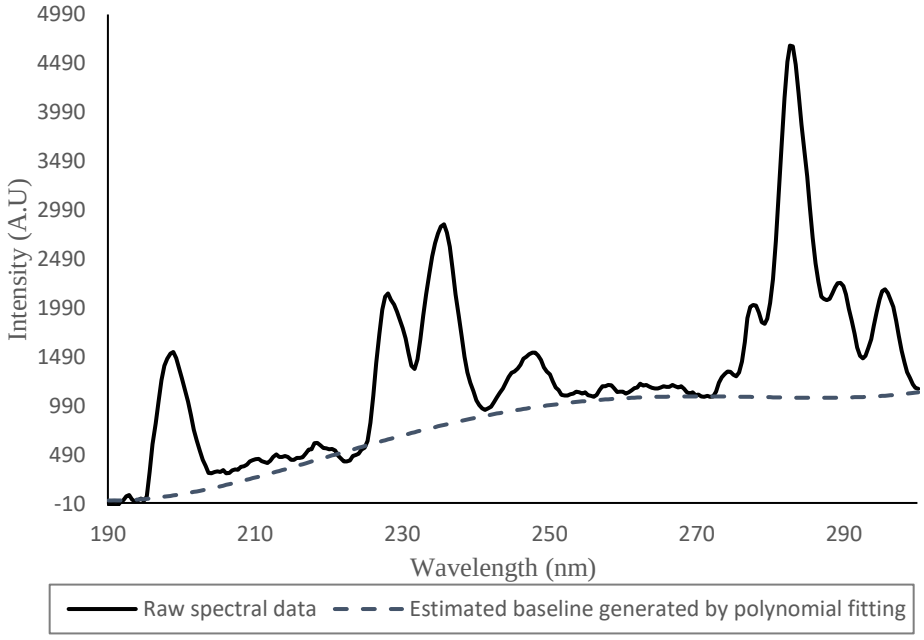

B.

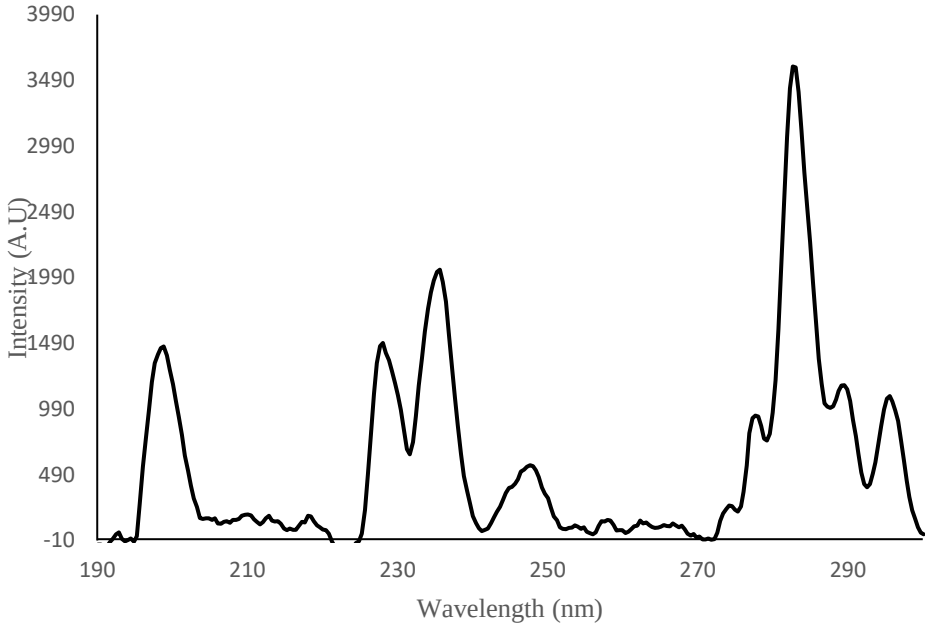

Figure 4.6: A. Raw spectral data for arsenic reaction trial, collected from helium microplasma along with baseline generated by polynomial fitting. B. Spectral data after background correction.

4.6.3.2 Processing Episodic Data Collected from Argon Microplasma

Episodic data was collected for arsenic reaction trials conducted with argon microplasma. Afterward, 22 episodes with the arsenic signal were added, starting from episodes beginning to show the arsenic signal. This added signal was plotted against the wavelength (in nm) to form an emission spectrum for each of the arsenic reaction trials at different observation position, p.

The data from this added signal in the wavelength range of 190 nm to 300 nm was imported into OriginPro 2023b software for background correction. The eleven anchor points for making the polynomial fit for baseline were placed on the emission spectrum by using the 2^{nd} Derivative (zeroes) method by the software. However, afterwards, the positions of these anchor points were manually adjusted to match the polynomial fit with the baseline of the emission spectrum, as illustrated in Figure 4.7. The anchor points were placed at similar wavelength positions over the emission spectra for different observation positions to get consistent results. The anchor points for emission spectra from argon microplasma were placed at: 194 nm, 206 nm, 211 nm, 220 nm, 223 nm, 240 nm, 251 nm, 260 nm, 269 nm, 293nm, and 299 nm. The polynomial function of order 5 (mentioned as poly5 in the software) was used to generate a polynomial fit which was subtracted from the spectral data.

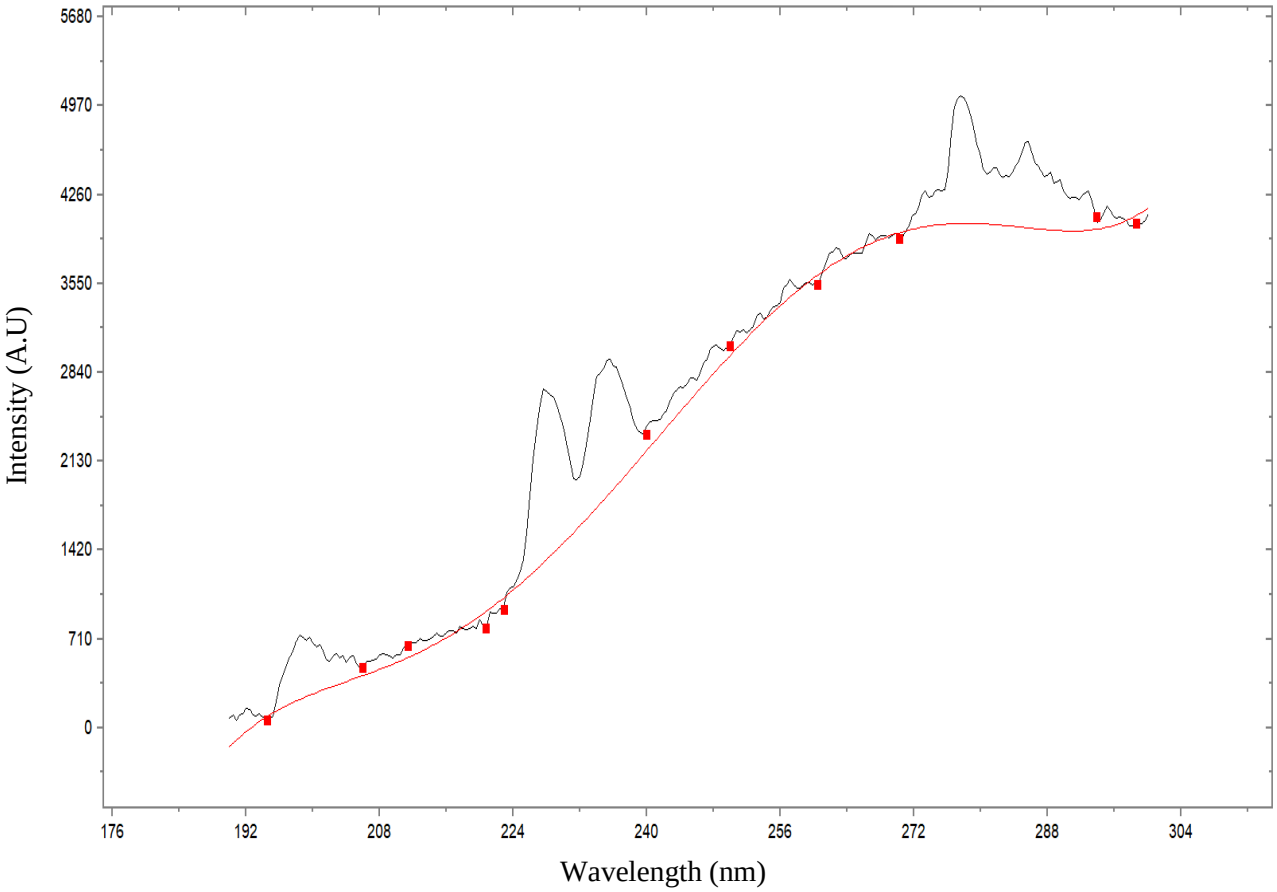

Figure 4.7: Emission spectrum for arsenic reaction trial after adding 22 episodes, imported into the OriginPro 2023b software for processing. The anchor points (■) used to generate the baseline (—) are shown.

A.

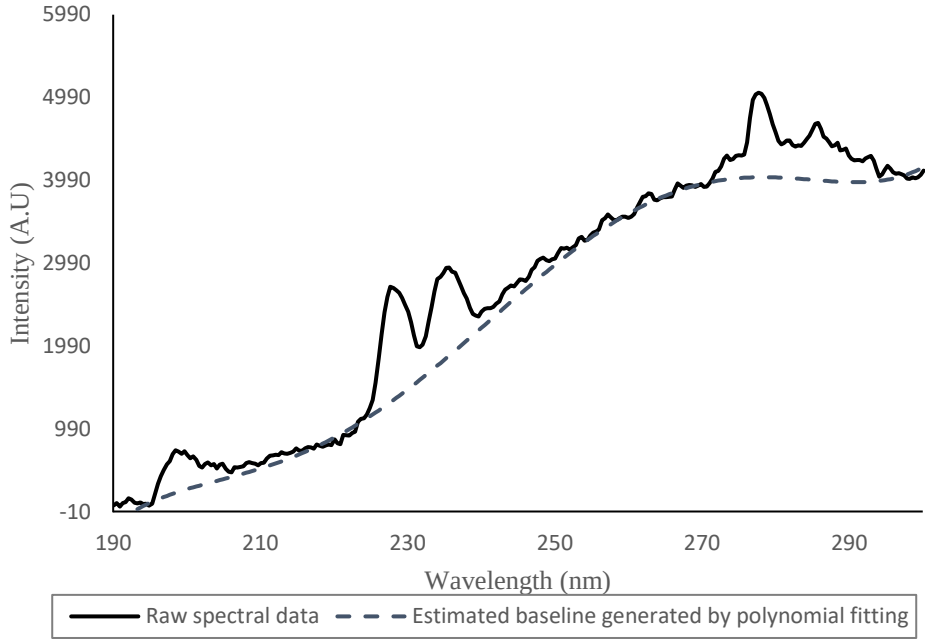

B.

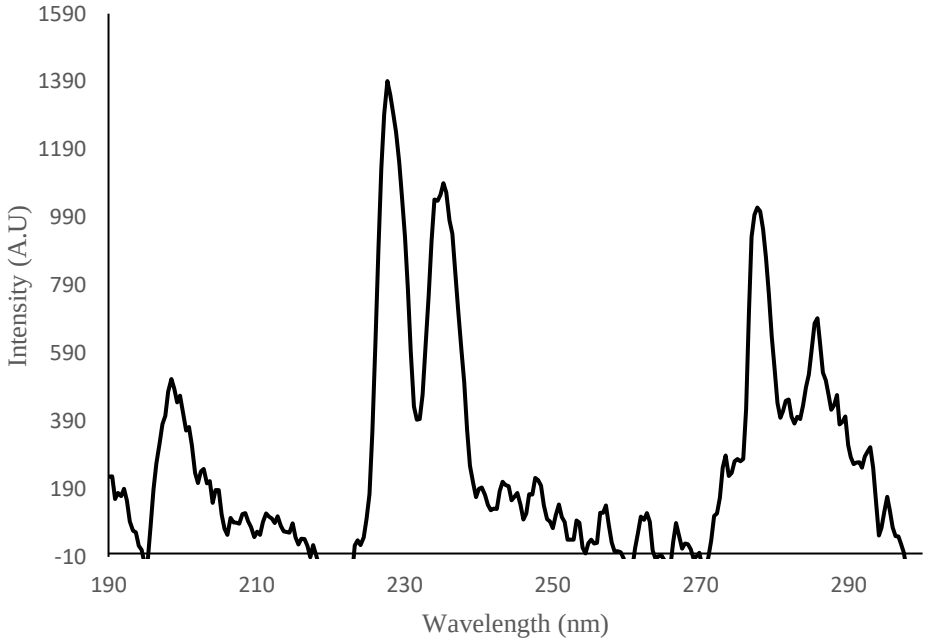

Figure 4.8: A. Raw spectral data for As reaction trial in argon microplasma with estimated baseline generated by a polynomial fitting. B. Spectral data after background correction.

4.6.4 Results for 14.9-watt Helium Microplasma

Hydride generation was coupled to helium microplasma for introducing arsenic into the microplasma and the best observation position for arsenic over the microplasma tube was determined by moving the optical fiber cable over the microplasma tube. The positions of the optical fiber cable, p, at which the arsenic signal was collected were 0 cm, 0.38 cm, 0.84 cm, 1.34 cm, and 1.84 cm. For each of the trials, the amount of reaction solution introduced in the GLS was 0.6 – 0.7 mL and episodic data was collected by the help of the integrating spectrometer. Afterwards, the initial 10 episodes showing the arsenic signal were added in the episodic data of each trial and compared for results. The emission spectra obtained after adding the first 10 episodes from each trial at a different observation position are given in Figure 4.9. All the emission spectra are plotted in the same figure for the purpose of comparison.

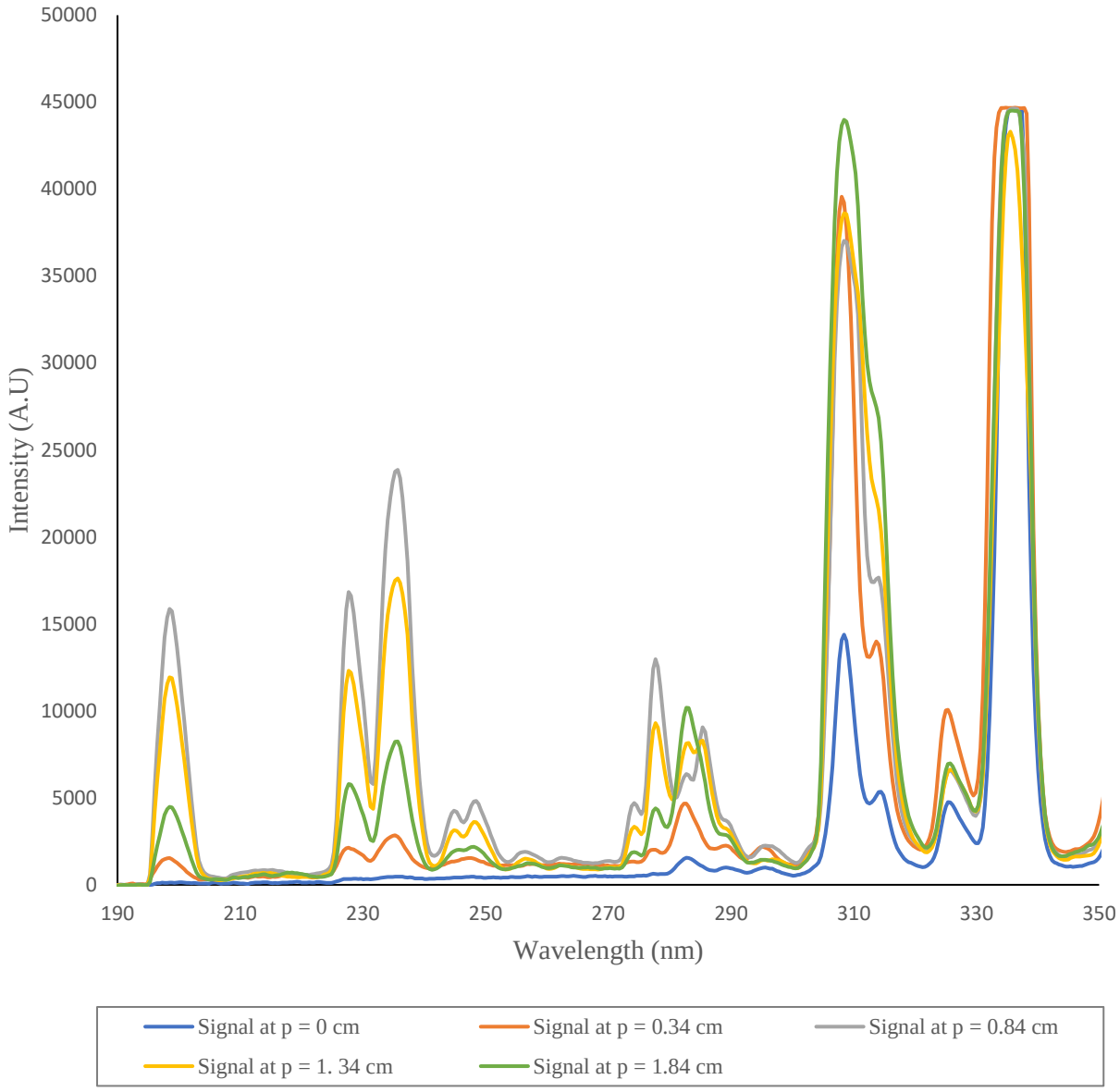

Figure 4.9: Emission spectra for arsenic reaction trials conducted for different observation positions, p, over the helium microplasma tube.

The arsenic peaks were very weak over and near the front electrode, through which the analyte and carrier gas were introduced. And moving the optical fiber cable away from the front electrode enhanced the intensity of the arsenic peaks. The intensity of arsenic peaks was the highest at a position of 0.84 cm from the front electrode. The other contributing factor in the change in intensity

of arsenic peaks was the impact of hydrogen on the emission spectrum. Moving the optical fiber cable away from the electrode made the impact of hydrogen more pronounced, even though the amount of hydrogen released from the reaction solution is not high enough to turn off the microplasma. At a position of 1.84 cm from the electrode, the arsenic signal seemed to dim after a few episodes, due to introduction of hydrogen in the microplasma tube. But at the position 0.84 cm, the dimming of the signal was not too significant. The reduction in intensity of helium peaks due to introduction of hydrogen in the microplasma tube also depended on the observation position.

The intensity of arsenic peaks at different observation positions is mentioned in Table 4.2 and plotted in Figure 4.10.

Distance of Optical Fiber Cable from Electrode (p)	**Intensity of Arsenic Peaks after Adding 10 Episodes from the Episodic Data and Applying Background Correction**		
	Intensity of As 197 nm	Intensity of As 228 nm	Intensity of As 235/237 nm
0 cm	133	150	203
0.34 cm	1465	1492	2050
0.84 cm	15817	16094	Saturates
1.34 cm	11888	11777	Saturates
1.84 cm	4410	5230	7578

Table 4.2: Emission intensities of different arsenic peaks observed at different positions over the helium microplasma tube.

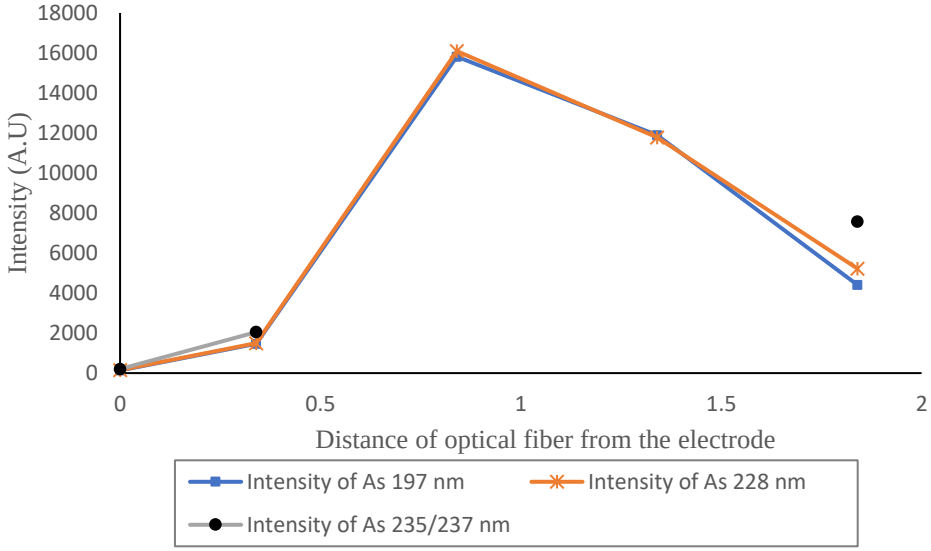

Figure 4.10: Graph showing the change in intensity of the arsenic peaks at 197 nm, 228 nm, and 235/237 nm with change in the observation position over the helium microplasma tube.

The As peak at 235/237 nm was saturating over a few episodes in the trials for positions at 0.84 cm and 1.34 cm, therefore, its true intensity cannot be determined for these trials. Hence, two points are missing in the graph of intensity VS position for this peak in Figure 4.10. This graph just proves that the arsenic signal has the highest intensity at 0.84 cm away from the front electrode.

4.6.5 Results for 6.2-watt Argon Microplasma

The positions of the optical fiber, p, at which the arsenic reaction trials were conducted were 0 cm, 0.38 cm, 0.74 cm, 1.34 cm, 1.84 cm, and 2.38 cm. The total volume of the reaction solution entering the GLS for each of the trials mentioned in this section was 0.4 mL. As mentioned earlier, the emission spectrum for each position was made by adding 22 episodes showing the arsenic signal.

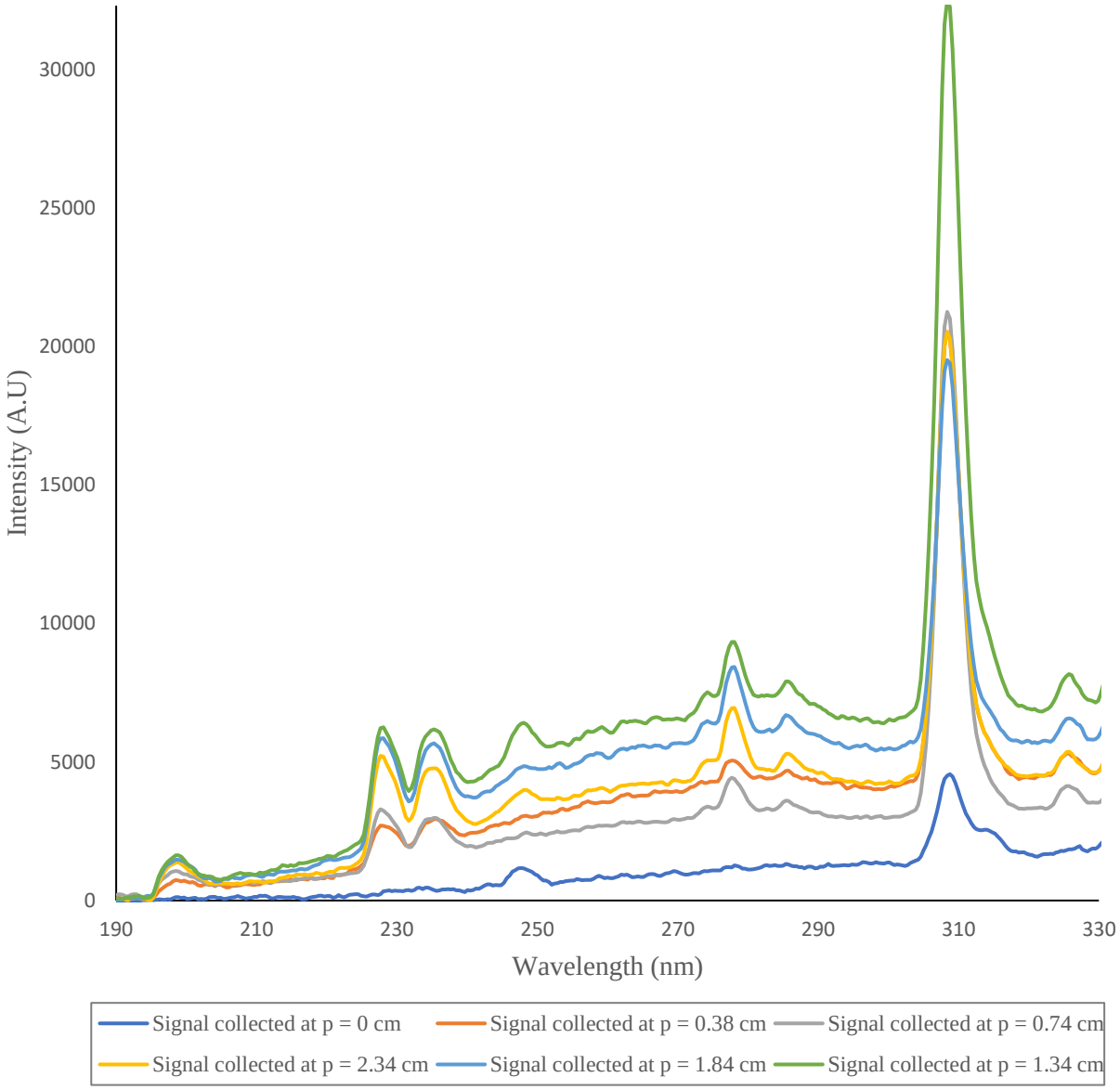

Figure 4.11: Emission spectra for arsenic reaction trials conducted for different observation positions over the argon microplasma tube.

It is only at a position, p, of 0 cm, where the argon peaks intensity is the highest. Whereas, for other observation positions, the argon peaks intensities were similar (not indicated in Figure 4.11), suggesting that the impact of hydrogen on the emission intensities of the argon peaks was not

position dependent. The intensity of OH peak at 308 nm is similar for different observation positions, indicating that the efficiency of the cold trap in removing water vapors was about the same for all these trials. The other changes seen in the emission spectra is the increase in background of emission spectrum due to hydrogen. The shift in background due to hydrogen is the least at position 0 cm and is higher for the positions 1.34 cm and 1.84 cm, as compared to other positions. Change in optical fiber position [6] and a small change in the amount of hydrogen released by the reaction solution caused due to small differences in the concentration of the $NaBH_4$ solution made for some trials, contributes towards a change in the intensity of the background caused by hydrogen.

Change in intensity of arsenic peaks can only be determined by applying a background correction, as mentioned in section 4.6.3 above. The intensities of the background corrected arsenic peaks at different observation positions are mentioned in Table 4.3 and are plotted in Figure 4.12.

Distance of Optical Fiber Cable from Electrode (p)	Intensity of Arsenic Peaks in Emission Spectrum (made by adding 22 episodes) after Background Correction		
	Intensity of As 197 nm	Intensity of As 228 nm	Intensity of As 235/237 nm
0 cm	Negligible	Negligible	Negligible
0.38 cm	514	1392	1091
0.74 cm	814	2081	1409
1.34 cm	1374	3735	2773
1.84 cm	1177	3741	2773
2.34 cm	1176	3654	2647

Table 4.3: Emission intensities of different arsenic peaks observed at different positions over the argon microplasma tube.

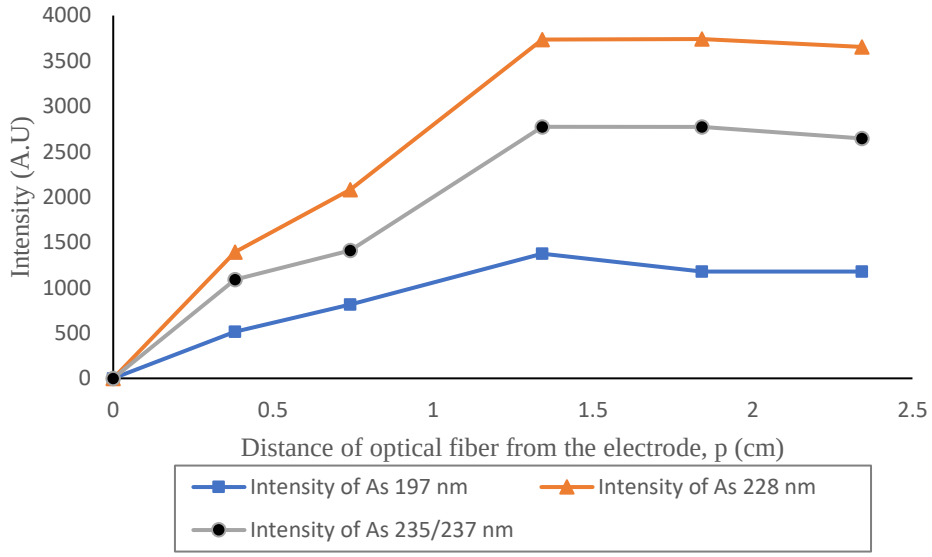

Figure 4.12: Graph showing the change in intensity of arsenic peaks at 197 nm, 228 nm, and 235/237 nm with change in observation position over the argon microplasma tube.

The curve for peak at 197 nm is slightly different from the other two curves because this peak is least impacted by the shift in background. The arsenic signals are more intense further away from the front electrode, more specifically at 1.34 cm to 1.84 cm from the front electrode. The difference in the emission intensities at positions 1.34 cm, 1.84 cm and 2.38 cm is not large.

By comparing the results for this experiment between helium and argon microplasma, it was found that the best observation position for the As signal is different for microplasma operated in different gases. This is because both helium and argon are different gases with different physical and chemical properties. Helium is ten times lighter than argon, therefore, its plasma has lower electron density as compared to argon plasma [58]. Argon is easier to ionize as compared to helium, therefore, for equi-operation plasma, the electron temperature of argon is always lower than that of helium plasma [58]. The difference in the properties of helium and argon microplasma, mainly electron density, seems to be responsible for the different results obtained in this experiment.

4.7 Difference in the Arsenic Signal Collected in Argon and Helium Microplasma

Coupling hydride generation with argon and helium microplasma generated different results. Although helium microplasma is more disturbed by the hydrogen generated from hydride generation reaction, its emission spectrum does not show high disturbance in the background, contrary to what is observed for argon emission spectrum. In addition to that, the arsenic signals were more intense in helium microplasma as compared to argon microplasma. Intensity of arsenic peaks in helium microplasma is about 6 – 9 times higher than that observed in argon microplasma. This can be seen in Figure 4.13 which shows the episodic data for the reaction of 30 ppm arsenic solution with a 0.05% (m/v) $NaBH_4$ solution (collected at IT = 100 ms). Figure 4.13A shows the

episodic data collected for helium microplasma and Figure 4.13B shows the episodic data collected for argon microplasma. The amount of reaction solution introduced in the GLS for both trials exhibited in Figure 4.13, was about the same, that is 0.8 mL. More intense arsenic signal in the helium microplasma may be due to the higher excitation potential of helium as compared to that of argon. It may also be due to higher power consumption by helium microplasma. As described earlier, it is only the input DC voltage of the HVAC power supply that can be adjusted manually; the input current adjusts on its own. Both the argon and helium microplasma were operated at 11.8 V, but the helium microplasma drew more current, resulting in its higher power input of 14.9 watts, instead of 6.2 watts, which was the power input for argon microplasma. Hence, helium microplasma provides a benefit of better sensitivity as it generates higher intensity arsenic signal with low background.

A.

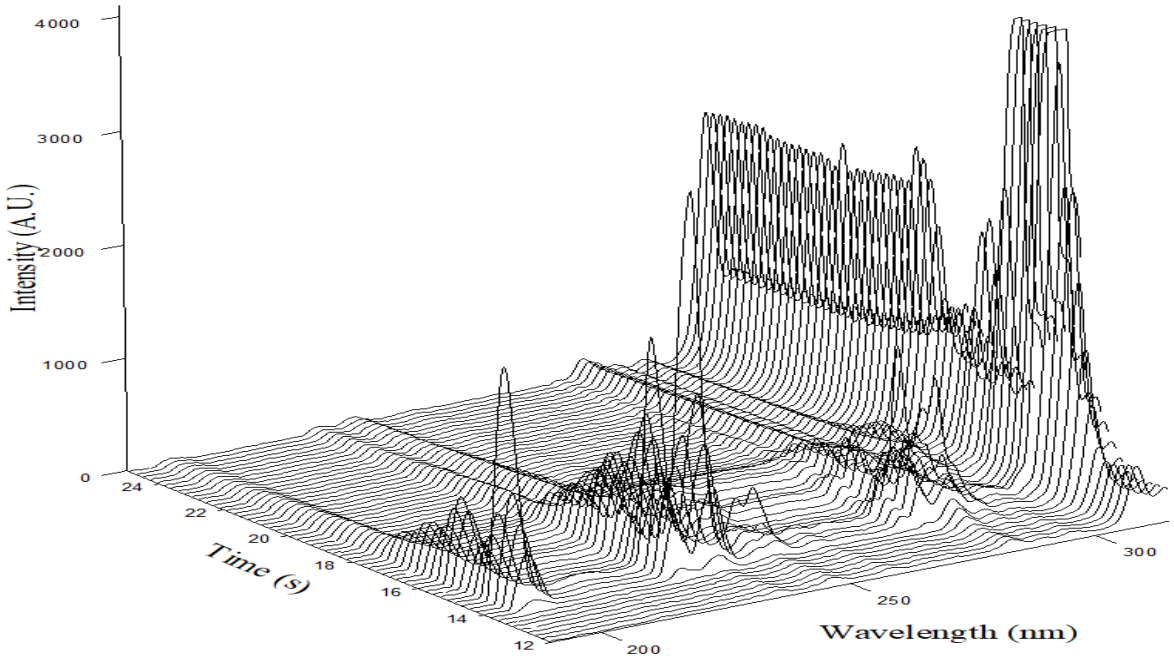

B.

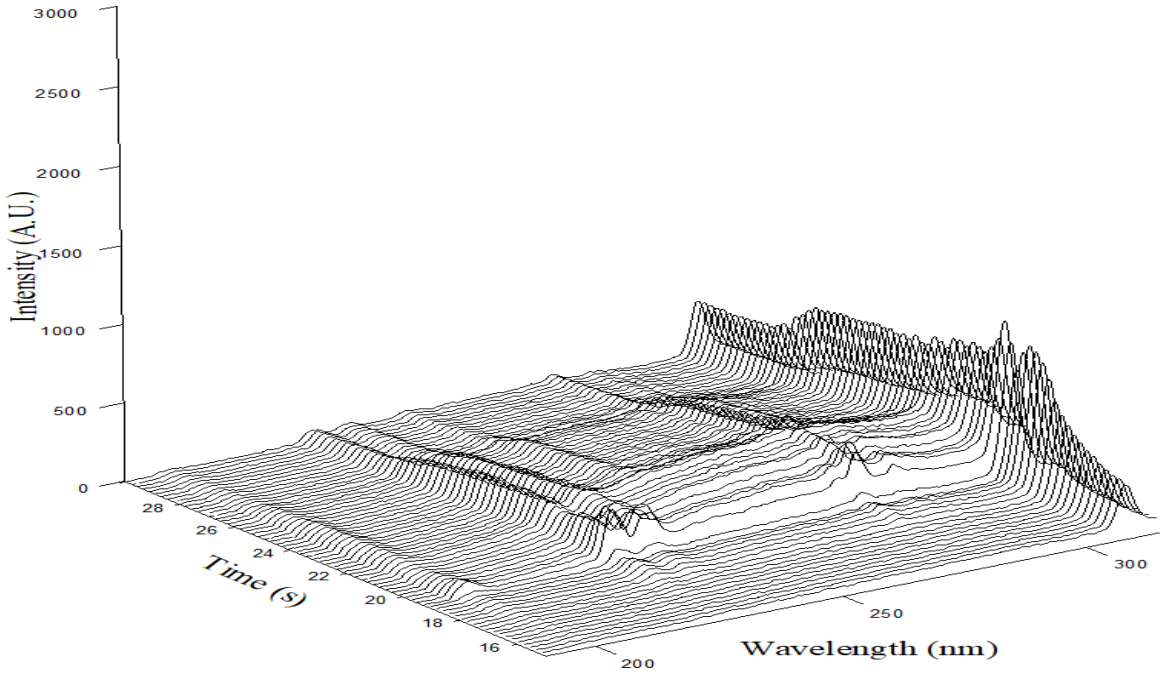

Figure 4.13: Episodic data for reaction of 30 ppm arsenic with 0.05% $NaBH_4$ solution collected for A. helium microplasma and B. argon microplasma, at IT = 100ms.

4.8 Estimating the Detection Limit

The limit of detection is defined as the smallest signal from the analyte that can be reliably seen against the background noise from an analytical instrument. It is the amount of analyte that generates a signal three times more intense than the background noise [76]. In this section, the limit of detection for arsenic in helium and argon microplasma is estimated.

4.8.1 Procedure for Running the Reaction Trials

The data for this section was collected in the same way as explained earlier in this chapter, but this time the episodic data for the first cleaning cycle was also collected. For helium microplasma, arsenic reaction trial with 30 ppm As solution and 0.05% $NaBH_4$ solution was run at IT = 100 ms. Whereas for argon microplasma, the arsenic reaction trial with 3 ppm As solution and 0.05% $NaBH_4$ solution was run with an integration time (IT) of 500 ms on the spectrometer. After collecting the data for the arsenic reaction trial, the sample reaction solution was ejected from the GLS by the help of its valve and the reaction solution in the reaction coil was ejected by the back flow of the carrier gas after the three-way valve was opened towards the ejection arm. The ejection through the reaction coil continued for 2 minutes (period set arbitrarily), but it did not get rid of all the arsenic reaction solution from the previously run trial, as some of the droplets from previous trial remained in the equipment. The pump for the blank reaction solution was connected to the solution inlet arm of the three-way valve and equilibration of the discrete flow system equipment with carrier gas was carried out for 1 minute (period set arbitrarily). After this equilibration, the episodic data for the first cleaning cycle was collected as the blank reaction solution was run through the equipment and introduced in the GLS. The first cleaning cycle often shows high intensity arsenic signal, as shown in section 4.5. Therefore, the arsenic signal collected for the first cleaning cycle can also be added to the arsenic reaction trial to improve the detection limit, as this

signal is caused by the solution left over from the prior trial. Moreover, the equipment is fully clean before the experiment is started and 3 – 5 cleaning cycles after each arsenic reaction trials clear all the memory.

As seen in Chapter 3, the influx of hydrogen into the microplasma often disturbs the background of the emission spectrum, especially for argon microplasma. Therefore, blank reaction trials, consisting of 9% (v/v) HCl and 0.05% (m/v) $NaBH_4$ were also conducted, and their episodic data was collected. The emission spectrum for the blank reaction can be subtracted from that of arsenic reaction to apply background correction.

For determining the detection limit, all the episodes showing the arsenic signal were added to avoid any signal loss.

4.8.2 Results for Helium Microplasma

For the emission spectrum collected from helium microplasma, the impact of hydrogen on the background was very low. Therefore, to apply the background correction to data for arsenic reaction trial, subtracting the first episode (episode collected without any influx of hydrogen or arsine into the microplasma) from all the episodes was sufficient to remove all the background. However, the blank reaction solution used for clean-up seems to have more dissolved air, which impacted its background. The peaks seen for the blank reaction trial may also be due to more excitation of impurities as the amount of hydrogen introduced in the microplasma was higher (hydrogen was not being used to make arsine).

To measure the detection limit, As peak at 197 nm is used as this peak has an intensity close to that of peak at 228 nm, but is not impacted by background from impurities in helium gas cylinder or from air dissolved in sample solution, and is baseline resolve

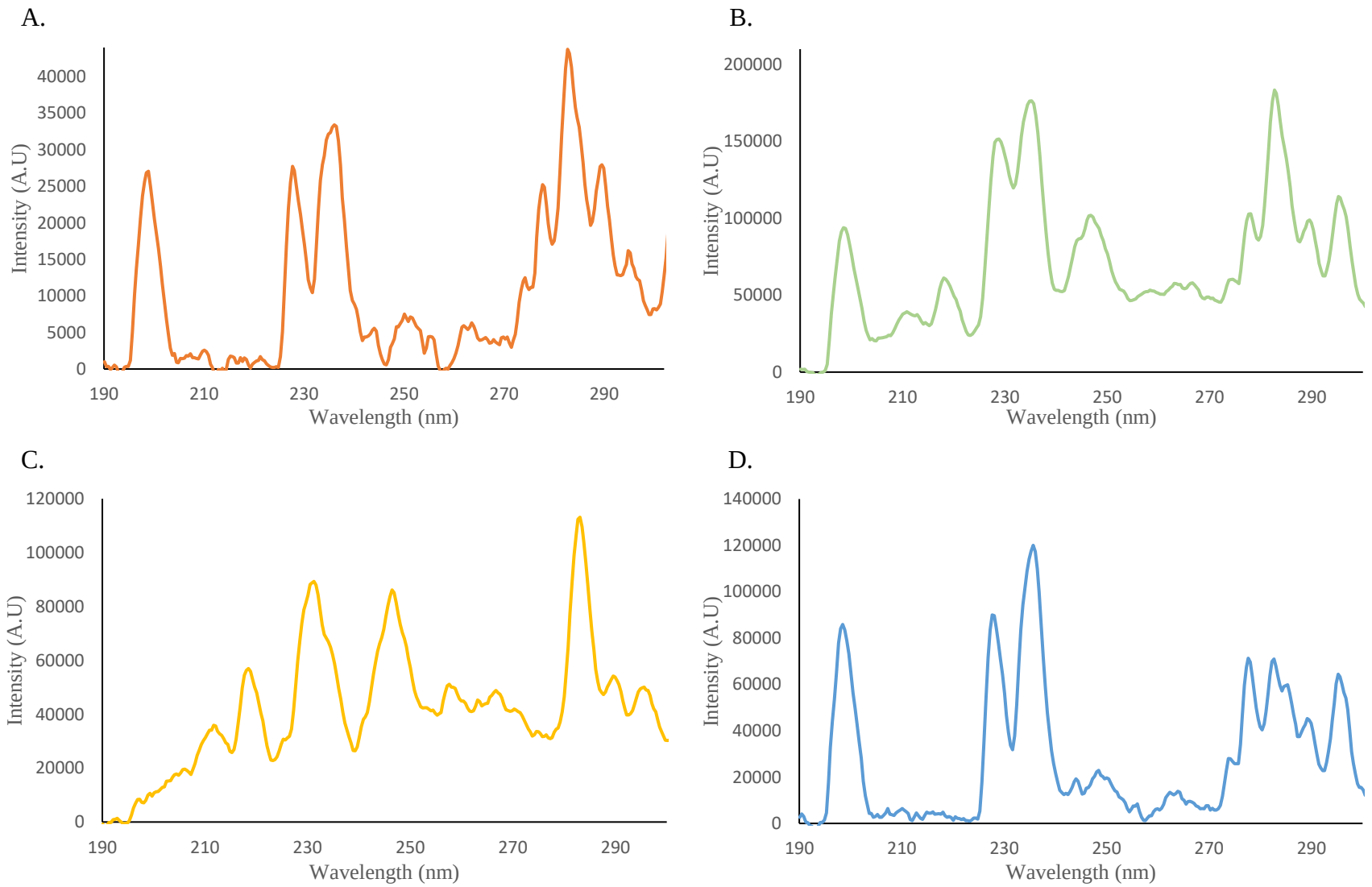

Figure 4.14: Emission spectrum for A. total signal collected for the arsenic reaction trial, B. sum of signal from the arsenic reaction trial and its cleaning cycle, C. blank reaction trial, and D. background corrected signal.

All the emission spectra in Figure 4.14 are plotted together in Figure 4.15 for comparison.

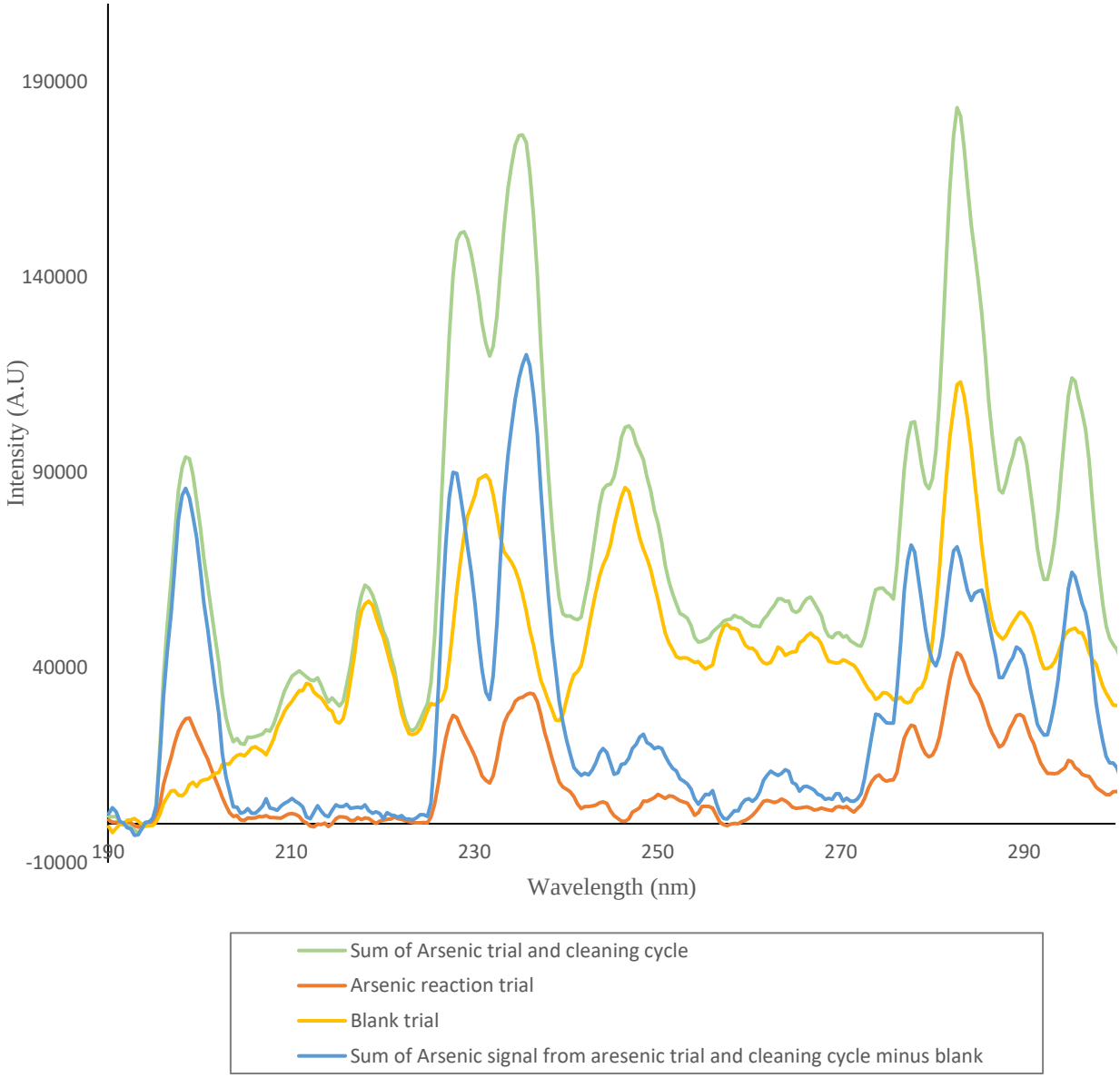

Figure 4.15: Overlapping emission spectra for total signal collected from the arsenic reaction trial, sum of signal from the arsenic reaction trial and its cleaning cycle, blank reaction trial, and background corrected signal.

4.8.3 Results for the Argon Microplasma

The emission spectrum showing the sum of all episodes for arsenic reaction trial and the sum of arsenic reaction trial, and its first cleaning cycle can be seen in Figure 4.13. This figure also shows the sum of episodes of the blank reaction trials.

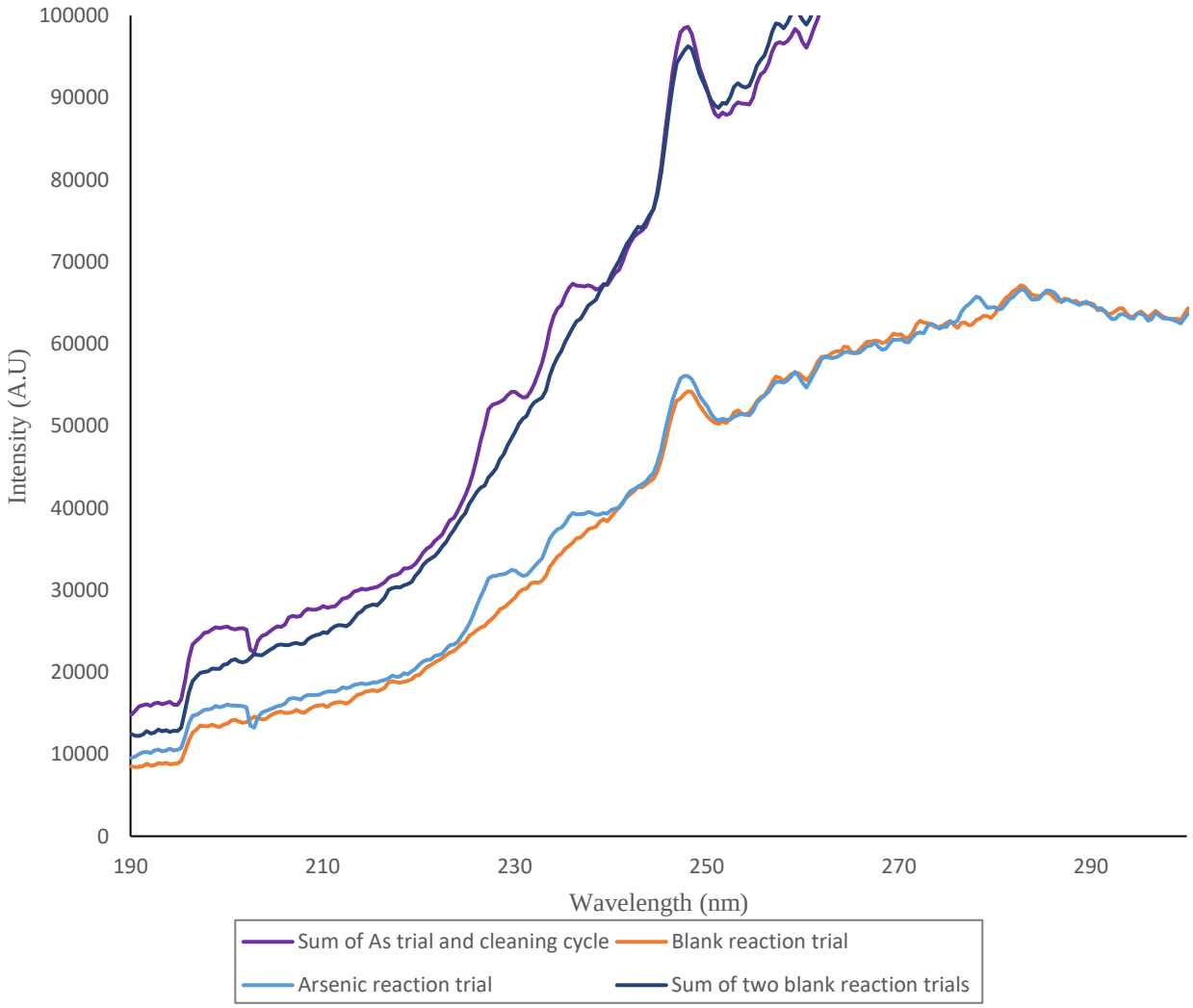

Figure 4.16: Emission spectrum for the arsenic reaction trial, sum the of arsenic reaction trial and its cleaning cycle and blank reaction trials.

The data for the blank reaction trial can be subtracted from the arsenic reaction trial and from the sum of the signal from arsenic reaction trial and its first cleaning cycle to apply background correction. The resultant signal is exhibited in Figure 4.17.

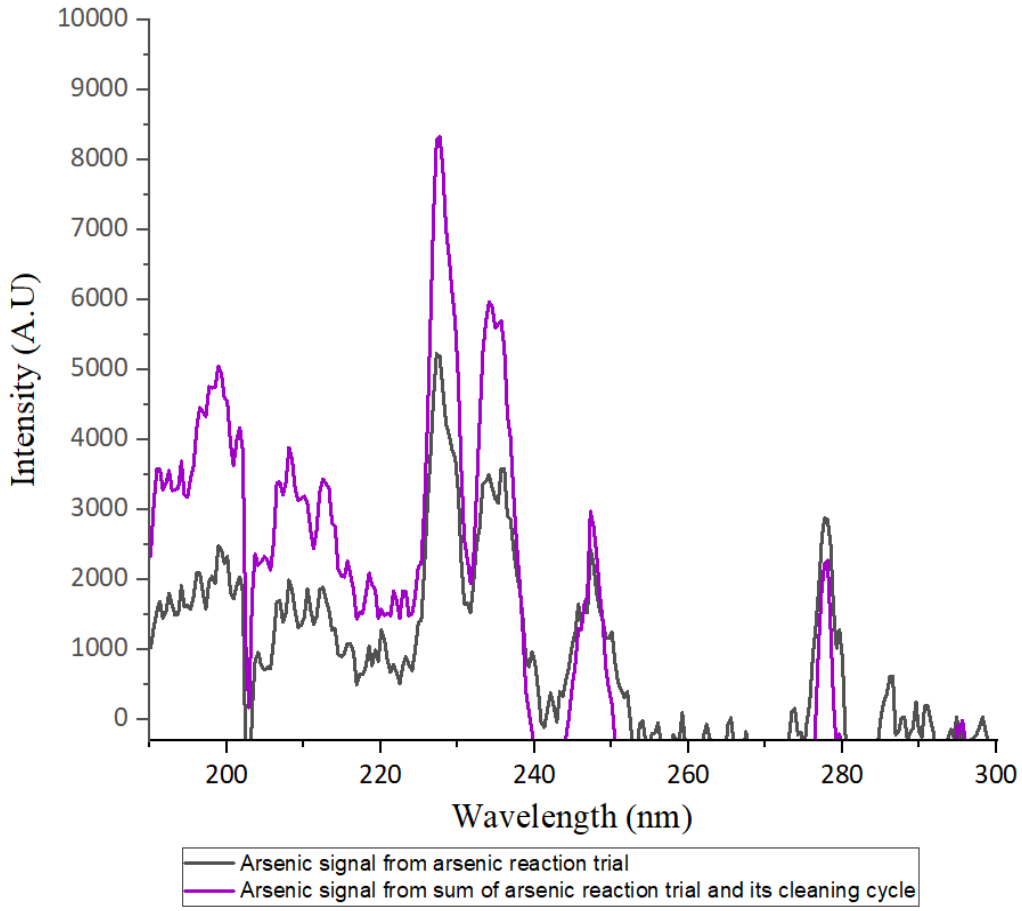

Figure 4.17: Background corrected arsenic signal for arsenic reaction trial and for sum of signal from arsenic reaction trial and its first cleaning cycle.

In the background corrected arsenic emission spectrum (shown in Figure 4.17), the As peak at 197 nm has a very low signal to noise ratio. This is because As peak at 197 nm usually has very low emission intensity in argon microplasma. The other two peaks at 228 nm and 235/237 nm

seem to have a slight overlap and are not baseline resolved due to low spectral resolution. The detection limit can be estimated by using the intensity of the peak at 228 nm. Although this peak is more impacted by the background than the As peak at 197 nm, it has much higher intensity as compared to that of peak at 197 nm. By using the peak at 228 nm, the detection limit calculated for the sum of arsenic reaction trial and first cleaning cycle is 0.040 ppm or 40 ppb.

4.8.4 Calculation for Estimating the Detection Limit:

The limit of detection is estimated from the signal to noise ratio (SNR) of the analyte and the quantity of the analyte used to generate the signal [77]. The signal to noise ratio is the ratio of required signal power to noise power. SNR quantizes the ability to resolve a signal from the noise it is embedded in [78]. SNR is determined by dividing the net signal by standard deviation in noise. The steps used for finding the detection limit for As in argon microplasma are given below [77]:

Step 1: Find the intensity of background corrected signal:

Intensity of Background corrected arsenic peak at 228 nm in the spectrum for sum of arsenic trial and cleaning cycle = 8289 A.U

Step 2: Find the peak-to-peak noise:

$$\text{Peak-to-peak noise} = 1689 - 1509 = 186$$

Step 3: Estimate the standard deviation in noise:

$$\text{Standard deviation in noise} = \frac{\text{Peak to peak noise}}{5} = \frac{186}{5} = 37.2$$

Step 4: Determine the signal to noise ratio:

$$\text{Signal to noise ratio (SNR)} = \frac{\text{Net signal}}{\text{standard deviation in noise}} = \frac{8289}{37.2} = 222.82$$

Step 5: Find the limit of detection:

Since the limit of detection (in this case) is SNR = 3, and the specified signal is produced by 3 ppm As sample, the limit of detection is determined by the equation:

$$\text{Limit of detection} = \frac{3\times\text{concentration of As sample}}{\text{SNR}} = \frac{3\times 3\text{ ppm}}{222.82} = 0.0404\text{ ppm or } 40.4\text{ ppb}$$

Hence, the limit of detection for arsenic in argon microplasma is estimated to be 40 ppb.

In this method, the standard deviation is estimated by using peak to peak noise instead of using its formula in Excel, because for the standard deviation to have the right value, there should be a considerable number of data points. This means that the measurement for standard deviation would need to include data points (intensity values) further away from the peak which is unrealistic because noise further away from the peak would not impact the peak [77].

4.8.5 Discussion of the Estimated Detection Limit

The detection limit of arsenic introduced into the microplasma by hydride generation depends on the amount of reaction solution introduced into the GLS and the type of spectrometer. The amount of arsine entering the microplasma relies on the amount of reaction solution in the GLS. Hence, with increasing amount of arsine, the signal for arsenic intensifies. However, as the amount of the reaction solution in the GLS increases, the amount of hydrogen released from the solution also surges, resulting in dimming of the microplasma and diminishing of the signal intensity. Hence, for measuring the detection limit, the amount of reaction solution in the GLS should be controlled, to not disturb the microplasma. The other factor that needs to be considered is the spectrometer. Integrating over 2048-pixel, the linear Photo Diode Array (PDA) detector- spectrometer was used in this experiment [41] with a fiber optic cable of length 2 m and diameter 600 µm. Using a shorter fiber optic cable of length 33 cm with diameter 1000 µm (labelled as F-1000-UV-VIS-SR) has

been known to improve the emission intensities of different peaks by 2 to 3 times [79]. Hence, using a smaller fiber optic cable will improve the detection limit of arsenic further. Secondly, a Heath 0.35 m Czerny-Turner scanning monochromator, equipped with 1200 mm^{-1} grating, adjustable entrance and exit slits and a photomultiplier tube detector [40] should be used to measure the detection limit. This detector has high sensitivity since it uses a photomultiplier tube [80] and collects more emission signal from the microplasma, as compared to the optical fiber. It also eliminates the need for an optical fiber cable which causes a loss of signal in the UV range [64]. Hence, the estimated detection limit for arsenic in argon and helium microplasma can be better than what is mentioned in this thesis.

4.9 Changes Needed for Improving the Reproducibility in the Reaction Trials and the Detection Limit for Arsenic

To ensure reproducibility in the arsenic reaction trials and to improve the detection limit of arsenic, the amount of reaction solution introduced in the GLS should be the same and the issue of peak tailing should be resolved. The amount of arsine that enters the microplasma tube depends on the amount of reaction solution in the GLS. Two reaction trials can be comparable only when the amount of reaction solution in the GLS for these trials is the same. During this research, the amount of reaction solution in the GLS was measured by the help of vernier calipers as distance between the valve of the GLS and the lower meniscus of the reaction solution in the GLS. It was very hard to control the amount of reaction solution in the GLS manually. This extended the experiment time as more arsenic reaction trials were conducted to get a desirable amount of reaction solution in the GLS for the trials. Therefore, changes in the equipment design are required to ensure that the same amount of reaction solution enters the GLS for each trial. The other problem that needs to be resolved is the peak tailing. Peak tailing occurs because the reaction solution in the GLS keeps on

emitting hydrogen and arsine over time. Peak tailing can be seen in the episodic data of arsenic reaction trial shown in Figure 4.13, in which the intensity of arsenic peaks is the highest in the first few episodes, when the reaction solution reaches the GLS, but then remains low for an extended period. This suggests that the carrier gas was not able to strip all the arsine from the reaction solution and that the mixing of carrier gas with the reaction solution in the GLS was not good enough. Gaseous arsine is partially soluble in water, resulting in its slow release from the reaction solution [46]. The solubility of arsine in water is 28 mg/100 mL at 20°C [33]. Hydrogen released from the reaction solution usually helps in the release of arsine from liquid solution. However, increasing the mixing of the carrier gas with liquid solution decreases the demand for $NaBH_4$ needed in the reaction trial [46]. If all the arsine generated from the reaction solution reached the microplasma at once, instead of tailing over time, the intensity of arsenic signal will strengthen, improving the detection limit. Hence, a change in the design of GLS is required to allow better mixing of the carrier gas with the reaction solution, as the carrier gas needs to strip arsine from the solution. This change in GLS design will improve the detection limit and reproducibility of the arsenic signal by compressing the signal in the time domain. In conclusion, changes should be made in the equipment to improve the reproducibility of arsenic reaction trials and the detection limit for arsenic.

4.10 Conclusion

In this chapter, the emission lines for arsenic in the microplasma were determined, which was followed by finding the best observation position for arsenic signal over the microplasma tube and estimating the detection limit for arsenic. The arsenic lines seen in microplasma are 197.3 nm, 228.8 nm, 234.4/235.0/237.0 nm cluster, 245.6 nm, 249.2 nm, 274.5 nm, 278.0 nm, 286.0 nm, and 289.9 nm (unresolved peak with low intensity). It was found that 3 and 5 cleaning cycles of a blank

reaction solution were needed to eliminate all the memory, after running arsenic samples with concentrations of 3 ppm and 30 ppm, respectively. The best observation position for arsenic signal was determined by collecting episodic data for arsenic reaction trials at different positions of the optical fiber over the microplasma tube. It was found that the arsenic signal was more intense further away from the front electrode, through which the carrier gas and the analyte were introduced. For helium and argon microplasma, the best observation positions were 0.84 cm and 1.34 cm away from the front electrode, respectively. Helium microplasma gave higher intensity arsenic signal as compared to argon microplasma. The detection limits for arsenic in helium and argon microplasma were estimated to be about 31 ppb and 40 ppb, respectively. Peak tailing of the arsenic emission signal occurred due to inefficient mixing of the carrier gas with the reaction solution. Using a more sensitive spectrometer and solving the issue of peak tailing will improve the detection limit of arsenic further in both helium and argon microplasma.

Chapter 5

Conclusion and Future Work

5.1 Outline

- Summary of all the work done and notable results
- Experiments that should be tried using hydride generation as a sample introduction technique.
- Cold vapor generation for detection of mercury using equipment for discrete flow system.
- Development of photochemical vapor generation technique.

5.2 Summary of Experiments and Results

In this project, the equipment for hydride generation was designed and tested for results. Mainly, two kinds of equipment were tested: the batch system and the discrete flow system. The equipment for the batch system had a smaller size and lighter weight but was not found to be suitable for hydride generation. It had an issue of slow and non-reproducible mixing of the sample solution with the reagent solution, in addition to allowing leakage of gas into and out of the system due to the permeability of the rubber septum. The discrete flow system was chosen for hydride generation because of its reproducible mixing in a reaction coil. The gas-liquid separator (GLS) for the discrete flow system was designed and a cold trap was used to remove water vapors escaping the GLS. The equipment for the discrete flow system was made of glass because glass is not permeable to gases.

Since the cold trap was used in the equipment and since water vapors and hydrogen were released from the hydride generation reaction, the microplasma operated in three different gases was tested for its response towards the cold trap, the water vapors and the hydrogen released from the hydride generation reaction. The three different gases tested were: helium, argon, and a mixture of argon with 1000 ppm hydrogen. It was found that microplasma operated in helium was the most drastically impacted by water vapors in the system. The microplasma operated in BIP argon was also negatively impacted due to water vapors, but this impact was lower as compared to that observed for helium microplasma. Whereas water vapors had almost no negative impact on the argon-1000 ppm hydrogen microplasma. The cold trap did not have any negative impact on the emission spectrum from the microplasma operated in any of the three different carrier gases, indicating that it can be used in the equipment. The cold trap was also very efficient in removing most of the water vapors released from the reaction solution. The hydrogen released from the hydride generation reaction also impacted the microplasma negatively. In fact, this released hydrogen would dim the microplasma if it was present in high amount. Therefore, 0.05% (m/v) $NaBH_4$ solution was used in the hydride generation reaction as hydrogen released from its reaction solution in the GLS did not dim the helium or argon microplasma. Microplasma operated in argon – 1000 ppm hydrogen could not even tolerate the hydrogen released from the 0.05% $NaBH_4$ solution. However, as the amount of hydrogen released from the reaction solution present in GLS depleted over time, the microplasma operated in argon, and argon-1000 ppm hydrogen regained its initial power very quickly. But the microplasma operated in helium took a longer time to regain its initial power (5 – 20 seconds, depending on the concentration of $NaBH_4$ used in the reaction). Higher concentration of $NaBH_4$ for the reaction solution would dim the microplasma momentarily.

In conclusion, the microplasma operated in different carrier gases was impacted differently by water vapors and hydrogen released from the reaction solution.

Afterwards, the emission spectra for arsenic were collected in helium and argon microplasma and detection limit of arsenic was determined for both carrier gases of microplasma. The arsenic lines seen in the microplasma were 197.3 nm, 228.8 nm, 234.4/235.0/237.0 nm cluster, 245.6 nm, 249.2 nm, 274.5 nm, 278.0 nm, 286.0 nm, and 289.9 nm. Out of these emission lines, the 245.6 nm, 249.2 nm, and 289.9 nm As lines were weaker than all other lines and were more observable in the emission spectrum collected from helium microplasma, as compared to that collected from argon microplasma. The peak 289.9 nm was the weakest peak and formed a cluster with neighboring 286.0 nm peak. Helium microplasma provided the benefit of a lower background in the emission spectrum. Emission spectra collected from argon microplasma, on the other hand, had a higher background due to release of hydrogen from the reaction solution and had a lower intensity for arsenic peaks as compared to that observed for helium microplasma. By collecting the arsenic signals at different positions on the microplasma tube, it was observed that arsenic signal was more intense further away from the front electrode – the electrode through which the carrier gas and analyte were introduced. In helium microplasma, the best position for observing arsenic signal was determined to be 0.84 cm from the front electrode. And for argon microplasma, the best position for obtaining high intensity arsenic signal was 1.34 cm away from the front electrode. Afterwards, the detection limit for arsenic in helium microplasma was estimated by measuring the intensity of As 197.3 nm peak, which turned out to be 31 ppb. And the detection limit for arsenic in argon microplasma was estimated by measuring the intensity of As peak 228.8 nm, which turned out to be 40 ppb. Using a smaller fiber optic cable for the fiber optic spectrometer with a linear Photo Diode Array (PDA) detector or using a more sensitive spectrometer can further

improve the detection limit for arsenic in both helium and argon microplasma. Similarly, solving the issue of peak tailing is also needed to ensure reproducibility and to improve the detection limit.

5.3 Future Experiments

5.3.1 Future Experiments with Hydride Generation

Hydride generation has been shown to work as a sample introduction technique for the microplasma during this research project. However, more research is needed in this field to improve the equipment used for hydride generation, and to study the detection limit for other hydride forming elements, the impact of other carrier gases on the experimental results and the impact of higher power input on the experimental results.

5.3.1.1 Changes in the Equipment Design

Changes are needed in the equipment design to enhance reproducibility and reduce the size of the equipment used for hydride generation. Reproducibility can be improved by controlling the amount of reaction solution that enters the GLS by automation and by changing the design of the GLS. Automation of introduction of reaction solution into the GLS is desired for precise results. This is because it was observed that the intensity of the arsenic signal depends on the amount of reaction solution in the GLS. Therefore, to get a reproducible signal, it is necessary to introduce equal amounts of the reaction solution into the GLS for each trial. During the experimentation, this amount was controlled manually by the help of a two-way valve between the reaction coil and the GLS. As it was not only the peristaltic pump that pushed the reaction solution into the GLS, but hydrogen gas made in the reaction coil also played a role in pushing the reaction solution forward. Therefore, controlling the amount of reaction solution in the GLS manually is hard, as it makes the experiment prone to personal errors. Automation of this process will eliminate this issue and

will also make the operation of the equipment easier. The size of the equipment can also be reduced further by testing smaller size reaction coils for their efficiency. Moreover, an automatic peristaltic pump pushing a specified amount of reaction solution into the GLS may eliminate the need for a two-way valve if the coil is small enough and if all the reaction solution in the coil is pushed into the GLS during the experimental trial. Thirdly, reproducibility of the reaction trials was also negatively impacted by the peak tailing. This peak tailing occurred due to inefficient mixing of the carrier gas with the reaction solution. The design of the GLS should be changed to eliminate this problem, as this will compress the signal in the time domain (resulting in an increase in its intensity) and improve sensitivity of the system. In short, automation of the peristaltic pump and change in the design of the GLS is required to improve reproducibility of the reaction trials and may further decrease the size of the equipment used for hydride generation. These changes should be made before proceeding to the next step in research into this topic.

5.3.1.2 Using a More Sensitive Spectrometer:

For measuring the detection limit for arsenic, a more sensitive spectrometer should be used. For this research portable fiber-optic spectrometer with an integrating 2048-pixel, linear Photo Diode Array (PDA) detector was used. The fiber optic cable used for this spectrometer had a diameter of 600 µm, and length of 2 m. Optical fibers often have a decreased transmission of UV light [64], therefore using a long optical fiber led to loss of the emission signal. For the same spectrometer, a smaller fiber optic cable with length 33 cm and diameter 1000 µm should be used. Using a smaller fiber optic cable is known to intensify the emission signal by 2 – 3 times [79]. Similarly, a more sensitive spectrometer, such as, a Heath 0.35 m Czerny-Turner scanning monochromator, equipped with 1200 mm^{-1} grating, adjustable entrance and exit slits and a photomultiplier tube

detector [40] will also improve the detection limit for arsenic. In conclusion, a more sensitive spectrometer is needed to improve the detection limit for arsenic in microplasma.

5.3.1.3 Experiment for Other Hydride Forming Elements

Using the experimental apparatus and procedure described in the thesis, the detection limit for other hydride forming elements should be measured. Hydride generation has been used for detection of various hydride forming elements, including As, Bi, Ge, Hg, Pb, Sb, Se, Sn, Te, and Hg [20,21,22,25] for microplasma. For each of these elements, the position on the microplasma tube where the emission intensity of the element is highest should be determined in the first step. This should be followed by measuring the detection limit of these elements, as described in Chapter 4.

5.3.1.4 Operating Microplasma in Other Gases

It has been observed previously that our microplasma can be operated in different carrier gases, including pure nitrogen, a mixture of argon and helium, a mixture of hydrogen and nitrogen, etc. Hydride generation should be coupled to microplasma operated in different carrier gases, and its experiments, as stated in Chapter 3, should be conducted for each carrier gas. Moreover, the impact of different carrier gases on the detection limit of different hydride-forming elements should also be studied.

Out of these gases, I suggest trying the carrier gas pure nitrogen, a mixture of nitrogen with 1% hydrogen, and a mixture of argon with nitrogen. The emission spectrum obtained from the microplasma operated in a mixture of nitrogen and hydrogen did not have the characteristic high background in the region 200 nm to 500 nm due to hydrogen, suggesting that hydrogen does not impact the background of a nitrogen emission spectrum. Although the emission spectrum for

nitrogen was very crowded due to the presence of nitrogen peaks, the emission spectrum was clear in region 190 nm to 290 nm [81], the region in which arsenic peaks usually appear. The emission spectrum for nitrogen published in the literature also do not show nitrogen lines in the region 190 nm to 300 nm [49,82]. Similarly, a mixture of argon with nitrogen should also be tried as a carrier gas when hydride generation is used as a sample introduction technique. A mixture of argon with nitrogen has been used as a carrier gas for various plasmas [15,83,84], however, this carrier gas mixture has not been tried for the microplasma in the lab. Different parameters of microplasma, like rotational temperature, gas temperature and electron density, operated in this mixture should be studied. In conclusion, the experiments described in Chapter 3 should be conducted with more carrier gases.

5.3.1.5 Higher Power Input

I suggest studying the effect of higher power input on the response of microplasma towards hydrogen released from the reaction solution and on the sensitivity of microplasma towards different analytes introduced by hydride generation. In this project, the microplasma operated in helium, argon, and argon-1000 ppm hydrogen had an input power of 14.8 watts, 6 watts and 6.5 watts, respectively. With the equipment being used right now, the input power of the microplasma can only be boosted by increasing the input DC voltage for the HVAC power supply. Since the maximum input voltage limit for the HVAC power supply is 12 volts, the power of the microplasma could not be exceeded beyond that mentioned in this paragraph. I suggest experimenting with higher power input and observing its impact on the microplasma and its response towards arsine and hydrogen released from the hydride generation reaction and towards water vapors. Hydrogen is known to disturb plasma [85] and often requires high power input for plasma to remain stable and operate [26,86]. Higher power input will allow the microplasma to

tolerate higher concentrations of $NaBH_4$ in hydride generation and will let the researcher study the effect of $NaBH_4$ concentration on the analytical signal. The concentration of $NaBH_4$ used for hydride generation coupled to the microplasma that has been published in literature is 0.2% (m/v) [20], 0.4% (m/v) [26], 0.8% (m/v) [25], and 1% (m/v) [21]; All of the reported concentrations of $NaBH_4$ are higher than what was used in this project, which is 0.05% (m/v). It is also hypothesized that higher power input will improve the intensity of the emission signal of the analyte, as the excitation capability of the microplasma is positively correlated with the input voltage [87]. The impact of the power input of the microplasma on the detection limit of different elements introduced into the microplasma through hydride generation should be studied. Moreover, literature publications for coupling hydride generation with microplasma have mentioned using a power input of 30 watts [21], 40 watts [26], and 77 watts [20] for microplasma, indicating some significance of higher power input. However, while using higher power input, care should be taken not to burn the microplasma tube. There is a limit to the amount of input power that can be tolerated by microplasma due to its small size. I suggest using an input power of 30 watts for argon microplasma and 40 watts for helium microplasma.

5.3.2 Coupling Other Chemical Vapor Generation Techniques with Microplasma

The other chemical vapor generation techniques that should be coupled with microplasma are cold vapor generation and photochemical vapor generation. The cold vapor generation technique is used for the detection of mercury only but uses the same equipment as that used for hydride generation. It offers the benefit of not releasing hydrogen during the reaction and therefore, can be coupled with a microplasma very easily [32]. The other chemical vapor generation technique that does not generate hydrogen as a by-product is photochemical vapor generation. Photochemical vapor generation expands the number of elements that can be detected but needs the development of a

flow-through photochemical reactor to generate chemical vapors [31]. In conclusion, other chemical vapor generation techniques can also be coupled to microplasma for the detection of various elements.

References

[1] T. Ichiki, T. Koidesawa, Y. Horiike, An atmospheric pressure microplasma jet source for the optical emission spectroscopic analysis of liquid sample, Plasma Sources Sci. Technol. 12 (2003) S16. https://doi.org/10.1088/0963-0252/12/4/315.

[2] M. Nie, R. Truckenmüller, S. Takeuchi, Chapter 10 - Microfabrication technology in tissue engineering, in: J. De Boer, C.A.V. Blitterswijk, J.A. Uquillas, N. Malik (Eds.), Tissue Engineering (Third Edition), Academic Press, 2023: pp. 329–353. https://doi.org/10.1016/B978-0-12-824459-3.00010-X.

[3] S.M. McBride, J. Remedios, V. Karanassios, Battery-operated microplasma coupled to a portable fiber-optic spectrometer and its application for the determination of nano-silver leaching from garments during washing, in: Next-Generation Spectroscopic Technologies XII, International Society for Optics and Photonics, 2019: p. 1098304. https://doi.org/10.1117/12.2519938.

[4] A. Postawa, C. Hayes, 8.1 Method Selection, in: Best Practice Guide on the Control of Iron and Manganese in Water Supply, IWA Publishing, 2013. https://app.knovel.com/hotlink/pdf/id:kt00U9VC1B/best-practice-guide-control/method-selection.

[5] S. Dubecky, M. Nyce, Lubricating Oils, in: S.J. Rand, A.W. Verstuyf (Eds.), Significance of Tests for Petroleum Products, ASTM International, West Conshohocken, 2018: pp. 267–285.

[6] S. Weagant, V. Chen, V. Karanassios, Battery-operated, argon–hydrogen microplasma on hybrid, postage stamp-sized plastic–quartz chips for elemental analysis of liquid microsamples using a portable optical emission spectrometer, Anal. Bioanal. Chem. 401 (2011) 2865–2880. https://doi.org/10.1007/s00216-011-5372-x.

[7] B.M. Dahal, M. Fuerhacker, A. Mentler, K.B. Karki, R.R. Shrestha, W.E.H. Blum, Arsenic contamination of soils and agricultural plants through irrigation water in Nepal, Environ. Pollut. 155 (2008) 157–163. https://doi.org/10.1016/j.envpol.2007.10.024.

[8] D.K. Nordstrom, Worldwide occurrences of arsenic in ground water, Science (1979). 296 (2002) 2143–2145. https://doi.org/10.1126/science.1072375.

[9] S. Wang, C.N. Mulligan, Occurrence of arsenic contamination in Canada: Sources, behavior and distribution, Sci. Total Environ. 366 (2006) 701–721. https://doi.org/10.1016/j.scitotenv.2005.09.005.

[10] M. Kuivenhoven, K. Mason, Arsenic Toxicity, in: StatPearls, StatPearls Publishing, 2023.

[11] K.S. Squibb, B.A. Fowler, CHAPTER 7 - The toxicity of arsenic and its compounds, in: B.A. FOWLER (Ed.), Biological and Environmental Effects of Arsenic, Elsevier, Amsterdam, 1983: pp. 233–269. https://doi.org/10.1016/B978-0-444-80513-3.50011-6.

[12] D. of E. and S. Affairs, THE 17 GOALS, 2021 (2021). https://sdgs.un.org/goals.

[13] M. Broussely, G. Pistoia, Industrial Applications of Batteries - From Cars to Aerospace and Energy Storage, Elsevier, Oxford, 2007.

[14] A.J.M. Mackus, S.B.S. Heil, E. Langereis, H.C.M. Knoops, M.C.M. van de Sanden, W.M.M. Kessels, Optical emission spectroscopy as a tool for studying, optimizing, and monitoring plasma-assisted atomic layer deposition processes, J. Vac. Sci. Technol. A. 28 (2009) 77–87. https://doi.org/10.1116/1.3256227.

[15] A. Barkhordari, A. Ganjovi, I. Mirzaei, A. Falahat, M.N. Rostami Ravari, A pulsed plasma jet with the various Ar/N2 mixtures, J. Theor. Appl. Phys. 11 (2017) 301–312. https://doi.org/10.1007/s40094-017-0271-y.

[16] L. Lin, Q. Wang, Microplasma: A New Generation of Technology for Functional Nanomaterial Synthesis, Plasma Chemistry and Plasma Processing. 35 (2015) 925–962. https://doi.org/10.1007/s11090-015-9640-y.

[17] H.R. Badiei, G. Stubley, R. Fitzgerald, M.S. and V. Karanassios, Computational Fluid Dynamics (CFD) Applied to a Glass Vaporization Chamber for Introduction of Micro- or Nano-Size Samples into Lab-Based ICPs and to a CFD-Derived (and Rapidly Prototyped Via 3D Printing) Smaller-Size Chamber for Portable Microplasmas, in: A. Ionescu (Ed.), Computational Fluid Dynamics, IntechOpen, Rijeka, 2018: p. Ch. 8. https://doi.org/10.5772/intechopen.72650.

[18] X. Jiang, Y. Chen, C. Zheng, X. Hou, Electrothermal vaporization for universal liquid sample introduction to dielectric barrier discharge microplasma for portable atomic emission spectrometry, Anal. Chem. 86 (2014) 5220–5224. https://doi.org/10.1021/ac500637p.

[19] X. Pan, Y. Lin, Y. Su, J. Yang, L. He, Y. Deng, X. Hou, C. Zheng, Methanol-Enhanced Liquid Electrode Discharge Microplasma-Induced Vapor Generation of Hg, Cd, and Zn: The Possible Mechanism and Its Application, Anal. Chem. (2021). https://doi.org/10.1021/acs.analchem.1c01091.

[20] M. Li, L. Kai, H. Lin, Z. Xiaoliang, W. Xi, H. Xiandeng, J. Xiaoming, Point discharge microplasma optical emission spectrometer: hollow electrode for efficient volatile hydride/mercury sample introduction and 3D-printing for compact instrumentation, Anal. Chem. 91 (2019) 7001–7006. https://doi.org/10.1021/acs.analchem.9b00045.

[21] Z. Zhu, H. He, D. He, H. Zheng, C. Zhang, S. Hu, Evaluation of a new dielectric barrier discharge excitation source for the determination of arsenic with atomic emission spectrometry, Talanta. 122 (2014) 234–239. https://doi.org/10.1016/j.talanta.2014.01.054.

[22] R. Guchardi, P.C. Hauser, A capacitively coupled microplasma in a fused silica capillary, J. Anal. At. Spectrom. 18 (2003) 1056–1059. https://doi.org/10.1039/B301659P.

[23] X.-P. Yan, Z.-M. Ni, Vapour generation atomic absorption spectrometry, Anal. Chim. Acta. 291 (1994) 89–105. https://doi.org/10.1016/0003-2670(94)85130-1.

[24] Z. Zhu, G.C.-Y. Chan, S.J. Ray, X. Zhang, G.M. Hieftje, Microplasma source based on a dielectric barrier discharge for the determination of mercury by atomic emission spectrometry, Anal. Chem. 80 (2008) 8622–8627. https://doi.org/10.1021/ac801531j.

[25] Y. Cai, Y.-L. Yu, J.-H. Wang, Alternating-current-driven microplasma for multielement excitation and determination by optical-emission spectrometry, Anal. Chem. 90 (2018) 10607–10613. https://doi.org/10.1021/acs.analchem.8b02904.

[26] P. Pohl, I.J. Zapata, N.H. Bings, E. Voges, J.A.C. Broekaert, Optical emission spectrometric determination of arsenic and antimony by continuous flow chemical hydride generation and a miniaturized microwave microstrip argon plasma operated inside a

capillary channel in a sapphire wafer, Spectrochim. Acta Part B At Spectrosc. 62 (2007) 444–453. https://doi.org/10.1016/j.sab.2007.04.007.

[27] Y. Zhang, X. Mao, D. Tian, J. Liu, C. Li, Trace arsenic analysis in edible seaweeds by miniature in situ dielectric barrier discharge microplasma optical emission spectrometry based on gas phase enrichment, Anal. Methods. 13 (2021) 4079–4089. https://doi.org/10.1039/D1AY01034D.

[28] H. Yu, C. Li, Y. Tian, X. Jiang, Recent developments in determination and speciation of arsenic in environmental and biological samples by atomic spectrometry, Microchem. J. 152 (2020) 104312. https://doi.org/10.1016/j.microc.2019.104312.

[29] P. Pohl, Recent advances in chemical vapour generation via reaction with sodium tetrahydroborate, TrAC Trends Anal. Chem. 23 (2004) 21–27. https://doi.org/10.1016/S0165-9936(04)00103-7.

[30] Y. Gao, R. Liu, L. Yang, Application of chemical vapor generation in ICP-MS: A review, Chi. Sci. Bull. 58 (2013) 1980–1991. https://doi.org/10.1007/s11434-013-5751-0.

[31] H. He, Z. Zhu, H. Zheng, Q. Xiao, L. Jin, S. Hu, Dielectric barrier discharge micro-plasma emission source for the determination of thimerosal in vaccines by photochemical vapor generation, Microchem. J. 104 (2012) 7–11. https://doi.org/10.1016/j.microc.2012.03.022.

[32] Y. Cai, S.-H. Li, S. Dou, Y.-L. Yu, J.-H. Wang, Metal carbonyl vapor generation coupled with dielectric barrier discharge to avoid plasma quench for optical emission spectrometry, Anal. Chem. 87 (2015) 1366–1372. https://doi.org/10.1021/ac5042457.

[33] National Center for Biotechnology Information, PubChem Annotation Record for ARSINE, Source: Hazardous Substances Data Bank (HSDB), (2023). https://pubchem.ncbi.nlm.nih.gov/source/hsdb/510#section=Solubility-%28Complete%29 (accessed June 19, 2023).

[34] J.D. G, L.B. B, C.R. R, T.M. C, K.T. F, Development of Chemical Reduction and Air Stripping Processes to Remove Mercury from Wastewater, J. Environ. Eng. (New York). 139 (2013) 1336–1342. https://doi.org/10.1061/(ASCE)EE.1943-7870.0000761.

[35] X. Yuan, G. Yang, Y. Ding, X. Li, X. Zhan, Z. Zhao, Y. Duan, An effective analytical system based on a pulsed direct current microplasma source for ultra-trace mercury determination using gold amalgamation cold vapor atomic emission spectrometry, Spectrochim. Acta Part B At Spectrosc. 93 (2014) 1–7. https://doi.org/10.1016/j.sab.2013.12.009.

[36] H. Deng, C. Zheng, L. Liu, L. Wu, X. Hou, Y. Lv, Photochemical vapor generation of carbonyl for ultrasensitive atomic fluorescence spectrometric determination of cobalt, Microchem. J. 96 (2010) 277–282. https://doi.org/10.1016/j.microc.2010.04.002.

[37] K.A. Romanovskiy, M.A. Bolshov, A. V Münz, Z.A. Temerdashev, M.Y. Burylin, K.A. Sirota, A novel photochemical vapor generator for ICP-MS determination of As, Bi, Hg, Sb, Se and Te, Talanta. 187 (2018) 370–378. https://doi.org/10.1016/j.talanta.2018.05.052.

[38] M. Liu, J. Liu, X. Mao, X. Na, L. Ding, Y. Qian, High Sensitivity Analysis of Selenium by Ultraviolet Vapor Generation Combined with Microplasma Gas Phase Enrichment and the Mechanism Study, Anal. Chem. 92 (2020) 7257–7264. https://doi.org/10.1021/acs.analchem.0c00878.

[39] S. Zhang, H. Luo, M. Peng, Y. Tian, X. Hou, X. Jiang, C. Zheng, Determination of Hg, Fe, Ni, and Co by Miniaturized Optical Emission Spectrometry Integrated with Flow Injection Photochemical Vapor Generation and Point Discharge, Anal. Chem. 87 (2015) 10712–10718. https://doi.org/10.1021/acs.analchem.5b02820.

[40] V. Karanassios, K. Johnson, A.T. Smith, Micromachined, planar-geometry, atmospheric-pressure, battery-operated microplasma devices (MPDs) on chips for analysis of microsamples of liquids, solids, or gases by optical-emission spectrometry, Anal. Bioanal. Chem. 388 (2007) 1595–1604. https://doi.org/10.1007/s00216-007-1273-4.

[41] S. Weagant, V. Karanassios, Helium–hydrogen microplasma device (MPD) on postage-stamp-size plastic–quartz chips, Anal. Bioanal. Chem. 395 (2009) 577–589. https://doi.org/10.1007/s00216-009-2942-2.

[42] StellarNet Inc, What is Exposure Time?, (2017). https://www.stellarnet.us/what-is-exposure-time/ (accessed November 7, 2023).

[43] StellarNet Inc, StellarNet Miniature Spectrometer Manual, (2011). https://mmrc.caltech.edu/StellarNet/StellarNet%20Documents/StellarNet%20Manual%202016.pdf (accessed November 7, 2023).

[44] B. Karlberg, G.E. Pacey, Flow Injection Analysis: A Practical Guide, Elsevier, Amsterdam, 1989.

[45] A.E. Kleckner, E. Kakouros, A. Robin Stewart, A practical method for the determination of total selenium in environmental samples using isotope dilution-hydride generation-inductively coupled plasma-mass spectrometry, Limnol. Oceanogr. Methods. 15 (2017) 363–371. https://doi.org/10.1002/lom3.10164.

[46] J. Dedina, D.L. (D Tsalev), Hydride generation atomic absorption spectrometry, John Wiley & Sons, Chichester, England, 1995.

[47] R. Massee, F.J.M.J. Maessen, J.J.M. De goeij, Losses of silver, arsenic, cadmium, selenium and zinc traces from distilled water and artificial sea-water by sorption on various container surfaces, Anal. Chim. Acta. 127 (1981) 181–193. https://doi.org/10.1016/S0003-2670(01)83974-X.

[48] M. Du, H. Xu, Y. Zhu, R. Ma, Z. Jiao, A comparative study of the major antimicrobial agents against the yeast cells on the tissue model by helium and air surface micro-discharge plasma, AIP Adv. 10 (2020) 025036. https://doi.org/10.1063/1.5110972.

[49] K. Shimizu, T. Ishii, M. Blajan, Emission Spectroscopy of Pulsed Power Microplasma for Atmospheric Pollution Control, IEEE Trans. Ind. Appl. 46 (2010) 1125–1131. https://doi.org/10.1109/TIA.2010.2044968.

[50] M. Bashir, S. Bashir, A. Javed, O.U. Noor, Characterization of helium microplasma generated in a flow focusing microfluidic device, J. Appl. Phys. 132 (2022) 063303. https://doi.org/10.1063/5.0097684.

[51] A. Kramida, Yu. Ralchenko, J. Reader, NIST ASD Team, NIST Atomic Spectra Database, National Institute of Standards and Technology, Gaithersburg, 2023. https://doi.org/10.18434/T4W30F.

[52] J.E. Sansonetti, W.C. Martin, S.L. Young, Handbook of Basic Atomic Spectroscopic Data, National Institute of Standards and Technology, Gaithersburg, 2005. http://physics.nist.gov/Handbook (accessed July 19, 2023).

[53] L. Bastarrachea, S. Dhawan, S.S. Sablani, Engineering Properties of Polymeric-Based Antimicrobial Films for Food Packaging: A Review, Food Eng. Rev. 3 (2011) 79–93. https://doi.org/10.1007/s12393-011-9034-8.

[54] P. Tiemblo, J. Guzmán, E. Riande, C. Mijangos, H. Reinecke, Effect of physical aging on the gas transport properties of PVC and PVC modified with pyridine groups, Polymer (Guildf). 42 (2001) 4817–4823. https://doi.org/10.1016/S0032-3861(00)00922-8.

[55] V. Siracusa, Food Packaging Permeability Behaviour: A Report, Int. J. Polym. Sci. 2012 (2012) 302029. https://doi.org/10.1155/2012/302029.

[56] X. Lu, S. Wu, J. Gou, Y. Pan, An atmospheric-pressure, high-aspect-ratio, cold micro-plasma, Sci Rep. 4 (2014) 7488. https://doi.org/10.1038/srep07488.

[57] K.-M. Weitzel, J. Mähnert, M. Penno, ZEKE-PEPICO investigations of dissociation energies in ionic reactions, Chem. Phys. Lett. 224 (1994) 371–380. https://doi.org/10.1016/0009-2614(94)00567-2.

[58] J. Jonkers, M. van de Sande, A. Sola, A. Gamero, J. van der Mullen, On the differences between ionizing helium and argon plasmas at atmospheric pressure, Plasma Sources Sci. Technol. 12 (2003) 30–38. https://doi.org/10.1088/0963-0252/12/1/304.

[59] Federal-Provincial-Territorial Committee on Drinking Water of the Federal-Provincial-Territorial Committee on Health and the Environment, Guidelines for Canadian Drinking Water Quality: Guideline Technical Document, Ottawa, 2006. https://healthycanadians.gc.ca/publications/healthy-living-vie-saine/water-arsenic-eau/alt/water-arsenic-eau-eng.pdf (accessed August 1, 2023).

[60] WHO, Arsenic, (2022). https://www.who.int/news-room/fact-sheets/detail/arsenic (accessed August 1, 2023).

[61] H.M. Anawar, Arsenic speciation in environmental samples by hydride generation and electrothermal atomic absorption spectrometry, Talanta. 88 (2012) 30–42. https://doi.org/10.1016/j.talanta.2011.11.068.

[62] Y. Zhang, J. Ma, X. Na, Y. Shao, J. Liu, X. Mao, G. Chen, D. Tian, Y. Qian, A portable and field optical emission spectrometry coupled with microplasma trap for high sensitivity analysis of arsenic and antimony simultaneously, Talanta. 218 (2020) 121161. https://doi.org/10.1016/j.talanta.2020.121161.

[63] Y. Liu, C. Yang, P.-J. Xing, X. Liu, J.-Z. Liu, Z.-L. Zhu, Highly sensitive determination of arsenic in water samples by hydrogen-doped solution anode glow discharge-optical emission spectrometry, J. Anal. At. Spectrom. 38 (2023) 742–750.

[64] K.F. Klein, P. Schließmann, E. Smolka, G. Hillrichs, M. Belz, W.J.O. Boyle, K.T.V. Grattan, UV-stabilized silica-based fibre for applications around 200 nm wavelength, Sens. Actuators B Chem. 39 (1997) 305–309. https://doi.org/10.1016/S0925-4005(97)80224-9.

[65] Y. Ozaki, Y. Morisawa, A. Ikehata, N. Higashi, Far-Ultraviolet Spectroscopy in the Solid and Liquid States: A Review, Appl. Spectrosc. 66 (2012) 1–25. https://doi.org/10.1366/11-06496.

[66] T.R. O'Brian, J.E. Lawler, Excited Level Lifetime Measurements, in: F.B. Dunning, R.G. Hulet (Eds.), Experimental Methods in the Physical Sciences, Elsevier Inc., 1996: pp. 217–254. https://doi.org/10.1016/S0076-695X(08)60794-2.

[67] N. OHNO, M.A. RAZZAK, H. UKAI, S. TAKAMURA, Y. UESUGI, Validity of Electron Temperature Measurement by Using Boltzmann Plot Method in Radio Frequency Inductive Discharge in the Atmospheric Pressure Range, Plasma Fusion Res. 1 (2006) 028–028. https://doi.org/10.1585/pfr.1.028.

[68] S. Weagant, G. Dulai, L. Li, V. Karanassios, Characterization of rapidly-prototyped, battery-operated, argon-hydrogen microplasma on a hybrid chip for elemental analysis of

microsamples by portable optical emission spectrometry, Spectrochim. Acta Part B At Spectrosc. 106 (2015) 75–80. https://doi.org/10.1016/j.sab.2015.01.009.

[69] R.S. Pappas, Sample Preparation Problem Solving for Inductively Coupled Plasma-Mass Spectrometry with Liquid Introduction Systems I. Solubility, Chelation, and Memory Effects., Spectroscopy (Springf). 27 (2012) 20–31.

[70] A. Ilander, A. Väisänen, The determination of antimony and arsenic concentrations in fly ash by hydride generation inductively coupled plasma optical emission spectrometry, Anal. Chim. Acta. 689 (2011) 178–183. https://doi.org/10.1016/j.aca.2011.01.043.

[71] G. Vujicic, I. Steffan, A new continuous hydride generator for ICP-AES, Mikrochim. Acta. 99 (1989) 267–272. https://doi.org/10.1007/BF01244681.

[72] P.J. Cadusch, M.M. Hlaing, S.A. Wade, S.L. McArthur, P.R. Stoddart, Improved methods for fluorescence background subtraction from Raman spectra, J. Raman Spectrosc. 44 (2013) 1587–1595. https://doi.org/10.1002/jrs.4371.

[73] H. Hu, J. Bai, G. Xia, W. Zhang, Y. Ma, Improved Baseline Correction Method Based on Polynomial Fitting for Raman Spectroscopy, Photonic Sens. 8 (2018) 332–340. https://doi.org/10.1007/s13320-018-0512-y.

[74] G.S. Salem Abdel-Badeeh Mohamed, 10.1.1 Background Removal Using Iterative Polynomial Fitting, Materials, Computer Engineering and Education Technology. (2021). https://app.knovel.com/hotlink/khtml/id:kt012ZHAM2/materials-computer-engineering/background-removal-using.

[75] V. Mazet, C. Carteret, D. Brie, J. Idier, B. Humbert, Background removal from spectra by designing and minimising a non-quadratic cost function, Chemom. Intell. Lab. Syst. 76 (2005) 121–133. https://doi.org/10.1016/j.chemolab.2004.10.003.

[76] M.G.T.E. Motarjemi Yasmine, 4.1.8 Conclusions, Encyclopedia of Food Safety. (2014). https://app.knovel.com/hotlink/khtml/id:kt00C6BRU2/encyclopedia-food-safety/overview-m-conclusions.

[77] A. Strum, A. Fenigstein, Complementary metal-oxide-semiconductor (CMOS) X-ray sensors, in: High Performance Silicon Imaging, Elsevier, 2014: pp. 348–372. https://doi.org/10.1533/9780857097521.2.348.

[78] Vassili Karanassios, From Micro-miniaturization to Nanoscale science and Nanotechnology, and to Electronic Measurements for Scientists, (2021): pp. 6.22-6.26.

[79] Scott Richard Weagant, Further Development of Atmospheric Pressure, Self-Igniting Microplasma Devices (MPDs) for Elemental Analysis of Liquid Microsamples Using Atomic Emission Spectrometry, University of Waterloo, 2011.

[80] A.A. Gaertner, H.W. Yoon, T.A. Germer, Chapter 3 - Dispersive Methods, in: T.A. Germer, J.C. Zwinkels, B.K. Tsai (Eds.), Spectrophotometry, Academic Press, 2014: pp. 67–95. https://doi.org/10.1016/B978-0-12-386022-4.00003-0.

[81] Laiba Qadeer, Observing the Microplasma and its Emission Spectra from its Under-development Analytical Instrument, Waterloo, 2020.

[82] S.I. Hosseini, S. Mohsenimehr, J. Hadian, M. Ghorbanpour, B. Shokri, Physico-chemical induced modification of seed germination and early development in artichoke (*Cynara scolymus* L.) using low energy plasma technology, Phys. Plasmas. 25 (2018). https://doi.org/10.1063/1.5016037.

[83] A. Qayyum, S. Zeb, M.A. Naveed, N.U. Rehman, S.A. Ghauri, M. Zakaullah, Optical emission spectroscopy of Ar–N2 mixture plasma, J Quant Spectrosc Radiat Transf. 107 (2007) 361–371. https://doi.org/10.1016/j.jqsrt.2007.02.008.

[84] H. Wiltsche, M. Wolfgang, F. Hallwirth, Effects of argon on the analytical properties of a microwave-sustained, inductively coupled, atmospheric-pressure plasma, J. Anal. At. Spectrom. 37 (2022) 1298–1308. https://doi.org/10.1039/D2JA00036A.

[85] C. Dietz, Y. Madrid, C. Cámara, P. Quevauviller, Simultaneous determination of As, Hg, Se and Sb by hydride generation-microwave induced plasma atomic emission spectrometry after preconcentration in a cryogenic trap, J. Anal. At. Spectrom. 14 (1999) 1349–1355. https://doi.org/10.1039/A902039J.

[86] R. Pereiro, M. Wu, J.A.C. Broekaert, G.M. Hieftje, Direct coupling of continuous hydride generation with microwave plasma torch atomic emission spectrometry for the determination of arsenic, antimony and tin, Spectrochim. Acta Part B At Spectrosc. 49 (1994) 59–73. https://doi.org/10.1016/0584-8547(94)80156-8.

[87] M. Li, Y. Deng, C. Zheng, X. Jiang, X. Hou, Hydride generation-point discharge microplasma-optical emission spectrometry for the determination of trace As, Bi, Sb and Sn, J. Anal. At. Spectrom. (2016) 2427–2433. https://doi.org/10.1039/C6JA00341A.

Appendix

A. Stoichiometric Calculation for the Amounts of Arsine and Hydrogen Released by the Reaction Solution

$$NaBH_4 + 3H_2O + HCl \rightarrow H_3BO_3 + NaCl + 8H \xrightarrow{E^{m+}} EH_n + H_2(\text{excess})$$

The following calculations assume that for 0.4 mL of reaction solution, 0.2 mL of 30 ppm As^{3+} sample solution reacts with 0.2 mL of 0.05% (m/v) $NaBH_4$, and that all the reactants are converted into products.

Concentration of As^{3+} sample solution = 30 mg/L

Amount of sample solution in Liter = 0.0002 L

Amount of As^{3+} in mg = 30×0.0002 = 0.006 mg

Number of moles of As = $\frac{0.006}{1000\times74.922} = 8.01 \times 10^{-8}$ mol

Concentration of $NaBH_4$ = 0.05% (m/v)

Volume of the reagent solution used = 0.2 mL

Mass of $NaBH_4$ in the reaction solution = $\frac{0.05\times0.2}{100} = 0.0001$ g

Number of moles of $NaBH_4$ = $\frac{0.0001}{37.84} = 2.64 \times 10^{-6}$ mol

Number of moles of arsine produced = Number of moles of As^{3+} in solution = 8.01×10^{-8} mol

Number of moles of $NaBH_4$ in excess = 2.64×10^{-6} mol $- 8.01 \times 10^{-8}$ mol $= 2.56 \times 10^{-6}$ mol

Number of moles of hydrogen gas produced = 2.56×10^{-6} mol $\times \frac{5}{2} = 6.41 \times 10^{-6}$ mol

So, when 0.2 mL of 30 ppm As^{3+} sample solution reacts with 0.2 mL of 0.05% (m/v) $NaBH_4$ solution, 8.01×10^{-8} moles of arsine and 6.41×10^{-6} moles of hydrogen are produced, assuming all the reactants are converted into products.

Similarly, when 0.4 mL of 30 ppm As^{3+} solution is reacted with 0.4 mL of 0.05% (m/v) $NaBH_4$ solution (making a total of 0.8 mL reaction solution), the amount of arsine released is 1.6×10^{-7} moles and the amount of hydrogen produced is 1.28×10^{-5}.

B. Photo of the Hydride Generation Equipment Used in the Lab

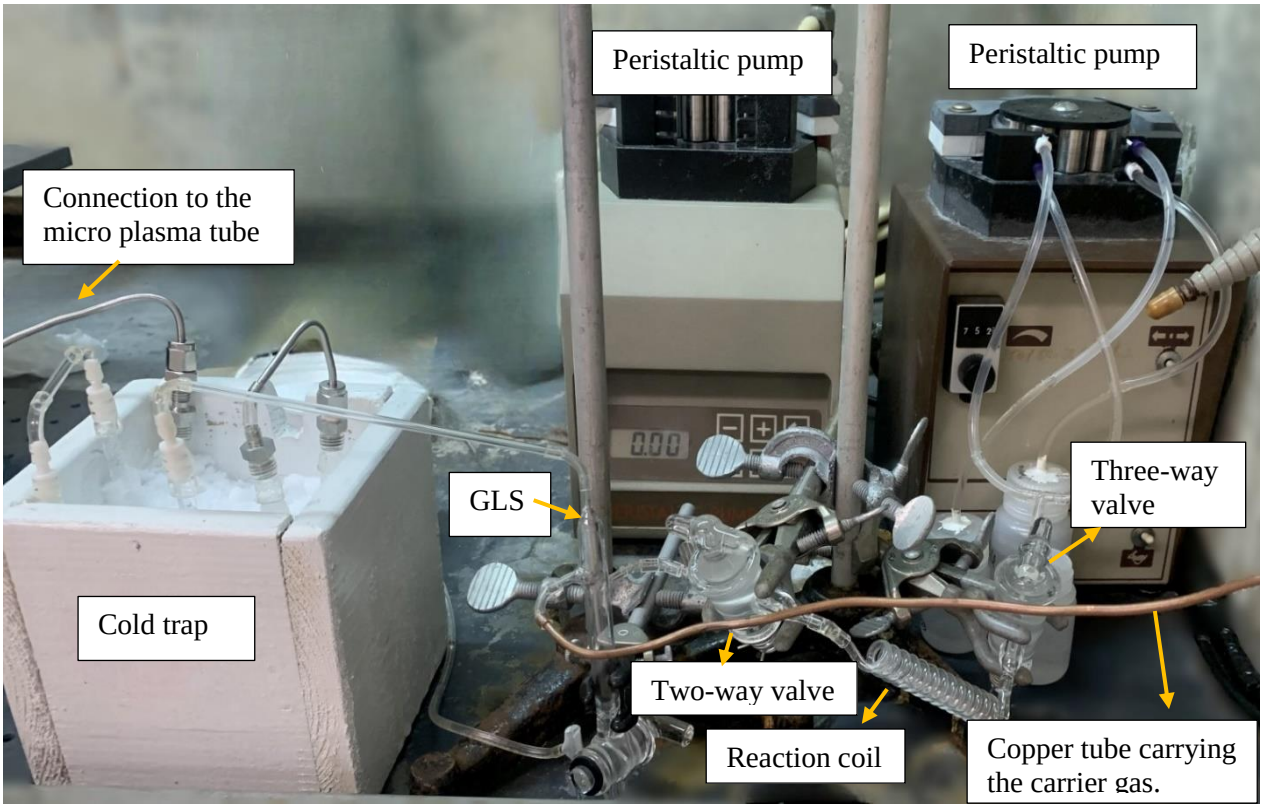

C. Photo of Microplasma Device Placed Inside the Fumehood